MODELING OF THE PHSICAL ENVIRONMENT AND ITS EFFECTS ON OYSTER DISEASE IN DELAWARE BAY: PAST, PRESENT AND FUTURE

By

ZHIREN (JOSEPH) WANG

A Dissertation submitted to the

Graduate School-New Brunswick

Rutgers, The State University of New Jersey

In partial fulfillment of the requirements

For the degree of

Doctor of Philosophy

Graduate Program in the Atmospheric Sciences

Written under the direction of

Professor Dale Haidvogel

And approved by

____

____

____

____

New Brunswick, New Jersey

October, 2013

ABSTRACT OF THE DISSERTATION

MODLING OF THE PHSICAL ENVIRONMENT AND ITS EFFECTS ON OYSTER DISEASE IN DELAWARE BAY: PAST, PRESENT AND FUTURE

By ZHIREN (JOSEPH) WANG

Dissertation Director: Professor DALE HAIDVOGEL

Delaware Bay is important to a variety of ecological and economic processes including the production of oysters. For this Bay we develop, validate and apply a high-resolution hydro-dynamical model, hindcast its largely unknown physical environment, investigate the roles of the physical environment influencing oyster diseases, the Multinucleated Spheres of unknown origin (MSX), and inquire into the future fate of the Bay in response to climate changes.

Model parameters are determined based on multiple experiments. Model validation against extensive *in situ* datasets shows that the model has significant skill in predicting variations in tracers and circulation.

The model is applied to inquire into the relationships between water properties and the observed MSX prevalence (MSXP), and simulations of concurrent physical conditions are performed. Correlation analyses indicate that MSXP is significantly correlated with river flow, salinity, and the salty-warm area (SWA) index that combines the effects of temperature and salinity. The positive river flow/temperature and the negative river flow/salinity correlations determined a negative temperature/salinity correlation with relatively small SWA, helping control MSX. An effective upper Bay transport mechanism, via timely spreading MSX with a MSXP gradient often available, may also contribute to MSXP in the upper Bay.

We inquire into the potential impacts on the physical environment in Delaware Bay arising from future climate change. Our sensitivity studies suggest that sea level rise (SLR) in 50-100 years may significantly change circulations and salinize the Bay mainly via weakened salinity gradient and salt advection, associated with intensified mixing induced by the widened Bay. Intensified river flow may not offset the SLR-induced salinization. Warmer surface air may significantly warm the shallow and thermally sensitive Bay. These new physical conditions would be generally unfavorable to oysters because they tend to promote oyster diseases (i.e., MXP and Dermo).

By fixing the coastline the salinization induced by the SLR would be substantially mitigated. The avoidance of dredging in the lower Bay would also mitigate the salinization to some extent. Similar processes related to salinization and warming may occur in other similar estuaries.

ACKNOWLEDGEMENTS

I would like to firstly thank my academic advisor Dr. Dale Haidvogel. With his broad knowledge and sharp vision in the field, he has helped me define my research questions and set me on the right track. The communications with him enlightened me a lot. With his great patience and academic rigor, he has cultivated my interests, enhanced my scientific understanding, and encouraged me to finish my research. His scientific attitude will be greatly beneficial to me in my future career.

Drs. James Miller, Mark Miller, David Bushek and Robert Chant are all very helpful to me. I learnt much from the communications with them and with Drs. John Wilkin, Maria Aristizabal, Enrique Curchitser (Institute of Marine and Coastal Sciences, Rutgers University). Dr. Robert Chant provided the salinity, temperature, and current data in 2010-2011 from the Delaware Bay Mooring Deployment Project-DBMDP. Drs. Eileen Hofmann (Department of Ocean, Earth and Atmospheric Sciences, Old Dominion University), David Bushek, Eric Powell, Susan Ford, Hal Brundage, and Jason Morson (Haskin Shellfish Research Laboratory, Rutgers University) provided supports including access to the Versar temperature and salinity in 2000 and MSX prevalence observations in 1958-2009. Drs. Kevin Brinson and Daniel Leathers (University of Delaware) provided the solar radiation from the Delaware Environmental Observation System. Research computing specialist Elias Hunter, computer experts David Robertson, Chuck Belmonte and Adam Porter, and PhD Candidate Greg Seroka (Institute of Marine and Coastal Sciences, Rutgers University) have all helped in computing and data issues.

It is a pleasant experience to work with the wonderful peoples above and other members of my department.

I specially thank my wife Hong and our parents as well as our sisters and brothers in the LORD (e.g., Zhiyuan Wang, Yuhui Lee, Guanglu Zhu, Jieqing Luo, I-qiang Lin, Peiling Xie, and Ruzheng Zhou) for their supports. Hong's trust, encouragement, patience and selfless support have been indispensable to my whole PhD studying process.

Funding was provided by, a full time Graduate Assistantship (September 2007-January 2009 and September 2011-June 2013) offered by Institute of Marine and Coastal Sciences of Rutgers University, and fellowship (January 2009-June 2011) offered by the DuPont Corporation, the New Jersey Agricultural Experiment Station, and the National Science Foundation Ecology of Infectious Diseases program (OCE06-22672).

Other non-profit data resources used here include: the North American Regional Reanalysis, the US Geological Survey, the National Water Level Program, the European Centre for Medium-Range Weather Forecasting, the Regional Ocean Modeling System, the Center for Operational Oceanographic Products and Services, the National Oceanic and Atmospheric Administration, the National Geophysical Data Center | U.S. Coastal Relief Model, the global Advanced Circulation Model, and the 119 cited papers.

Table of contents

List of tables

List of illustrations

§1. Literature review and background

§1-1. The physical environment in Delaware Bay

Delaware Bay is located between Atlantic Ocean and Delaware River on the Northeast seaboard of the United States and neighbored with three states (i.e., New Jersey, Delaware, and Pennsylvania) and their large cities such as Newark, Jersey City, Wilmington, and Philadelphia. Estuaries like Delaware Bay are of great importance for their high productivity of organic matter, their protective habitats for wildlife and aquatic life, their ecological roles in providing freshwater resources, and their economic value through commercial and recreational activities (Fig. 1).

Delaware Bay has relatively small volume, shallow depth, and narrow mouth and body and is very sensitive to changes in sea level and surface air temperature. Its shallow and narrow topography helps limit the salt-intrusion and maintain a large horizontal gradient of salinity together with the river flow input from the upper Bay to keep the upper water fresher and provide a habitable ("refuge") area for biota such as oysters.

The primary inputs of freshwater to Delaware Bay are from six rivers (the Delaware, Schuylkill, Maurice, Cohansey, Brandywine and Rancocas). Based on daily USGS river flow data for the period 1974-2011, the average freshwater input rate into Delaware Bay through the six rivers is approximately 478 m^3s^{-1}, about 76% and 18% of which are from the Delaware River and the Schuylkill River, respectively. Some 28%, 36%, 17%, and 19% are input into the Bay in winter (DJF), spring (MAM), summer (JJA), and fall (SON), respectively. The daily river flow varies greatly, ranging from 69 m^3s^{-1} (on 1 May 1981) to 7786 m^3s^{-1} (on 29 June 2006). High levels of nutrients are input into Delaware Bay from the Philadelphia area (Sharp *et al.*, 2009).

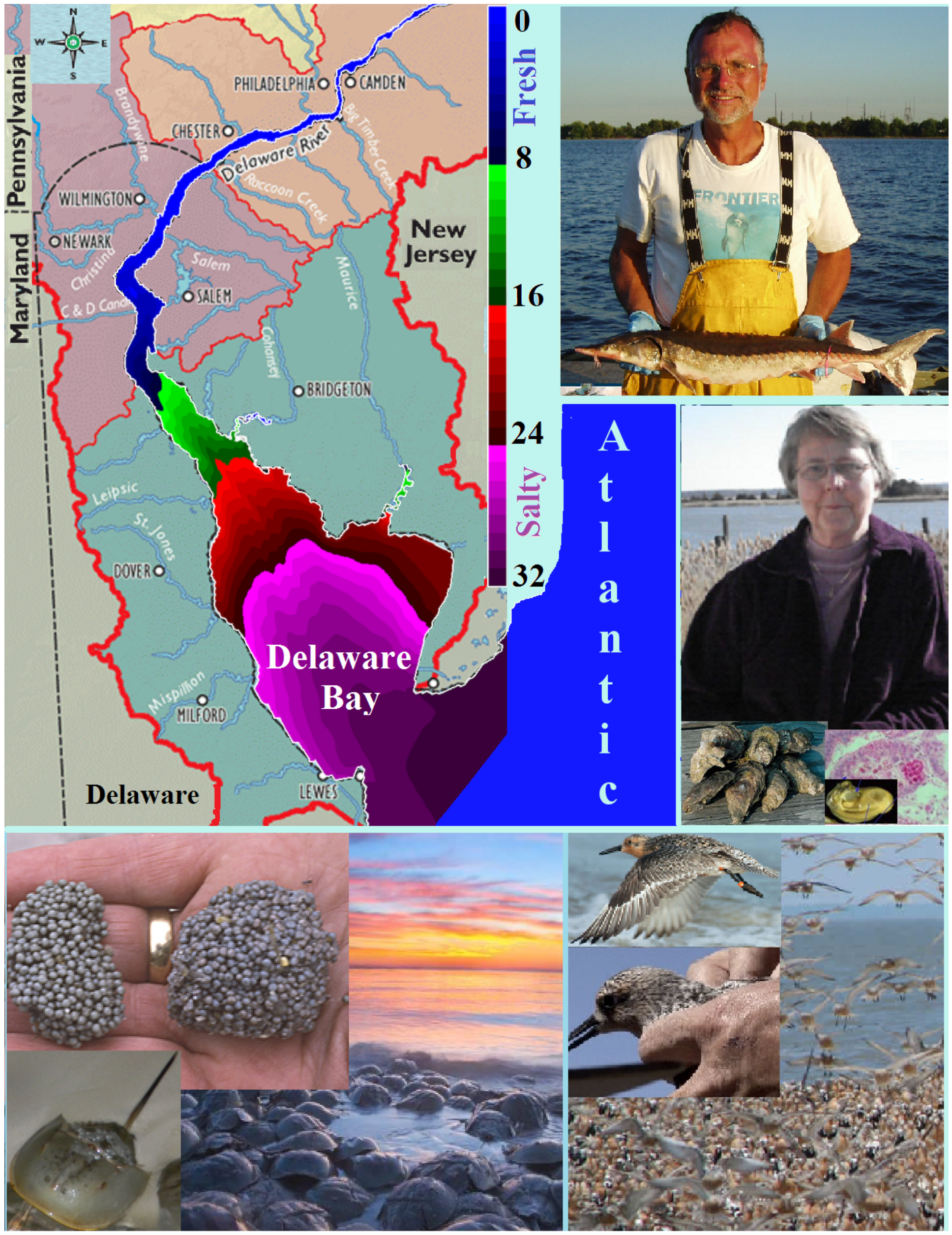

Figure 1. The unique Delaware Bay. Salinity plotted in the left upper frame is from numerical simulation temporally averaged within 1974-2009 and vertically averaged within the entire water column. Other parts of this figure are re-edited from the pictures from Principal Hal Brundage (Environmental Research and Consulting, Inc.) and published on: http://www.delawareestuary.org, http://hsrl.rutgers.edu, http://www.udel.edu, http://www.state.nj.us, and EC Press Releases List.

The physical environment, including circulation and tracers, in Delaware Bay displays abundant spatial and temporal variation on multiple scales. The water level is controlled primarily by tidal processes and secondarily by longer-period signals from (e.g.) atmospheric forcing. The mean sea level range can reach 4.5 meters. Salinity is affected by many factors such as the variations in river inputs, salt intrusion and mixing processes. The spatial variation of salinity can reach 30, from zero in the upper Bay to 30 in the lower Bay. Temperature signals are dominated by the seasonal cycle of surface air temperature and heat fluxes. The seasonal variation of temperature can be up to 25^{o}C; its spatial variation is small since the Bay is small in areal extent.

The intensity of vertical mixing is proportional to the cube of the tidal current amplitude but inversely proportional to the depth of the water column (Simpson *et al.*, 1978; Haidvogel and Chant, 2011). Therefore, because of its shallow water column, Delaware Bay has effective vertical mixing by the tides (Wong, 1995) which maintains a small top-to-bottom salinity difference (Wong, 1994A) and contributes to efficient exchange (e.g., of oxygen) between the atmosphere and the Bay (Sharp *et al.*, 2009). Strong shear is observed primarily in the lower Bay where there exists a two-layer vertical structure with shallow outflow (buoyancy flux from riverine inflow toward the lower Bay through the upper layer) and inflow at depth (with saltier water that intrudes from the lower Bay via the lower layer). The salinity in Delaware Bay (of a volume of ~13.2 km^3) is sensitive to variations in fresh water input.

The low-lying areas neighboring the Bay and the shallowness of the Bay itself leave the Bay susceptible to changes in sea level and temperature. The area of the Bay increases rapidly with SLR (Fig. 2). Likely related to the long-term interaction between the high tide and the land near the coastline, the topography near the coastline (0 to 50 cm above sea level) of the Bay is rather flat and therefore the water area is very sensitive to sea level rise (SLR). A 50 cm SLR increases the water area by approximately 53%; a 100 cm SLR will enlarge the water area by approximately 55%, with water area extending westward by about 7 km. The temperature of the shallow (less than 50 meters) water column is strongly related to the sea surface air temperature, the higher the sea surface air temperature, the higher the sea temperature.

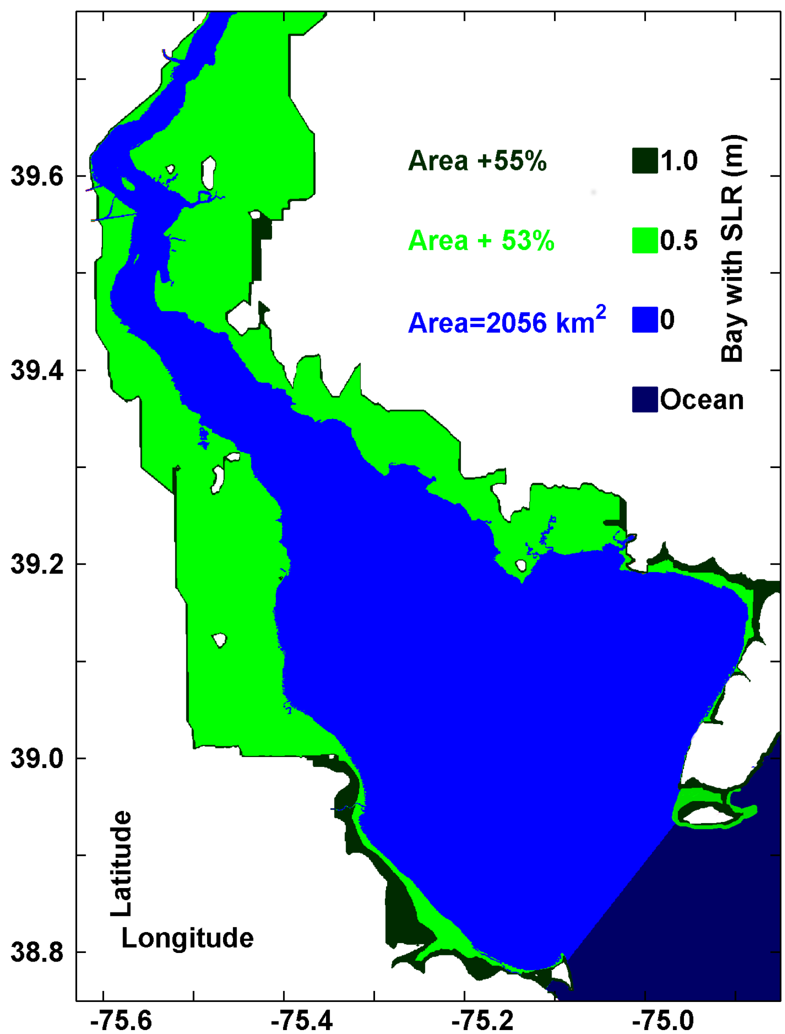

Figure 2. Sea level and coast-line of Delaware Bay. NGDC 3-second topography is used in this figure.

§1-2. Theoretical studies and numerical modeling pertinent to Delaware Bay

Circulation and tracers (especially salinity) in Delaware Bay are characterized by substantial spatial-temporal variability and are highly responsive to the applied forcing, which together with the inherent dynamical complexity of the estuarine circulation offers a big challenge for both theoretical and numerical modeling studies.

Delaware Bay is fundamentally driven by tides. Tides provide energy for vertical mixing (Simpson *et al.*, 1978) and induce strong currents (~5 m/s) (Knauss, 2005). Tidal harmonic analysis gives the relative amplitude and periods of tidal motion for tidal constituents, e.g., of the principle lunar (M_2, with a period of 12.42 hours and the most dominant amplitude), luni-solar diurnal (K_1, 23.93 hours and 58.4% of M_2-amplitude), principle solar (S_2, 12.00 hours and 46.6% of M_2-amplitude), principle lunar diurnal (O_1, 25.82 hours and 41.5% of M_2-amplitude), principle solar diurnal (P_1, 24.07 hours and 19.4% of M_2-amplitude), larger lunar elliptic (N_2, 12.66 hours and 19.2% of M_2-amplitude), and lunisolar semidiurnal (K_2, 11.97 hours and 12.7% of M_2-amplitude). The M_2, S_2 and N_2 produce spring and neap variability at 14.8 and 27.3 days respectively; the K_1 and O_1 can induce diurnal inequality to tidal period variability.

An inter-play between river input, exchange flow, and mixing determine the estuarine structure of current shear and the along-channel salinity gradient (MacCready, 2004), and the spring-neap mixing variation leads to changes in the estuarine structure (MacCready, 2007). The time-dependent salt-intrusion distance (SID), which is the distance from the estuary mouth to the point where the salinity reaches the river salinity (Nguyen, 2008), is the primary measure of the salinity structure and the adjustment time for a given section-averaged velocity. The inflow gradually rises and joins the outflow as it move towards the upper Bay, producing the exchange flow. The highly variable salinity structure including an accompanying salt front is produced through highly variable riverine inflow and saltier water intrusion which is highly sensitive to the water depth (MacCready and Geyer, 2010). Water inflow is centered over the deepest section and freshwater outflow is situated over each flank (Wong, 1994B) because vertical eddy viscosity is significant with an Ekman depth close to the overall water depth (Kasai *et al.*, 2000).

Horizontal currents are approximately geostrophic, with Kelvin numbers (ratio of current width to internal Rossby radius) exceeding 1 in the Delaware Estuary (Garvine, 1995; Holton, 1992; Knauss, 2005). Substantial transverse variability in salinity and residual circulation results from gravitational effects and wind forcing (Wong, 1994A), and from lateral (secondary) circulation (MacCready and Geyer, 2010). Lateral variations in depth and a strong momentum shear produce a transverse circulation of 5−10 cm/s in the Delaware River estuary (Lerczak and Geyer 2004). In the bottom layer, shear drives entrainment to cause estuarine boundary layer mixing (Chant *et al.*, 2007).

Delaware Bay is usually vertically well mixed due to tidal mixing whose intensity is proportional to the cube of the tidal current amplitude but inversely proportional to the depth of the shallow water column (Simpson *et al.*, 1978). Shear is determined by the balance between vertical mixing and the spatially inhomogeneous inputs of freshwater and heat (Haidvogel and Chant, 2012). A well-mixed water column tends to be produced if vertical mixing overcomes the surface heat flux that produces shear. In the open ocean where salinity is relatively spatially uniform, temperature influences density more significantly than salinity (Stommel, H., 1961), but this is not the case in Delaware Bay where there is a strong salinity contrast between riverine inflow and saltier water intrusion. Shear is also influenced by the wind. For a partially stratified estuary, up-estuary wind reduces shear, while down-estuary wind effects shear depending on the competition between wind straining which induces shear and direct wind mixing which reduces shear (Chen and Sanford, 2009).

The time dependency of the salt-intrusion distance (SID) that is highly sensitive to the depth and cross-sectional area of the estuaries (MacCready and Geyer, 2010), river flow (Aristizabal and Chant, 2013) and bathymetry (Ralston *et al.*, 2008). Mixing (turbulence) and diffusion (Mello and Yamada, 1974, 1982; Warner et al., 2005a; Umlauf and Burchard, 2003) change the salinity and current structure. For Delaware Bay of the generally shallower depth, smaller size and narrow mouth should limit salt-intrusion. However, as shown below, sea level rise will change geometry and therefore salinity and current structure significantly (see Chapter 4 for details).

Theoretical studies have quantitatively described the important circulation and salinity structures, based upon simplifying assumptions. However, numerical modeling is required to study the real coastal circulation and other physical conditions by applying more realistic (e.g., non-linear) control equations, atmospheric forcing, and initial and boundary conditions.

A few modeling studies have been conducted to explore the circulation in Delaware

Bay or adjacent estuaries. The buoyant outflow in Delaware Estuary has been simulated and the simulation compared with observations of the lateral salinity pattern and vertical structure, with the lower Bay well simulated but the along-estuary salinity gradient over-estimated (Whitney and Garvine, 2006). A larval transport model with realistic tidal forcing, bottom bathymetry, wind stress and river flow has been applied in Delaware Bay to reproduce observed blue crab recruitment in 1990-92 and in 1989, with the wind stress dominant in the determination of the timing of settlement events (Tilburg *et al.*, 2005). The role of turbulent salt fluxes in maintaining the salinity intrusion and the complex spatial and temporal interplay between turbulent mixing and the shape of the isohaline have been highlighted using an analytical model and using results from a three-dimensional numerical model (MacCready and Geyer, 2001). The New York Bight has been studied under idealized conditions of an unforced buoyant river plume, under upwelling and downwelling wind forcing, using adjoint sensitivity analysis (Zhang, *et al.*, 2009). A comprehensive skill assessment has been conducted via ROMS-based numerical simulations of the Hudson River estuary with different turbulence closure methods to effectively reproduce the observed variations in salinity and current structure (Warner *et al.*, 2005).

Aristizabal and Chant (2013) perform theoretical and modeling studies in Delaware Bay to describe the spatial and temporal structure of the exchange flow and the salinity field using the regular bathymetry driven by M2 and S2 tidal components and the steady river flow input from Delaware River. A steady shear dispersion and a tidal oscillatory salt flux are larger during neap tide than during spring (also see Lerczak *et al.*, 2006). The lateral flows cause the temporal variability of the tidal oscillatory salt flux via bringing velocity and salinity out of quadrature, and the stronger stratification during neap tide enhances the tidal oscillatory salt flux. Associated with the steady shear dispersion and a tidal oscillatory salt flux, the role of river flow input in controlling salt intrusion distance is determined to be weaker than that from the classical results of Hansen and Rattray (1966) and Monismith *et al.* (2002).

These prior studies help our understanding of the dynamics of the Delaware Bay circulation and lay the basis for us to do further works in developing the model, hindcasting the physical environment, studying the roles of the physical environment, and exploring the potential response of the physical environment to climate change. Oyster diseases are chosen to study how physical environment influence function in Delaware Bay and in the next section we will introduce the background of oyster diseases.

§1-3. Oysters, oyster diseases and EID project background

Oysters (*Crassostrea virginica*) are of great commercial value as food, and of environmental importance as part of a healthy ecosystem. They live along salinity gradients and are sensitive to their physical environment. Limited by disease mortality, oyster population abundance in Delaware Bay was high during 1970-1985, but low during 1953-1969 and 1985-1999, and very low since 2000 (Ford, 1996; Powell *et al.*, 2008; Mann *et al.*, 2009). In six consecutive years since 1999, the condition of the oyster resource deteriorated with recruitment below average (less than 0.5 spat per oyster per year in 2005) in Delaware Bay, compared to the 53-year record for which detailed survey data are available (1953-2005, US Army Corps of Engineers Philadelphia District, 2006).

Oyster population abundance is closely related to environmental fluctuations, harvest and recruitment levels and oyster mortality controlled by two lethal diseases: MSX (Multinucleated Sphere of unknown origin) and Dermo (Hofmann *et al.*, 2009).

MSX is caused by a protozoan parasite, *Haplosporidium nelsoni* (Sprague, 1979; Burreson *et al.*, 2000; Ford and Tripp, 1996). The first recorded outbreak of MSX disease was in 1957 in Delaware Bay. It killed 90-95% of the oysters in lower Delaware Bay and about half of those in the upper Bay in 1957-59 (Haskin *et al.*, 1966). Natural mortality was mostly low before the first outbreak of MSX disease in 1957, but remained above 10% after 1957 (Powell et al., 2008). About 70-75% of the oysters in the upper Bay died over a two-year period in 1985 and 1986 when MSX was most prevalent in Delaware Bay (Powell *et al.*, 2008; Hofmann *et al.*, 2009). MSXP displays a significant temporal (seasonal and inter-annual) and spatial variability over a 52-year period since 1958. In the upper Bay, it is higher in 1960s, 1980s, and 1990s, but lower in 1970s and 2000s. In the lower Bay, it is persistently higher except in the falls of 1990s and 2000s. After approximately 1993 MSXP decreased significantly (Fig. 3) and the majority of the population has developed a relatively high level of resistance (Ford and Bushek, 2012). Despite this resistance, MSXP remains systematically higher in the lower Bay than in the upper Bay, providing a potential transport gradient for infective particles (Ford et al., 2012). It is unknown how infective particles move around the bay

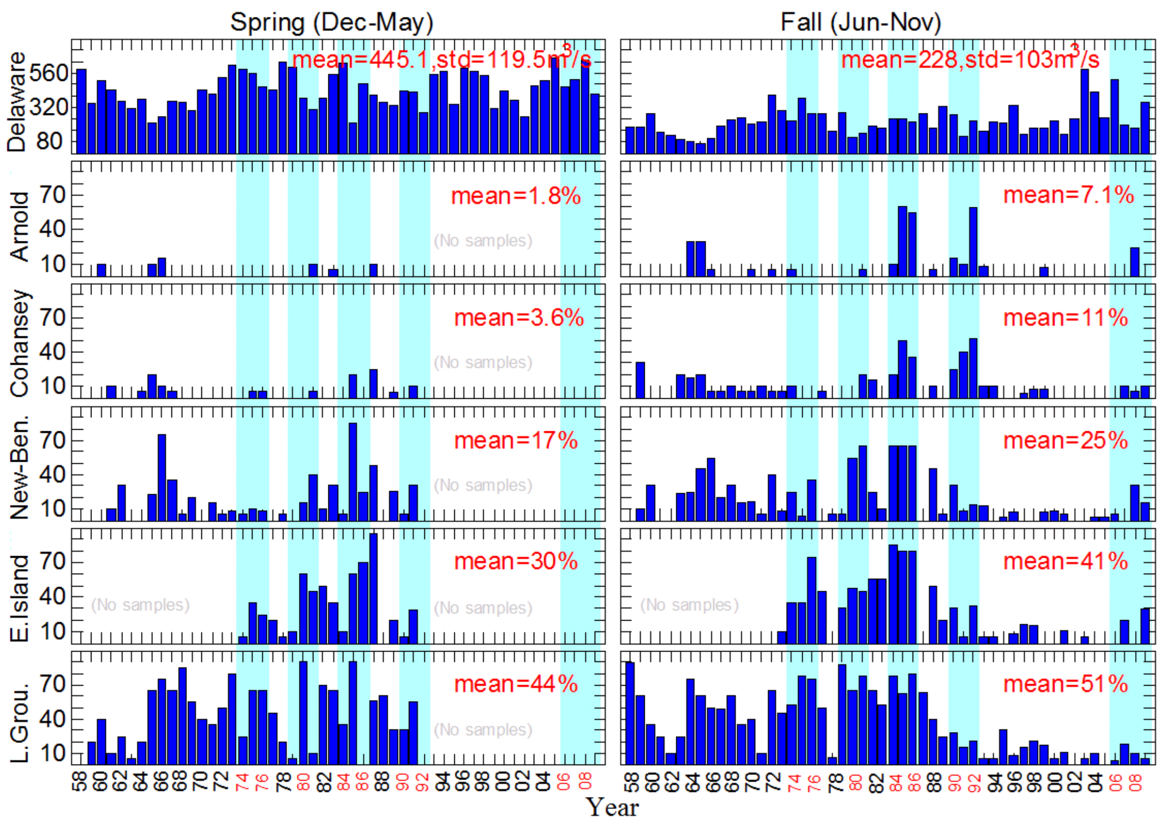

Figure 3. Time series of river flow input in to Delaware Bay and *Haplosporidium nelsoni* prevalence (MSXP). The river flow (m^3/s, row 1, with its mean and standard deviation provided in red numbers) and MSXP (%, rows 2-6, with its mean provided in red numbers) are observed in spring (Dec-May, column 1) and fall (Jun-Nov, column 2). MSXP was observed at Arnolds, Cohansey, New Beds-Bennies, Egg Island, and Leased Grounds. The highlighted periods 1974-76, 1979-81, 1984-86, 1990-92, and 2006-09 are the five scenarios used for our comparison. MSXP is defined as 100*number of infected oysters/number of oysters sampled, assessed using tissue-section histology for the first four periods and using both histology and polymerase chain reaction for the last.

Dermo is caused by a water-borne protozoan parasite (*Perkinsus marinus*) that was found in Delaware Bay in the mid 1950s. It became undetectable following a restriction of oyster imports from infested areas, but has influenced on oyster abundance increasingly since the late 1980s (Bushek *et al.*, 2012). This study focuses on MSX prevalence (MSXP) as part of a larger study to understand the mechanisms that permitted much of the oyster population in Delaware Bay to develop resistance to an introduced pathogen (Hoffman *et al.*, 2009).

Environmental fluctuations and disease are a crucial influence on oyster population abundance (e.g., Haskin and Ford, 1982). A central element of this project is the 53-year database of oyster surveys in the Bay, providing long-term records for both MSX and Dermo diseases. Shortly after the initial MSX outbreak in 1957, MSXP has been assayed one to two times per year on five sites in Delaware Bay (Arnolds, Cohansey, New Beds-Bennies, Egg Island and Leased Grounds). Between 1958 and 2010, all beds were assayed in the fall. From 1958 through 1991 the beds were also assayed in spring. Delaware Bay river flow is generally lower in 1960s and 1980s, but higher in 1970s, 1990s, and 2000s. The temperature, salinity, and circulation in Delaware Bay are largely unrecorded and need to be "recovered" through modeling. Salinity and temperature are the primary physical controls on MSX, with MSX requiring salinity >10 and temperature about 5-20^{o}C; infection prevalence generally decreases along a salinity gradient with salinity. Infection prevalence can be eliminated from oysters at salinity <10, providing a disease refuge, but high salinity does not always guarantee high MSX levels, nor does low salinity always prevent the parasite from appearing in the upper Bay. Oysters and the parasite are relatively inactive at 5^{o}C and below; the parasite multiplies faster than the oysters can control between about 5^{o}C and 20^{o}C (Andrews, 1966; Haskin and Ford, 1982; Ford, 1985). Both MSX and Dermo multiply fast at higher temperature (above 18-20^{o}C) and higher salinity (above approximately 12; reviewed in Ford and Tripp, 1996; Cook *et al.*, 1998).

However, the method(s) of transmission and the role of the physical environment, particularly the role of circulation on the dispersal of infective MSX particles are unknown. That MSXP is systematically higher in the lower Bay and that low salinity does not always prevent the parasite from appearing in the upper Bay might imply the importance of some, yet unexplored, transport mechanism.

The issues the overarching research program funded through NSF's EID program has been studying include: the rapid genetic changes probably induced by environmentally modulated selection, the temporal and spatial variability in the number of parents that successfully produce offspring, the mechanism(s) for the refugia to persist in the very low-salinity regions, modeling studies on the origin of larvae that set in different regions of the Bay, the oyster-disease interaction with climate change, etc. The important methods the EID program has applied to study these issues include coordinated field and laboratory studies of genetics and disease, and integration of data sets via genetic, population and circulation models. The overall goal of these collaborative studies has been improving understanding of disease resistance and prevalence in estuarine populations, and their response to climate change.

§1-4. Climate changes and Delaware Bay

The climate system is changing and thereby influencing the coastal oceans and estuaries such as Delaware Bay that are sensitive to variability in sea surface height, sea surface temperature, winds, precipitation, etc. Sea-level could rise 40-65 cm by the year 2100 due to predicted greenhouse-gas-induced climate warming with sea surface temperatures increasing by about 2~3^{o}C. Such a sea-level rise would threaten coastal cities, ports, and wetlands (Gornitz, 1995). Coastal erosion, offshore bathymetric changes (Copper and Navas, 2004), inundation, and ecosystem losses will affect hundreds of millions of people. By mid-century, runoff is projected with high confidence to increase by 10 to 40% at higher latitudes, but decrease by 10 to 30% at some dry mid-latitudes and tropics. Records show that the U.S. Northeast climate has changed with global warming with spring arriving sooner, summer growing hotter, winter becoming warmer and less snowy, and with seasonal precipitation changes (UCS, 2006).

Climate change will influence the tracers, circulation, and ecosystems in Delaware Bay. As we will see in Chapter 3, in Delaware Bay, salinity and temperature are normally out of phase because enhanced river flow reduces salinity and increases with temperature. A warmer climate produces stronger river flow through intensified precipitation and ice-snow melting, further reducing salinity and upper Bay transport.

However, concurrent warmer and saltier conditions can occur in Delaware Bay, and such occurrences may become more frequent with climate change. The “irregular mode” with salinity and temperature being more in-phase has occurred in the persistently drier and warmer period 1984-85 when MSXP was high. This might be related to the irregularly strong La Niña with an irregular general circulation pattern in 1984-85 after the unusually strong El Niño in 1982-83. Warmer and saltier conditions can also be induced by global warming, a salt-intrusion intensified by SLR, and less river flow with reduced precipitation and available snow. Consequently, higher temperature does not necessarily guarantee stronger river flow. The detailed introduction to climate changes associated with Delaware Bay and studies on the effects from climate changes on Delaware Bay will be given in Chapter 4.

§1-5. Approaches and goals of this study

Prior observations, theories, and modeling leave much room for improved understanding of the estuarine dynamics and ecosystem response in Delaware Bay. Here, we develop, validate and apply a high-resolution hydro-dynamical model based on the Regional Ocean Modeling System (ROMS) for Delaware Bay. Implementation and validation of the model is described in Chapter 2. In particular, it is shown that the model has low bias (less than 1^{o}C in temperature, less than 2 in salinity) and high skill in simulating tracers and circulation. Next, we apply ROMS to investigate the relationships between observed MSXP and the simulated physical environment. Excluding the sensitivity tests used to design the model and the multiple tests for particle transport study, 19 years of simulation have been conducted for model validation (years 2000 and 2010-11, Chapter 2) and for exploration of inter-annual variations in observed MSXP (years 1974-76, 1979-81, 1984-86, 1990-92, and 2006-09; Chapter 3); 48 years of simulation for 17 cases (2-3 years for each case) have been done for climate sensitivity studies that are conducted and analyzed in Chapter 4. Lastly, a summary and discussion for this dissertation is presented in Chapter 5.

§2. Delaware Bay Model: implementation and validation

§2-1. ROMS overview

ROMS is a terrain-following, free-surface, primitive-equation ocean model with accurate and efficient physical and numerical algorithms, several vertical mixing schemes, multiple levels of nesting and composed grids, and several coupled models for biogeochemical, bio-optical, sediment, and sea ice applications. The primitive equations are vertically discretized over variable topography using stretched terrain-following coordinates (Song and Haidvogel, 1994). The stretched coordinates allow increased resolution in areas of interest, such as the thermocline and the bottom boundary layer. A staggered Arakawa C-grid (Arakawa and Lamb, 1977) is applied. Coastal boundaries can also be specified as a finite-discretized grid via land-sea masking.

ROMS has various options for advection schemes (e.g., second- and forth-order centered differences, third-order upstream biased differences), sub-grid-scale parameterizations, horizontal mixing of momentum and tracers (local or nonlocal closure schemes, applied along terrain-following levels, geopotential surfaces, or isopycnic surfaces; Shchepetkin and McWilliams, 1998). For computational economy, a split-explicit time-stepping scheme is used in ROMS, based on a robust and stable third-order accurate predictor (Leap-Frog) and corrector (Adams-Molton) time-stepping algorithm. For more detailed descriptions of ROMS, please refer to the published papers of, e.g., Haidvogel *et al.*, 2000 and 2008; Shchepetkin and McWilliams, 2003, 2005, and 2006; Warner *et al.*, 2005, 2008A,B; Budgell, 2005; Umlaugh and Burchard, 2003; Mellor and Yamada, 1982; and Durski *et al.*, 2004.

ROMS has been applied to several pysical and ecological processes. For examples, ROMS was used to simulate the circulations in the North Atlantic Ocean (Haidvogel, *et al.*, 2000), in North Pacific Ocean (Curchitser *et al.*, 2005), in the Peru and central California current systems (Penven *et al.*, 2005 and 2006), and in the southern Agulhas Current (Lutjeharms *et al.*, 2003). ROMS has also been applied for some dynamical and ecological studies in Delaware Bay (e.g., Wang *et al.*, 2012; Narváez *et al.*, 2012; Aristizabal and Chant, 2013).

§2-2. Implementation for Delaware Bay

§2-2-1. Grid and resolution

The Delaware Bay model covers the domain 74.1^{o} to 75.6^{o}W and 38.1^{o} to 40.2^{o}N. An Arakawa C-grid is applied to 98×386 horizontal cells using orthogonal curvilinear stretching to enhance horizontal resolution in the upper Bay and tidal river (~230 meters) compared to the adjacent coastal ocean (~1500 meters) where the domain extends to approximately the 50 meter isobath (shown in Fig. 4a,b)[1]. The minimum water depth is 2 meters. The time step is 60 seconds and the barotropic mode is temporally integrated 25 times within each baroclinic step using the split-explicit method (Shchepetkin and McWilliams, 2005). The Delaware River extends as far as Trenton, NJ, the head of the tidal regime and the location of the USGS river flow monitoring station. For the lower Bay from about the Schuylkill (~39.8^{o}N) to the mouth of the Bay (~38.7^{o}N), we set 20 vertical levels in a generalized topography-following coordinate weighted to give highest resolution near the sea surface. The horizontal spacing ranges from 300 to 1500 meters.

§2-2-2. Choice of model parameters and related sensitivity studies

The choice of appropriate values for certain model parameters is essential. For example, the temperature of the shallow and turbid water column is sensitive to the depth scale assumed for solar radiation absorption (the so-called "water type") and to the net heat flux (solar shortwave radiation, SSWR) and the circulation of the shallow water column is sensitive to the bottom drag options.

---

[1] To minimize the number of "land" cells within the ROMS grid, the river cells above 39.8^{o}N have been folded back onto the grid to the south. The results below will be shown in the correct, unfolded geometry.

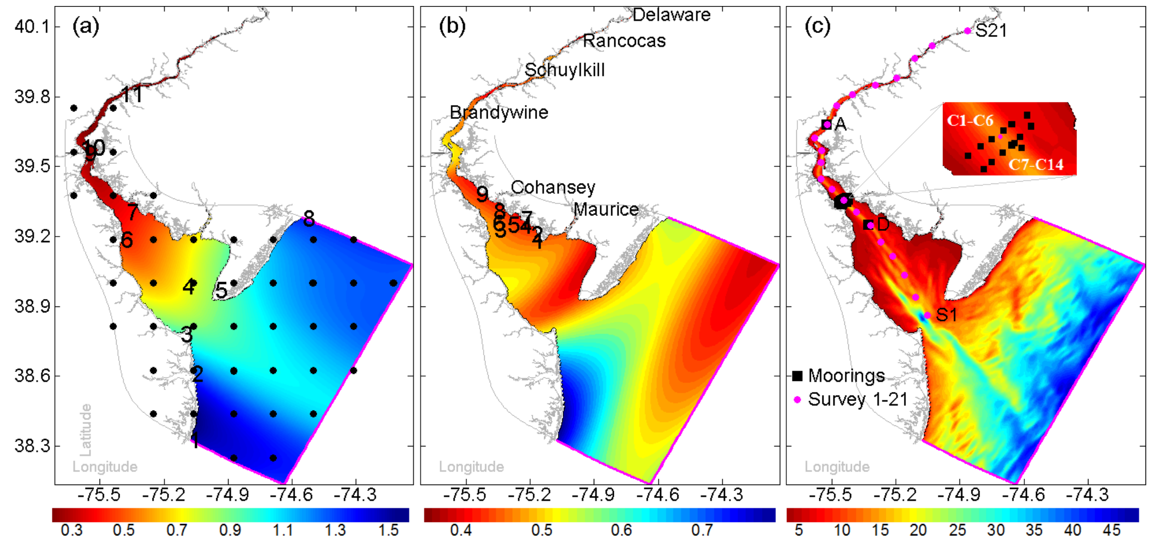

Figure 4. Delaware Bay model implementation. (a) cross-Bay spacing (km), eleven water level stations (numbers), and surface atmospheric forcing stations (black dots); (b) along-Bay spacing (km), 6 river input stations, and 9 Versa salinity-temperature stations (numbers for Section554, Egg Island, Lower Middle, New Bed, Bennies, Over the Bar, Nantuxent, Ship John and Arnolds, respectively); and (c) bathymetry (m) and the stations for Delaware Bay Mooring Deployment Project: black squares for moorings, A, D, and C1-C14, pink dots for survey S1-S21 (detailed in Tabs.3a,b). The pink lines indicate the open boundaries. The depths of the water level at stations 1 to 11 are 10.2, 6.4, 3.2, 8.2, 5.3, 2.5, 7.4, 17.5, 4.0, 5.1, and 5.5 meters, at the Versar stations 1 to 9 are 5.9, 5.4, 4.5, 5.7, 5.2, 5.4, 3.4, 5.5, and 5.7 meters, respectively.

SSWR: In Delaware Bay, the SSWR from the North American Regional Reanalysis (NARR) was discovered to be systematically higher than the SSWR observed near ground by the Delaware Environmental Observation System (DEOS, http://www.deos.udel.edu), which in turn produces an overly warm simulation. The SSRW ratios of DEOS to NARR are 77.4%, 77.1%, 76.7%, 76.2%, and 76.8% respectively for winter, spring, summer, fall, and the whole year, based on a comparison of the original 5-min interval DEOS SSWR and 3-hr interval NARR SSWR for the contemporary period 2005 through November 2009 when both DEOS and NARR SSWR are available (Fig. 5). The systematic percentage difference is nearly independent of season, which makes the correction of SSWR straightforward. In the simulations reported below, NARR SSWR was reduced by 20%.

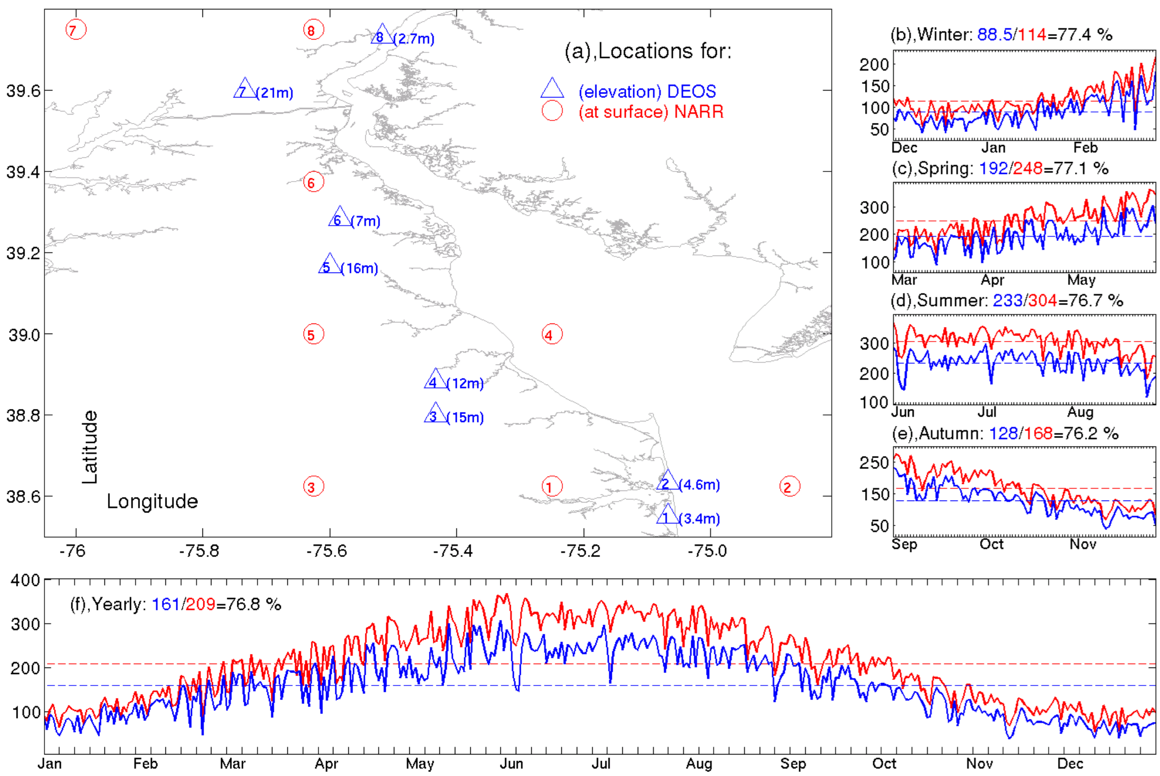

Figure 5. NARR- and DEOS- downward solar short wave radiations (Wm^{-2}, red and blue lines) in (b) winter, (c) spring, (d) summer, (e) fall and (f) entire year. Both NARR and DEOS data are averaged from 2005 to 2009 for all the eight stations shown in (a). Circles and triangles indicate the stations of NARR (at surface) and DEOS (at 2.7-21 meters above surface), respectively. The numbers in (b) to (f) indicate the seasonal and yearly mean downward solar short wave radiations for DEOS/NARR. Comparison based on station by station (1-8) gives about the same result. DEOS: Delaware Environmental Observation System, NARR: North American Regional Reanalysis.

Water types: In ROMS, the SSWR absorption profile is represented as two exponential functions following Paulson and Simpson (1977), with parameters determined by an assumed "water type" that defines the fraction of incident solar shortwave radiation flux penetrating the water column to a specified depth z = $A\ e^{z/B} + (1\text{-}A)\ e^{z/C}$ in meters (<0). The first/second term is the stronger/weaker attenuation of light in the red/blue-green part of the spectrum. A is the relative amount of red light incident on the sea surface, B and C are attenuation lengths (m) for the red and blue-green bands, respectively (Cahill *et al.*, 2008). A = 0.78, 0.5 and 0.5, B = 1.4, 0.01 and 0.2, and C = 7.9, 4.9 and 0.2 for water types 5, 6 and 7, respectively. We compared these three water types before choosing water type 7. Water types 5 and 6 characterize a cleaner water column, whereas water type 7 better fits the turbid water column in Delaware Bay, thereby concentrating absorption nearer the surface.

With the original NARR SSWR applied, simulated bottom temperature is approximately 1.9 ^{o}C and 1.8^{o}C warmer than the Versar data for June-August period using water types 5 and 6, respectively while water type 7 produces a better simulated temperature that is closer to Versar data (section 2-3-1) by approximately 0.3^{o}C or larger at lower water column (Fig. 6). In the future, ROMS could perhaps be improved with a water type that is space (i.e., depth and turbidity) dependent.

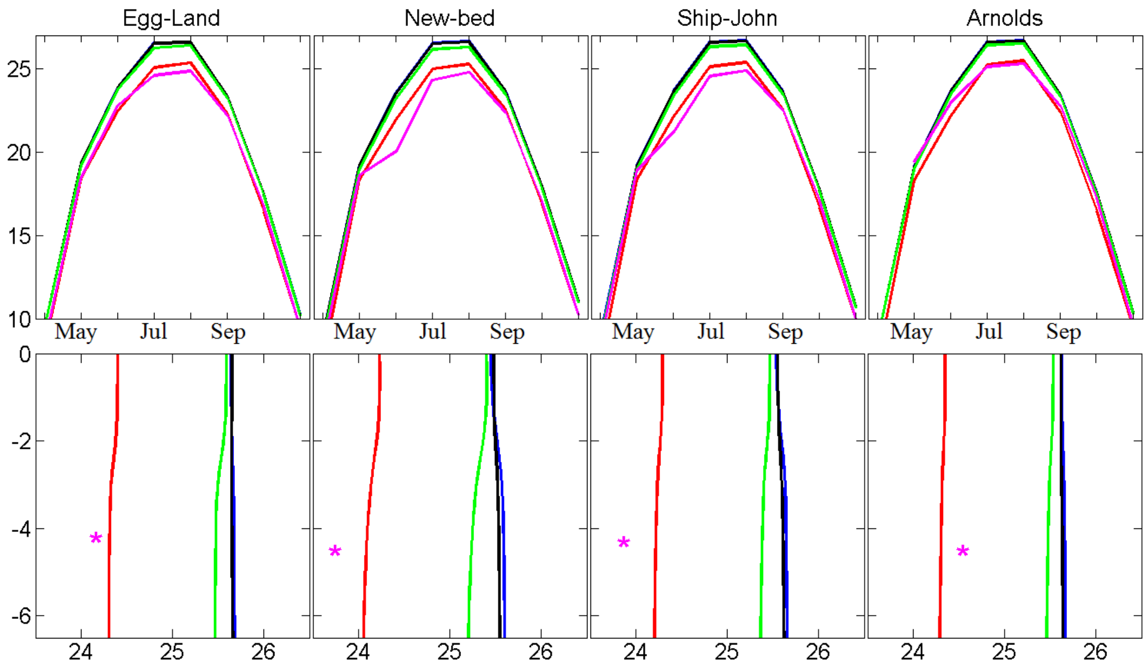

Figure 6. Mean observed and simulated temperature under different water types and solar radiation. The pink lines and stars indicate observed, blue, black, green and red lines indicate simulated temperature (^{o}C) using water type5, 6, 7 and water type7 plus 20%-reduced NARR short wave radiation at stations Egg Land (column 1), New bed (column 2), Ship John (column 3), and Arnolds (column 4) (with stations described in Fig. 3b). The temperature is averaged monthly at the observation depths in the first row, but averaged in June-to-August period at all depth (m, y-axis) in the second row, based on the 15-minute-interval Versar as described in Table 2 (Chapter 2) and simulated temperature from 13 May to 12 November 2000 and from 08 March to 12 April 2001.

Bottom drag: To examine the role of bottom stress in regulating the amplitude of the tidal currents, we ran two cases for years 2010-2011, one with a bottom resistance coefficient set to its standard value 3×10^{-3} and another with a value increased by 50%. The standard bottom resistance produces an along-Bay current 0.96~1.43 times that observed at the Bay from about 39.2~39.7^{o}N. This drag permits a strong tidal response and produces a better salinity variation (0.6~1.3 times of that observed). Enhanced bottom resistance decreases the along-Bay current to 0.73~1.25 times that observed and the variations of tide and salinity get too weak in the upper Bay. Therefore, the standard bottom resistance was employed in this study.

Number of vertical layers: Twenty levels are sufficient for the simulations described below. We conducted a sensitivity study with enhanced vertical resolution (40 layers) for the year 2000. The modification makes negligible difference to model skill.

§2-2-3. Forcing

The Delaware Bay model is forced by the following inputs: 6-hourly surface atmospheric fluxes from the ERA-40 data of European Centre for Medium-Range Weather Forecasting (ECMWF, http://data-portal.ecmwf.int) and 3-hourly atmospheric fluxes from the North American Regional Reanalysis (NARR available since 1979, http://nomads.ncdc. noaa.gov, Mesinger *et al.*, 2006; input locations shown in Fig. 4a); daily river transport from the US Geological Survey (USGS, http://waterdata.usgs.gov) input at six river locations (Fig. 4b); and climatological means of tidal elevations and currents at the domain perimeter with seven tidal constituents (M_2, N_2, S_2, K_1, O_1, M_4, and M_6) from the Global Advanced Circulation Model (ADCIRC, http://www.unc.edu/ims/adcirc/index.html). The annually averaged river transport rate from the six rivers is 283 to 880 m^3/s, with most of the input from the Delaware River (225 to 691 m^3/s, or 71.6 to 80.2%) and Schuylkill River (43 to 146 m^3/s, or 15.2 to 21.0%), for the 19 modeling years (Tab. 1).

Table 1. Annual mean river freshwater input rate into the Delaware Bay from the six rivers (Fig. 4b). The mean values shown are for the entire period from 1974-2011.

year	Delaware		Schuylkill		Brandywine		Maurice		Rancocas		Cohansey		Total
	m^3/s	%	m^3/s	%	m^3/s	%	m^3/s	%	m^3/s	%	m^3/s	%	m^3/s
1974	385	78.5	79.7	16.3	12.3	2.5	4.1	0.8	5.0	1.0	4.1	0.8	**490**
1975	449	73.4	123	20.2	20.3	3.3	6.5	1.1	6.2	1.0	6.5	1.1	**612**
1976	363	77.7	79.7	17.0	12.4	2.7	4.0	0.9	4.0	0.9	4.0	0.9	**467**
1979	446	73.9	109	18.1	25.4	4.2	7.6	1.3	7.8	1.3	7.6	1.3	**604**
1980	229	75.3	51.2	16.9	11.5	3.8	4.2	1.4	3.8	1.2	4.2	1.4	**304**
1981	225	79.3	43.0	15.2	6.7	2.4	2.9	1.0	3.1	1.1	2.9	1.0	**283**
1984	386	71.6	113	21.0	20.8	3.9	6.3	1.2	6.4	1.2	6.3	1.2	**539**
1985	249	77.8	53.2	16.6	8.4	2.6	3.4	1.1	2.7	0.8	3.4	1.1	**320**
1986	354	79.3	70.4	15.8	10.6	2.4	3.7	0.8	3.9	0.9	3.7	0.8	**446**
1990	387	77.3	86.4	17.3	12.5	2.5	4.7	0.9	5.3	1.1	4.7	0.9	**500**
1991	243	74.5	60.2	18.5	10.3	3.2	4.1	1.3	4.5	1.4	4.1	1.3	**326**
1992	266	76.7	61.6	17.8	9.1	2.6	3.1	0.9	4.0	1.1	3.1	0.9	**346**
2000	339	76	80.9	18.1	14.7	3.3	3.9	0.9	4.1	0.9	3.9	0.9	**447**
2006	482	77.0	114	18.3	14.8	2.4	4.8	0.8	5.1	0.8	4.8	0.8	**625**
2007	367	76.3	85.4	17.8	14.5	3.0	4.8	1.0	4.6	1.0	4.8	1.0	**481**
2008	435	80.2	85.5	15.8	11.6	2.1	3.3	0.6	3.6	0.7	3.3	0.6	**543**
2009	370	74.7	96.1	19.4	14.7	3.0	4.8	1.0	4.9	1.0	4.8	1.0	**495**
2010	364	75.4	85.1	17.6	15.9	3.3	6.1	1.3	5.4	1.1	6.1	1.3	**483**
2011	691	78.5	146	16.6	21.6	2.5	7.7	0.9	5.9	0.7	7.7	0.9	**880**
Mean	**362**	**75.7**	**87.8**	**18.4**	**14.4**	**3**	**4.6**	**1**	**4.8**	**1**	**4.6**	**1**	**478**

§2-2-4. Advection and mixing schemes

The advection terms in the 3D primitive equations are computed using the multidimensional positive-definite advection transport algorithm (MPDATA; Smolarkiewicz and Grabowski, 1990; Smolarkiewicz and Szmelter, 2005) for tracers, and using a 3D 4th-order centered discretization for momentum. The Generic Length Scale mixing scheme (Umlaugh and Burchard, 2003) is applied with k-kl closure parameters (Mellor and Yamada, 1982).

§2-2-5. Boundary conditions

On the open boundaries a radiation condition is applied whose algorithm is described by Marchesiello *et al.* (2001) and Chapman (1987). In particular, a radiation extrapolation for u and v (the current components in the cross-Bay and along-Bay directions), and their vertical averages, is applied for outward propagation to allow the information from the interior solution to pass through the boundary without excessive reflection. The climatological means of tidal elevations and inward propagating u and v and their vertical averages are used as the boundary values at the temporal and spatial points as needed. At the open (east, west and south, Fig. 4) boundaries, salinity and temperature are extrapolated using a zero gradient condition. A closed wall condition is applied for the northern coastal boundary.

§2-2-6. Initial conditions

Initial zeta, current, temperature and salinity are required to numerically solve the developing equations. There are no accurate initial zeta, current, temperature and salinity available. Fortunately, Delaware Bay is small in size and highly sensitive to both dynamical and thermo-dynamical forcing, which permits the initialized zeta, current and temperature to quickly (~2 weeks for Delaware Bay, this value can be years for global models) be adjusted to the current and temperature that can serve as initial current and temperature.

For zeta and current, the model was started 2 weeks before the simulation window with zero-zeta and zero-current conditions.

The initial temperature field contributes directly to the feedback from the sea surface heat fluxes and is quickly adjusted to a state consistent with the applied thermo-dynamical forcing. For example, if the initial temperature is too high, the water column loses more heat via faster exchange of sensible heat, latent heat and longwave radiation at the surface. With this in mind, the initialized temperature field was obtained, first, from a short, two-month run prior to the simulation window. The output temperature was then corrected by using the observed temperature (Versar data for 2000 and Mooring data for 2010, see section 2-3-1 for detail) at all the available stations as shown in Figure 4b and c. The corrected temperature, after vertically averaged to remove any stratification, was used again as the initialized temperature of the model to simulate the whole observed temperature. If any bias exists between the simulated and observed temperature at each of the stations, the bias is used to correct the initial temperature again, with this temperature adjustment repeated until the output temperature is close to the observed temperature. The model was given an additional two weeks to adjust to this initial temperature prior to the simulation window.

In contrast to temperature, salinity applies almost no feedback onto its forcing such as river flow input, evaporation and tidal intrusion. It therefore takes a long time (depending on the salinity field adopted and the applied river flow, two months are about sufficient for our case) for an overly salty or fresh initial salinity field to be adjusted to its proper level. An approximate salinity field (the more observed salinity near the initial time, the better) was used as the initial model salinity, which was then run for two months, driven by the observed forcing. The output salinity was then corrected by using the observed salinity at all the available stations as shown in Figure 4b and c (Versar data for 2000 and Mooring data for 2010, see section 2-3-1 for detail). The corrected salinity was used again as the initialized salinity of the model to repeat the model salinity adjustment until the output salinity is close to the observed salinity. Then the output salinity was vertically averaged to remove the any vertical salinity structure. Finally, the model was given two weeks to adjust this initial salinity prior to the simulation window.

§2-2-7. Simulation performed

A total of sixty-nine years of simulation have been conducted for three primary purposes: for model validation (years 2000 and 2010-2011; see section 2-3), for exploration of inter-annual variations in observed *H. nelsoni* infection prevalence (years 1974-1976, 1979-1981, 1984-1986, 1990-1992, and 2006-2009 for tracer simulation and 2007-2009 for particle transport simulation; sections 3), and for climate sensitivity studies (2000-2002, the reference case, three-year simulations for each of the thirteen future cases, and two-year simulations for each of the three diagnostic cases; section 4). In addition, various sensitivity studies have been carried out to assess the influence of alternate parametric choices (e.g., the number of vertical layers, water types, the SSWR correction, and bottom drag, as explained in section 2-2-2) and operative dynamics including the role of wind forcing (2008 cases with and without wind to investigate the role of wind forcing, section 3-3-2).

§2-3. Model validation

Our objectives include the application of the Delaware Bay model to reproduce, or hindcast, for selected years the physical environment (temperature, salinity, currents, and circulation with associated particle transports) in Delaware Bay and to examine the sensitivity of these physical states to anticipated environmental changes in the future (50-100 years). To achieve these objectives, we must first verify if our model can give accurate simulations of the contemporary evolution of circulation and tracers (temperature and salinity) and their spatial and temporal structure (e.g., stratification/shear, horizontal gradients, and seasonal variation).

§2-3-1. Data availability and validation schemes

Taking into consideration data availability and data quality, we choose two time periods, years 2000 and 2010-11 (see **§2-3-1a** and **§2-3-1b** for details), for model validation. These data and the corresponding simulations permit the validation of our model for temperature and salinity in 2000, for temperature, salinity, and currents in 2010-11, and for vertical and horizontal differences of temperature, salinity, and currents in 2010-11 (along- and cross- Bay current components are obtained by using principal component analysis). These data have higher temporal resolution (10-60 minutes), are observed over two to four seasons, and span a large area in the Bay.

Data and their availability in 2000: For 2000, the observed Versar water temperature and salinity are available, obtained at the nine oyster beds (Fig. 4b) from moorings placed one-meter from the bottom. Data are from the Pre-Construction Oyster and Water Quality Monitoring Study for the Main Channel Deepening Project (prepared by Versar, Inc., http://www.versar.com), provided by Dr. Eric Powell (Haskin Shellfish Research Laboratory, Rutgers University, Port Norris, NJ). The recording interval is 15 minutes for the period of 13 May through 12 November 2000 (Tab. 2). These data span from Section 554 (~39.18^{o}N) to Arnolds (~39.38^{o}N) and cover most of the important oyster beds. The year-2000 water level observations are obtained from the National Water Level Program (NWLP) and the National Water Level Observation Network (NWLON) at http://tidesandcurrents.noaa.gov. There are eleven stations (Fig. 4a) in Delaware Bay where the observed water levels are available from 12 June to 31 December 2000 with a one-hour interval.

Table 2. Availability of 2000-2001 temperature and salinity observed at 1 meter above bottom

Period	Beginning		May12	Jun 15	Jul 11	Jul 27	Aug 10	Aug 25	Sep 22	Oct 23	Mar08
	Ending		Jun 08	Jul 05	Jul 24	Aug 08	Aug 22	Sep 11	Oct 18	Nov 13	Apr12
stations	longitude	latitude	sample size with 15-minute interval								
1,Section554	-75.1903^{o}	39.1838^{o}	2595	1890	1226	1131	1137	1618	2492	2003	3346
2,Egg land	-75.1917^{o}	39.2117^{o}	2595	1890	1226	1131	1137	1618	2492	2003	3346
3,Lower middle	-75.3659^{o}	39.2309^{o}	2595	1890	1226	1131	1137	1618	2492	2003	3346
4,New bed	-75.2483^{o}	39.2483^{o}	2595	1890	1226	1131	1137	1618	2492	2003	3346
5,Bennies	-75.3017^{o}	39.2517^{o}	2595	306	1226	1131	1137	1618	2492	2003	3346
6,Over the bar	-75.3746^{o}	39.2583^{o}	2595	1890	1226	1131	1137	1618	2492	2003	3346
7,Nantuxent	-75.2450^{o}	39.2733^{o}	2595	1890	1226	741	1137	1618	0	2003	3346
8,Ship John	-75.3683^{o}	39.3083^{o}	2595	694	1226	1131	1137	1618	2492	2003	3346
9,Arnolds	-75.4500^{o}	39.3830^{o}	2595	1890	1226	1131	1137	1618	2492	2003	0

Table 3. Availability of salinity (S), temperature (T, °C) and current (U, V, m/s). For U and V, distance = P+Q*i (i=1, N) (m, above bottom) with P,Q and N listed; for S & T, distance=depth (m), with depth listed. For mooring data, recording interval is mostly 10 minutes.

Table3a (data in 2010)	Distance		Begin	End		
	S, T	U, V	S, T, U, V	S	T	U, V
A: -75.5249, 39.6792	12.2	1.15,.5, 19	Jul 15, 00:00	Sep30,01:50	Nov17,23:50	Nov17,23:50
C1: -75.4641,39.3462	1.5	.95, .25, 16		SAA	SAA	SAA
C2: -75.4561, 39.3505	1.5, 5.15	.87, .25, 22		SAA	SAA	SAA
C3: -75.4490,39.3543	1.5, 6.6, 12	(None)		SAA	SAA	(None)
C4: -75.4415,39.3584	SAA	(None)		Sep07,20:30	SAA	(None)
C5: -75.4362,39.3616	1.5, 7.2	.87, .25, 20		Sep30,01:50	SAA	Aug13,12:10
C6: -75.4267, 39.3660	1.5	1.15, .25, 16		SAA	SAA	Nov17,23:50
D:- 75.3293,39.2511	1.5, 14.3	1.5, .5, 21		SAA	SAA	Sep20,08:30

Table3b (data in 2011)	Variable	Distance	Begin	End	Depth	Begin	End
A -75.5249, 39.6792	S, T	1.5, 12.6	Mar 23	Jun 03	1.5, 12.2	Jun 05	Sep 01
	U,V	1.15, .5, 19			1.15, .5, 19		
C7 -75.4540,39.3397	S, T	1.5	Apr 08, 00:00	Jun 26	1.5	Jun 29	Aug 10
	U,V	(None)		(None)	.95, .25, 19		
C8 -75.4488, 39.3431	S, T	1.5,5.1,8.75		Jun 26	1.5, 5.1		Aug 10
	U,V	.87,.25,25			.87, .25, 3		Aug 11
C9 -75.4421, 39.3475	S, T	10.7			10.7		Aug 11
	U,V	.87,.25,32		May 15	.87, .25, 35	Jun 30	
C14 -75.4301,39.3501	S, T	17.1		May 19	16.9		Aug 10
	U,V	1.12,.25,31		Jun 27	1.12,.25,46		Sep 26
C11 -75.4345,39.3525	S, T	11.4		Jun 26	11.5	Jun 29	Aug 10
	U,V	.87,.25,34	Apr 16		.88, .25, 35		
C12 -75.4309, 39.3555	S, T	1.5	Apr 08		1.5, 8.2		Jul 31
	U,V	(None)			1.15, .25, 26		Aug 10
C13 -75.4239, 39.3605	S, T				1.5, 6.8		
	U,V				2.23, .5, 7		
C10 -75.4364, 39.3513	S, T				1, 4, 8.5		
	U,V				(None)		
D -75.3294,39.2511	S, T	1.5, 12.9	Mar 23	Jun 03	1.5 12.9	Aug 01 Jun 04	Sep 16
	U,V	1.5,.5,18		May 07	(None)		

Table3c	Salinity and temperature at along-Bay at depths 1.0+i/4 (m, i=1,40)s				
Time	Sep 12-13, 2010	Dec13-14,2010	Mar 21-22,2011	Jun 03-04,2011	Sep 16-17,2011
Station	S_1-S_{21}, along deep cannel from approximate 38.9 to 40.1°N (see Fig. 3c)				

Data and their availability in 2010-2011: There are mooring data and along-Bay surveys covering the period from July 2010 to September 2011 (Tab. 3 and Fig. 4c), provided by Dr. Robert Chan (Institute of Marine and Coastal Sciences, Rutgers University, New Brunswick, NJ, Delaware Bay Mooring Deployment Project-DBMDP). There are 16 moorings (A, D, and C1-C14) where salinity, temperature, and currents are observed at multiple depths and with intervals as short as 10 minutes. In addition, we have used five surveys carried out along the Bay to observe salinity and temperature at multiple depths on 12-13 September 2010, 13-14 December 2010, 21-22 March 2011, 3-4 June 2011, and 16-17 September 2011 and spanning from 38.86N to 40.07N.

Table 4. Data-application schemes [In season (MAM: Spring, JJA: Summer, SON: Fall) rows, the unit of the number is day. The number of hours is the sample size of the statistics.]

Time series at bottom or at the only observation depth

Mooring		A	C1	C2	C3	C4	C5	C6	C7	C8	C9	C11	C12	C14	D
S,T	MAM	70	0	0	0	0	0	0	54	54	54	54	54	21	70
	JJA	129	48	48	40	48	48	48	69	58	68	69	59	43	81
	SON	75	78	78	78	47	60	78	0	0	0	0	0	0	94
	Hour	6578	3025	3025	2843	2269	2587	3025	2954	2684	2930	2954	2714	1535	5858
U,V	MAM	70	0	0				0		54	33	46		46	45
	JJA	139	48	48				48		65	42	69		87	48
	SON	79	78	78				78		0	0	0		25	19
	Hour	6903	3025	3025				3025		2863	1808	2750		3785	2686

vertical difference between surface and bottom at moorings

S,T	A	C2	C3	C4	C5	C8	D
MAM	70	0	0	0	0	54	70
JJA	91	48	40	48	48	58	33
SON	1	78	78	47	60	0	79
Hour	3878	3025	2843	2269	2587	2684	4351

U,V	A	C1	C2	C6	C8	C9	C11	C14	D
MAM	70	0	0	0	54	33	45	46	45
JJA	139	48	48	48	56	25	69	87	46
SON	79	77	77	77	0	0	0	25	19
Hour	6894	2993	3004	3001	2639	1404	2733	3775	2614

horizontal gradient between moorings

S,T	A-D	C1-C3	C1-C6	C4-C6	C7-C9	C8-C12
MAM	70	0	0	0	54	54
JJA	67	40	48	48	68	48
SON	67	78	78	60	0	0
Hour	4882	2843	3025	2587	2930	2444

U,V	A-D	C1-C2	C1-C6	C2-C5
MAM	45	0	0	0
JJA	48	48	48	30
SON	19	78	78	0
Hour	2686	3025	3025	709

Validation schemes: To objectively validate our simulations with the available data, we use all data that cover at least 2 seasons. All the available data in July of 2011 are used for exploring along- and cross- Bay currents with the time interval being 10 minutes. Surveys on S_1-S_{21} stations of a few times in each season will be concatenated to form one time-space series to have a larger sample size (>1400) and span the Bay. The simulation accuracy in amplitude and phase of temperature, salinity, currents, as well as their vertical and horizontal gradients will evaluated using correlation (COR) and its confidence (%, CON), standard deviation normalized to data (NSTD), root mean square (RMS) and the Warner skill score for evaluation of the amplitude and phase, the centered-pattern RMS for evaluation of the amplitude of anomaly and phase, and bias for comparing amplitudes. Sometimes the bias is small/large but the amplitude is also small/large. In this situation, small/large bias does not indicate a good/poor simulation. Here we provide relative bias (%, rbias), relative to the amplitude of the observation, for comparing amplitudes. The centered-pattern RMS (CRMS) and the Warner skill score (WSK) are described as follows:

• CRMS (Taylor, 2001) is the square root of the mean square difference between the observed and simulated de-mean time series), defined as,

$$CRMS = \frac{1}{N_s} \sum_{n=1}^{Ns} \{[X_{obs}(n) - X_{obsm}] - [X_{\mathrm{mod}}(n) - X_{obsm}]\}^2 \tag{1}$$

• WSK (Warner *et al.* 2005b) is defined as,

$$WSK = \{1 - \frac{\sum_{n=1}^{Ns} |X_{\mathrm{mod}}(n) - X_{obs}(n)|^2}{\sum_{n=1}^{Ns} [|X_{\mathrm{mod}}(n) - X_{obsm}| + |X_{obs}(n) - X_{obsm}|]^2}\} \times 100\% \tag{2}$$

here, X_{mod} or X_{obs} is a time series of simulation or observation, X_{modm} is a temporal mean of X_{mod} , X_{obsm} *is* a temporal mean of X_{obs}. N_s is the number of samples.

We apply an enhanced Taylor diagram to summarize the COR, WSK, NSTD, bias, and CRMS. In the original Taylor diagram (Taylor, 2001; Fig. 7), there are four basic statistical quantities as summarized above: 1) the COR indicated on the azimuthal axis of a Taylor diagram, 2) the NSTD expressed by the radial distance from the origin to the "test" points, 3) the CRMS measured by the distance from the star to a "test" point, and 4) the bias. The WSK is also added. For a perfect simulation, COR=1, CON=100%, NSTD=1, WSK=100%, CRMS =0 (or RMS=0), bias =0, and rbias=0%.

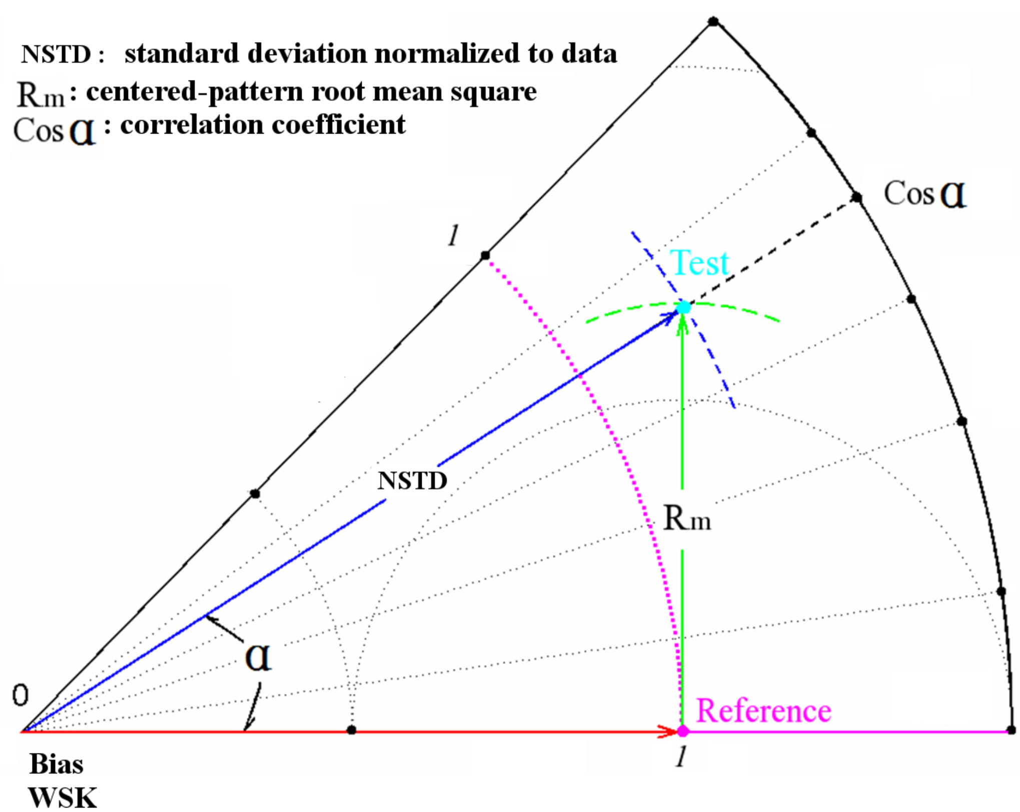

Figure 7. An enhanced Taylor Diagram

§2-3-2. Simulation of salinity, temperature, and currents

The salinity, temperature and current fields exhibit variations on multiple time and space scales. Both the observed and simulated data generally display consistent variations. Temperature is dominated by the seasonal cycle with variation up to 25 ^{o}C, tidal-frequency signals are small (STD = 4.13 ^{o}C, 4.12 ^{o}C, and 0.25 ^{o}C for total, low-pass, and high-pass temperature, respectively). Salinity is dominated by longer-period signals and secondarily by variations at tidal frequencies with variation up to 10 at a given location and changing from zero in the uppermost Bay to 30 near the mouth (STD = 2.9, 2.8, and 0.89 for total, low-pass, and high-pass salinity, respectively). Current speed is dominated by variations at tidal frequencies (STD = 0.22 m/s, 0.07 m/s, and 0.21 m/s and the mean speeds are 0.41 m/s, 0.41 m/s, and -0.0 m/s for total, low-pass, and high-pass current, respectively) (Fig. 8).

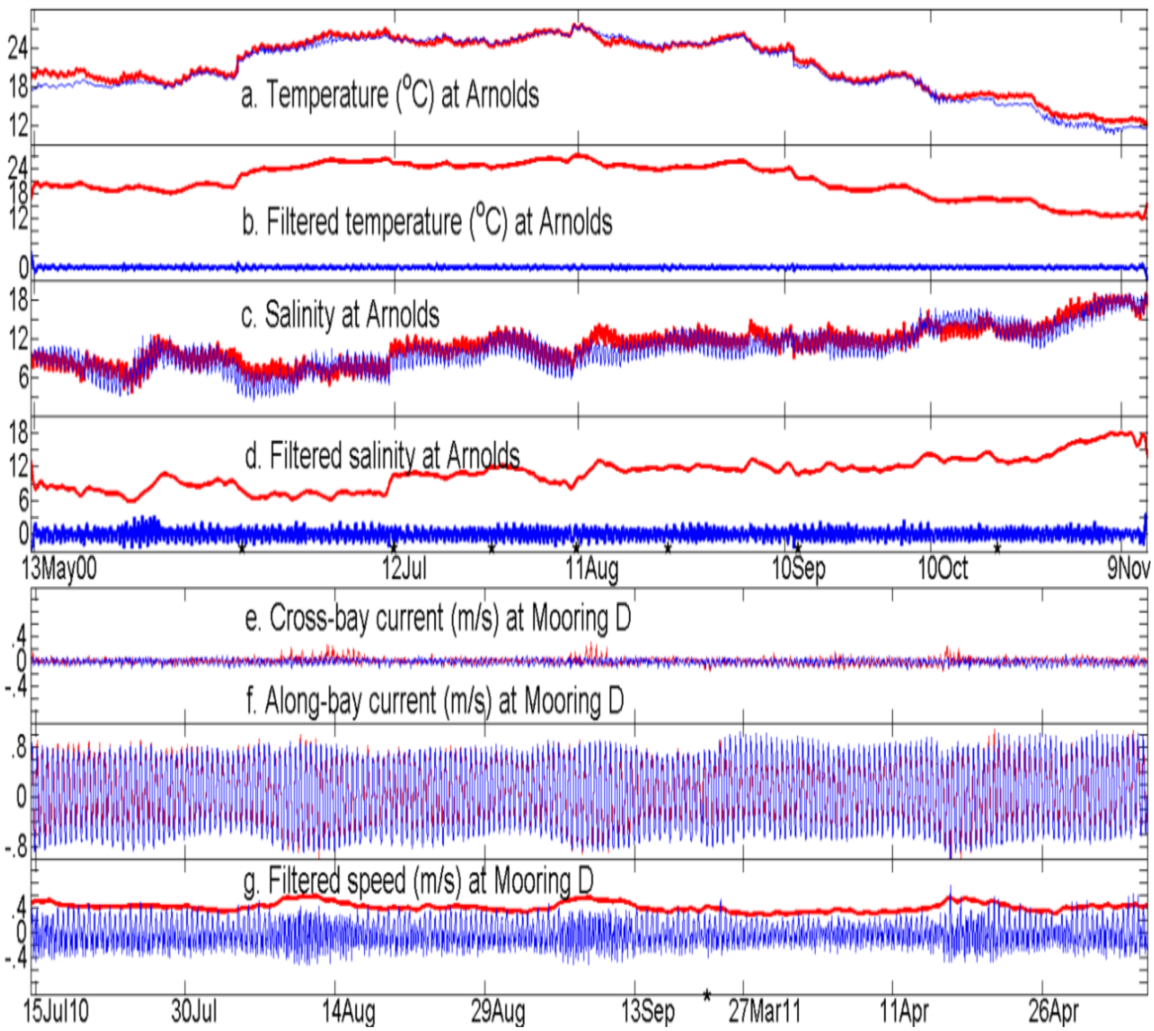

Figure 8. Time series of hourly observed (red lines) and simulated (blue lines) temperature (A), salinity (C) and vertically averaged cross-Bay (E) and along-Bay (F) current as well as their low-passed (red lines) and high-passed (blue lines) observations (B, D and G, respectively). Time windows are cut off at the black stars if no data available. The standard deviations are 4.13, 4.12 and 0.25°C; 2.9, 2.8 and 0.89; 0.22, 0.07 and 0.21m/s for total, low-passed, and high-passed temperature, salinity, and current, respectively. The mean speeds are 0.41, 0.41 and -0.00 m/s for total, low-pass, and high-passed current, respectively. To distinguish between the tidal-frequency signals and those with longer periods, signals of periods shorter than/no shorter than 32 hours are filtered in the low-/high-passed temperature and salinity, and current.

§2-3-2a. Concatenated temporal and spatial variations:

The comparison of observed salinity and temperature from surveys with their corresponding simulations can show the general simulation effect because "concatenated" data series cover five seasons (September 2010, December 2010, March 2011, June 2011, and September 2011) and span the Bay from 38.9 to 40.1°N and from bottom to surface. The seasonality, along-Bay gradient, and vertical profiles of salinity and temperature are well reproduced. For the "concatenated" 105 samples of salinity, COR>0.94 with 100% CON for surface and bottom salinity and the salinity difference between surface and bottom, bias<=0.4 for surface and bottom salinity, bias=-0.089 for the salinity difference between surface and bottom, or rbias=-0.8% (Fig. 9). For bottom salinity, NSTD=0.99, WSK=99.7%, RMS=1.29, and rbias = 1.8%. See Table 5 for more validation quantities.

The changes in the observed and simulated salt fronts track each other consistently. The salt front extends to 39.8°N with a relatively weaker gradient in September 2010, but retreats to about 39.4~39.45°N with a relatively stronger gradient in December of 2010, and March, June, and September of 2011 (Fig. 9a and b). Both observed and simulated salinity differences between the surface and bottom consistently change along the Bay and with survey dates that cover five seasons, and consistently display the salt wedge around 39.1~39.3°N where the fresh river flow in the upper layer from the upper Bay meets the salty inflow in the lower layer from the ocean. A stronger vertical salt gradient occurs near the salt wedge in December of 2010 and in March and September of 2011 when the along-Bay salt gradient is also stronger (Fig. 9c).

Table5. Summarized simulation results for tracers and circulation

(SU is the data concatenated along the Bay on S_1-S_{21} of the five cruises to form 105 salinity and temperature samples. MO is the data on the 16 moorings. VE / HO is the vertical / horizontal differences. Along- and cross- Bay current components are obtained by using principal component analysis.)

	Quantity	COR	NSTD	WSK	RMS	bias	rbias	Amp.	Size
2000									
	Water level (m)	.76~.98	.95~1.41	96~99.8	.12~.53	-.1~.07	-11.9~8.3	.84	4872
	Versar salinity	.70~.91	.82~1.18	78~93	1.25~2.17	-.99~1.11	-10.6~12	9.3	4416
	Versar temperature (^{o}C)	.99~.99	1.03~1.14	99~99.5	.57~.83	-.38~.22	-3.6~2.1	10.4	4416
2010-2011									
SU	Bottom salinity	.994	.99	99.7	1.29	.40	1.8	21.9	105
SU	Bottom temp. (^{o}C)	.969	.97	97.2	2.48	1.79	13.5	13.2	105
MO	Salinity	.73~.96	.6~1.3	81~96	1.1~2.6	-.5~1.1	-3.6~8.0	13.7	1535~6578
MO	Temperature (^{o}C)	.93~.99	.99~1.06	99~99.9	.4~1.3	-.4~.4	-2.7~2.7	14.9	1535~6578
MO	Current (m/s)	.89~.97	.96~1.43	89~98	.14~.25	-.03~.07	-2.3~5.1	1.4	1808~6903
VE	Salinity	.29~.88	.31~1.44	44~86	.36~3.25	-.72~.79	-6.5~7.0	11.3	2269~3878
VE	Temperature (^{o}C)	.54~.85	.96~1.76	40~80	.29~.95	-.36~.23	-12.0~7.7	3.0	2269~3878
VE	Current (m/s)	.65~.87	.64~1.20	73~93	.12~.29	-.06~.10	-5.6~9.3	1.07	1404~6894
HO	Salinity	.44~.82	.90~1.93	60~88	1.20~2.76	-.45~.47	-3.6~3.7	12.6	2269~4882
HO	Temperature (^{o}C)	.28~.87	.61~1.95	47~87	.37~1.26	-.49~.51	-12.6~13	3.9	2269~4882
HO	Current (m/s)	.54~.83	.41~1.33	51~96	.08~.22	-.07~.06	-5.0~4.3	1.39	709~3025
Along- (C9 & A) and across-Bay (C7,C9,C11 & C12) currents at 20 depths in July 2011 (10-min)									
	Across-Bay current (m/s)	.86~.95	1.02~1.36	82~95	.09~.15	-.028~.001	-3.4~.1	.82	4464*20
	Along -Bay current (m/s)	.93~.95	.85~1.12	95~95	.26~.27	-.065~.053	-4.1~3.3	1.60	4464*20

For the concatenated temperature with 105 samples, COR>0.96 with 100% CON and bias<1.8^{o}C (or rbias<13.5%) for surface and bottom temperature (Fig. 10). Near bottom, WSK=97.2%, NSTD=0.97, RMS=2.48 ^{o}C. For temperature difference between surface and bottom, COR=0.83 and bias= -0.26 ^{o}C or rbias=-6.5%. See Table 5 for more validation quantities.

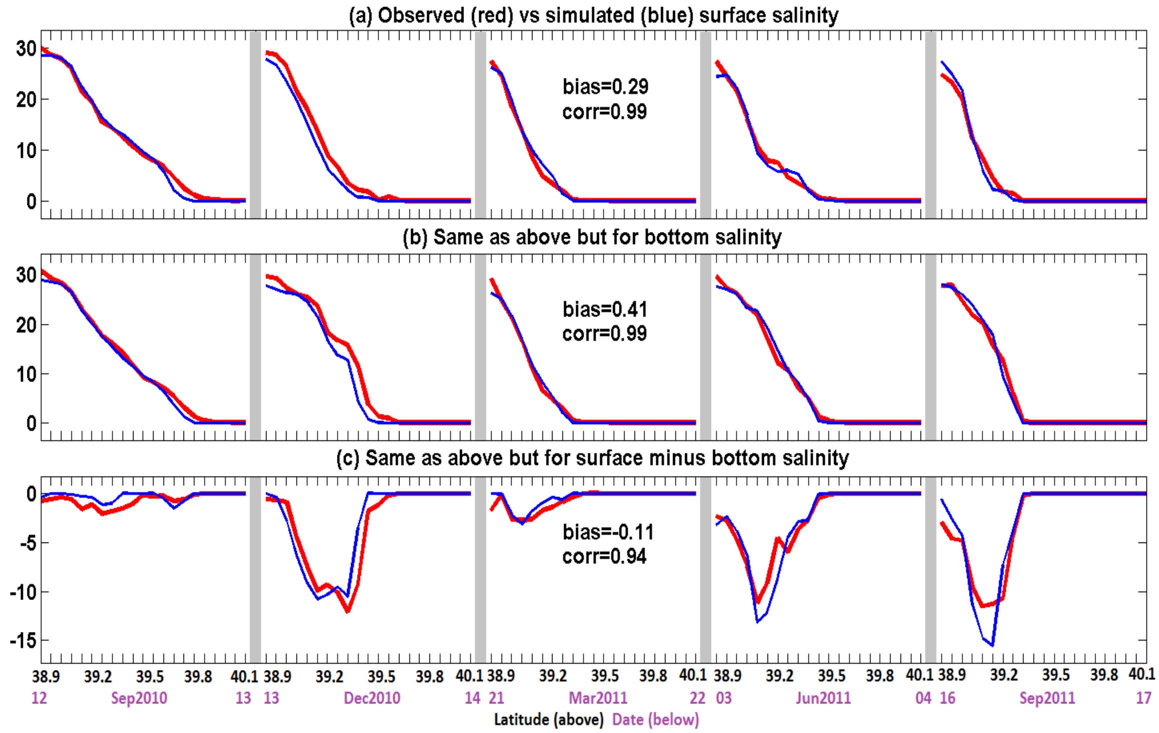

Figure 9. Observed (grey line) and simulated (black line) salinity at surface (a) and bottom (b) and its surface-bottom difference (c). Data cover five seasons from September 2010 to September 2011 from left to right frames and span from low (38.9°N) to up (40.1°N) Bay. In each season, there is one survey lasting a few days (indicated on the last line of the Figure) to observe once salinity on each of the twenty-one locations (latitude range is given on the last but one line). There are 105 salinity samples at each depth for the five surveys on the twenty-one locations. These 105 salinity samples are concatenated to form one "time-space" series for statistical analysis between the observed and simulated salinity. The data are provided by Dr. Bob Chant (see text) .

Although the spatial gradient of temperature in the Bay is very small, both observed and simulated temperatures consistently display weak along-Bay gradients that change seasonally: positive (temperature decrease from low to upper Bay) in December, neutral (temperature gets even along the Bay) in March, and negative (temperature increase from low to upper Bay) in June. A stronger vertical temperature gradient occurs in the lower Bay in June and September of 2011, but is absent in the other three surveys. Simulated temperature is lower than observed near the mouth of the Bay. Our model applies uniform water type 7 for the whole Bay. Water type 7 fits a shallow and turbid water column that restricts the penetration of shortwave radiation to a more shallow depth and allows the ocean to lose more heat through heat exchange between sea surface and the atmosphere. Near the mouth of the Bay, the water gets deeper and less turbid. A spatially dependent water type is suggested here to be developed in the future.

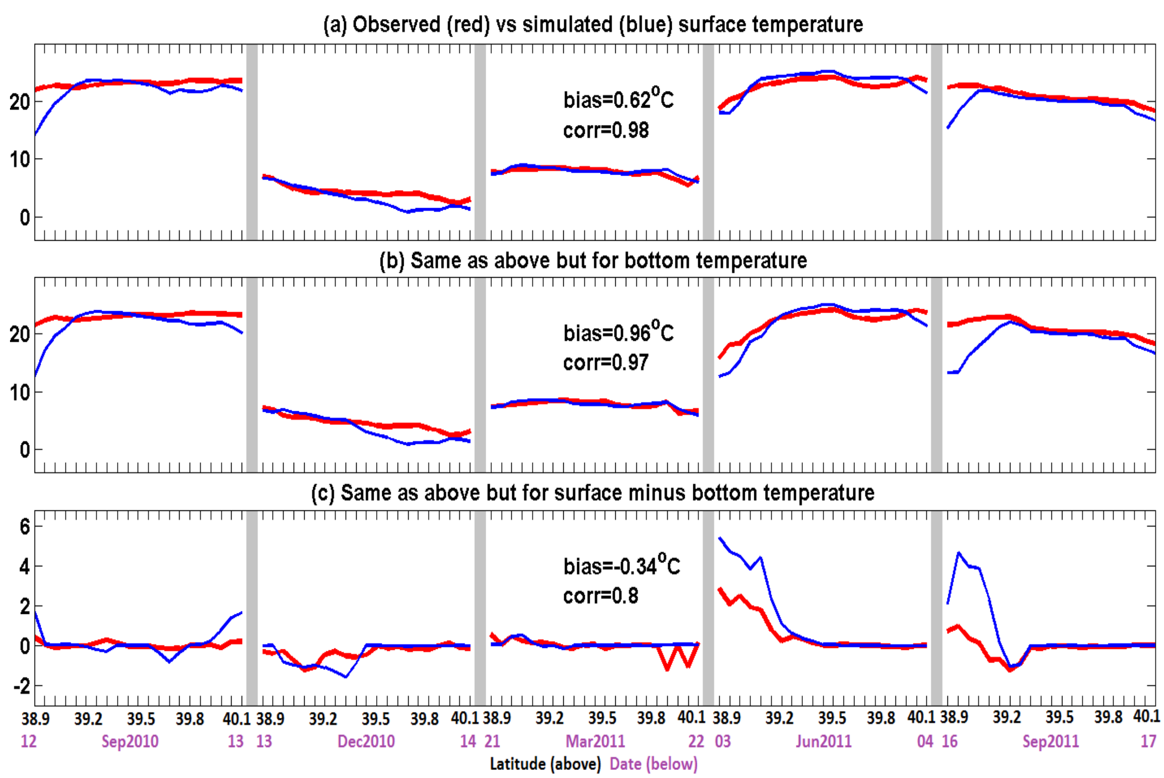

Figure 10. Same as **Figure 9** but for temperature.

§2-3-2b. Time series at different stations and in different periods

Now we compare the observed and simulated salinity, temperature, vertically averaged along-Bay currents, and water level observed at different stations and in different periods as described in Tables 3 and 4. The salinity and temperature are evaluated at the 9 stations whose locations are shown in Figure 3b, with 4416 samples from 13 May to 12 November 2000, and at the fourteen moorings whose locations are shown in Figure 3c, with 1535-6578 samples from July 2010 to September 2011. Water level is evaluated at the 11 stations shown in Figure 3a, with 4872 samples from 12 June to 31 December 2000. The vertically averaged along-Bay current is evaluated at nine moorings (A, D, C1-2, C6, C8-9, C11 and C14) whose locations are shown in Figure 3c with sample sizes 1808-6903 from July 2010 to September 2011. These data cover three seasons and span from 39.2 to 39.68^{o}N.

For salinity (Fig. 11a), COR is higher than 0.7 at all stations, and generally higher than 0.8. NSTD is about 0.6 to 1.3. WSK=75~96%. Bias is from about -0.99 to 1.0 (greatest at the most down-Bay location where the simulated salinities exceed observations by about 1.0, suggesting contamination of the salinity signals from the open boundaries at which no independent salinity information is being supplied). Rbias is -10.6% to 11.9%.

For temperature (Fig. 11b), COR is over 0.99 and NSTD about 1.03~1.1, WSK 99~100%, except for surface temperature at mooring 12 where COR=0.92, WSK=92%, NSTD=1.2. Bias is less than a half ^{o}C (-0.4 to 0.4), or rbias=-3.6~3.6%. See Table 5 for more validation quantities.

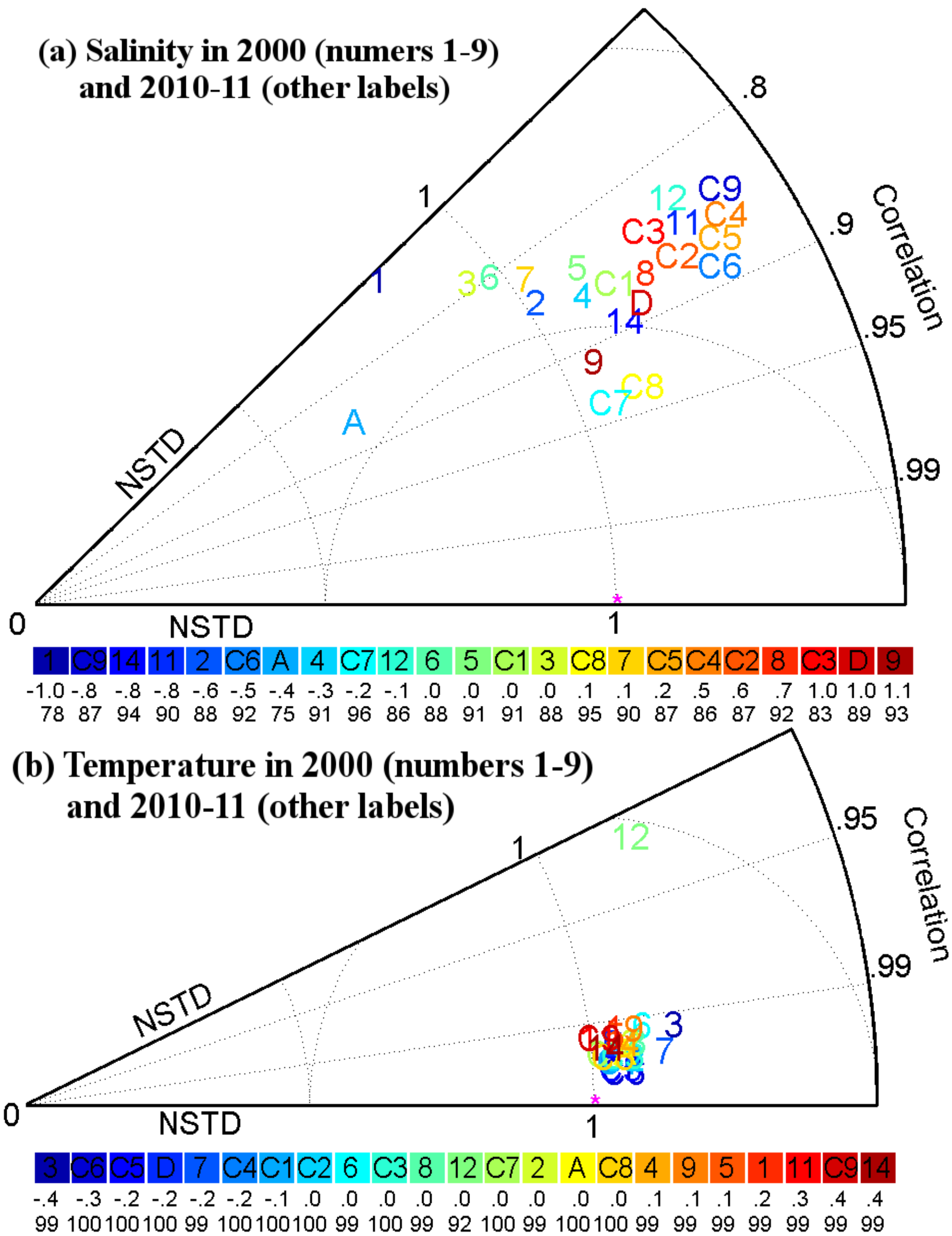

Figure 11. Taylor diagram showing model-data comparisons for (a) salinity and (b) temperature. Warner skill (%) is shown with the numbers on the last line. The salinity and temperature compared here are observed at the 9 stations (number 1-9, black color) whose locations are shown in Figure 4b, based on 4416 hourly data from 13 May to 12 November 2000, and at the fourteen moorings (near surface at A, D, C1-C8, and C12; but near bottom at C9, C11 and C14, number 11, 12 and 14 indicate C11, C12 and C14 respectively, grey color, letter "C" is omitted) whose locations are shown in Figure 3c, based on 1535-6578 data from July 2010 to September 2011.

For water level (Fig. 12a), COR=0.76~0.98 with CON=100%, NSTD=0.95~1.41, WSK= 96~99.8%, bias=-0.1~0.07 meter, and rbias=-11.9~8.3%. Tidal excursion, as measured by normalized standard deviation of the simulated water level, is well predicted in the lower Bay, but higher than observed by approximately 30-45% in the upper Bay.

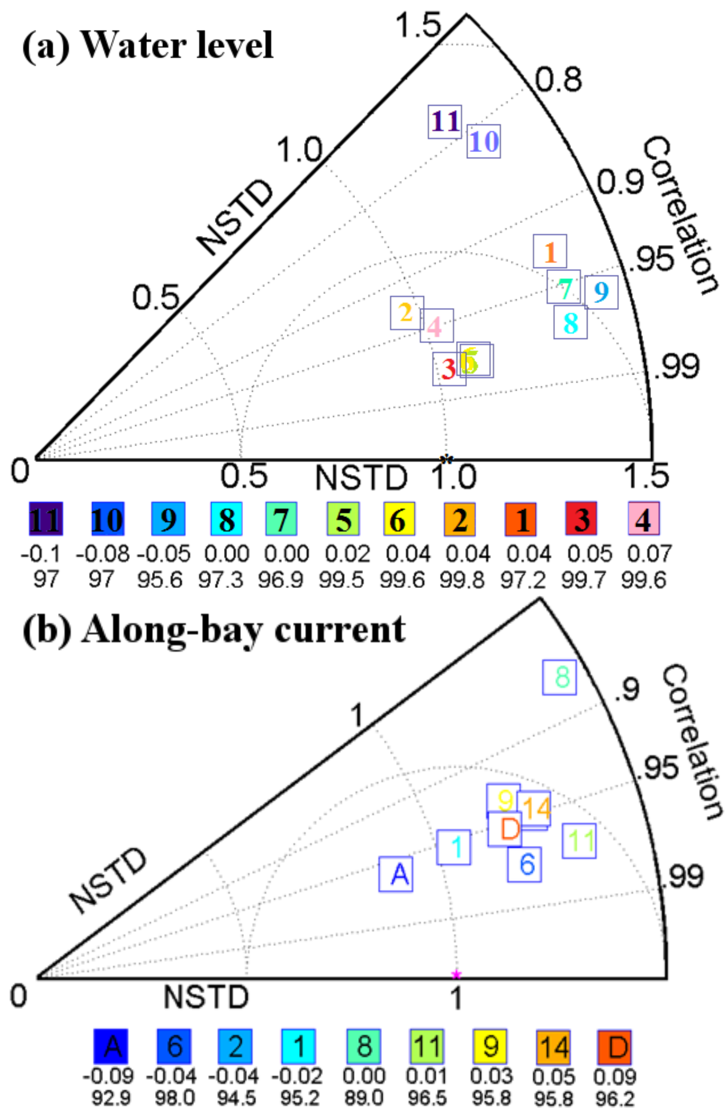

Figure 12. Taylor diagram for (a) water level (m) at the 11 stations shown in Figure 4a, computed from hourly data 12 Jun-31 Dec 2000 and (b) vertically averaged along-Bay current at nine moorings (A, D, C1-2, C6, C8-9, C11 and C14, Fig. 3c) with sample sizes 1808-6903 from July 2010 to September 2011.

For vertically averaged along-Bay current that dominates the total vertically averaged current (Figs.8 and 12b), COR=0.89~0.97 with CON=100%, NSTD=0.96~1.43, WSK=89~98%, bias= -0.03~0.07 m/s, and rbias=-2.3~5.1%. See Table 5 for more validation quantities.

§2-3-2c. Vertical structure

Here we use the differences between surface and bottom salinity, temperature, and current to indicate the stratification of salinity and temperature and the current shear. Seven moorings are available for the stratification of salinity (Fig. 13a) and temperature (Fig. 13b), with sample sizes 2269-3878, and nine moorings are available for current shear (Fig. 13c), with sample sizes 1404-6894 (mostly larger than 2000). These data cover three seasons from July 2010 to September 2011 (no data in winter, Tabs.3 and 4) and are located from about 39.2^{o}N to about 39.68^{o}N (Fig. 4c).

For salinity stratification, COR=0.29~0.88 with CON = 100%, NSTD = 0.31~1.44, WSK = 44~86%, bias = -0.72~0.79, and rbias = -6.5~7.0%; for temperature stratification, COR = 0.54~0.85 with CON = 100%, NSTD = 0.96~1.76, WSK = 40~80%, bias = -0.36~0.23, and rbias = -12.0~7.7%; for current shear, COR = 0.65~0.87 with CON = 100%, NSTD = 0.64~1.2, WSK = 73~93%, bias = -0.36~0.23, and rbias = -12.0~7.7% (see Table 5).

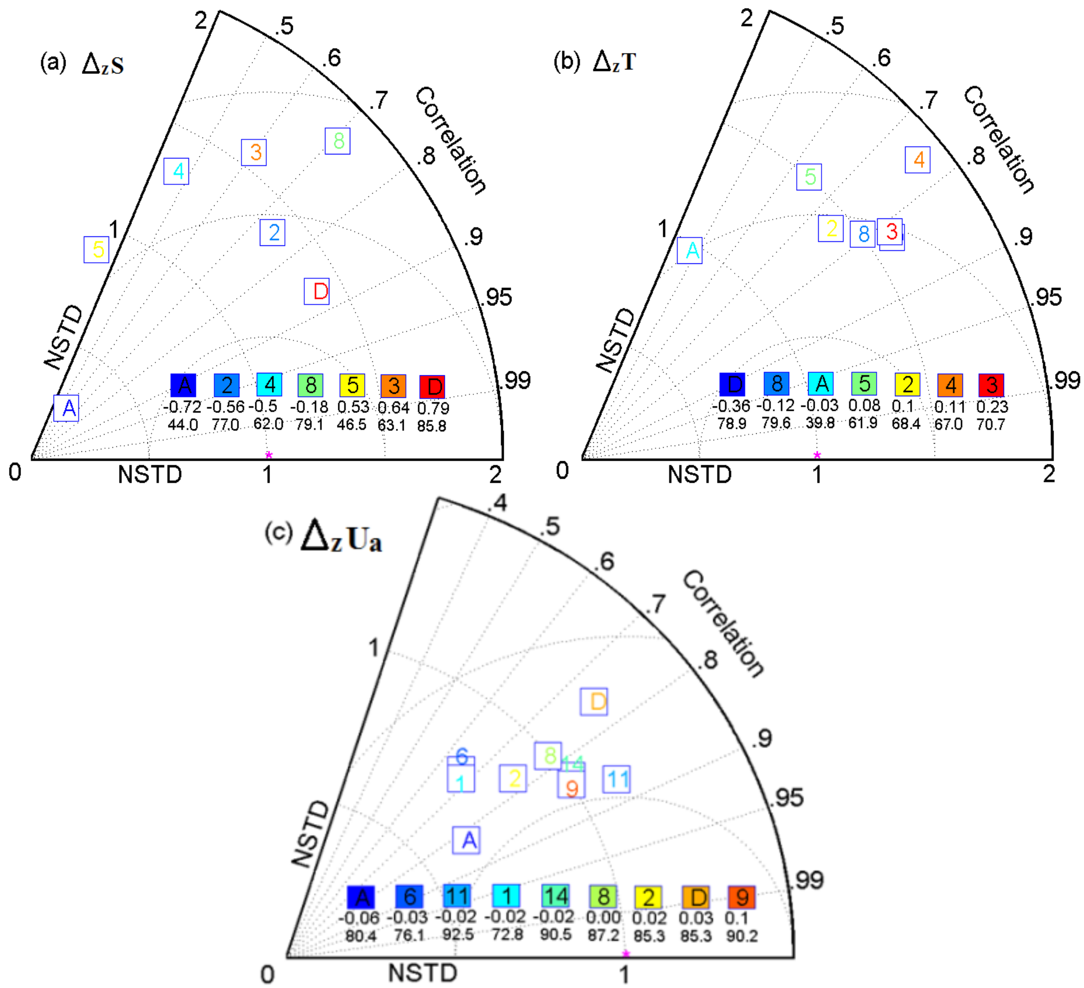

Figure 13. Taylor diagrams for the vertical differences of (a) salinity, (b) temperature, and (c) along-Bay current at nine moorings (Fig. 4c). These data (2269-3878 salinity and temperature and 1404-6894 current samples) cover three seasons from July 2010 to September 2011 (Tabs. 3 and 4).

Checking vertical shear of the along-Bay current with 10-minute interval data for one month (July 2011) at moorings A and C9, the simulated vertical structure basically follows the observations, but with stronger simulated current especially during low tide when the current goes toward the lower Bay with an amplitude bigger than 0.5 m/s at mooring C9 (Fig. 14).

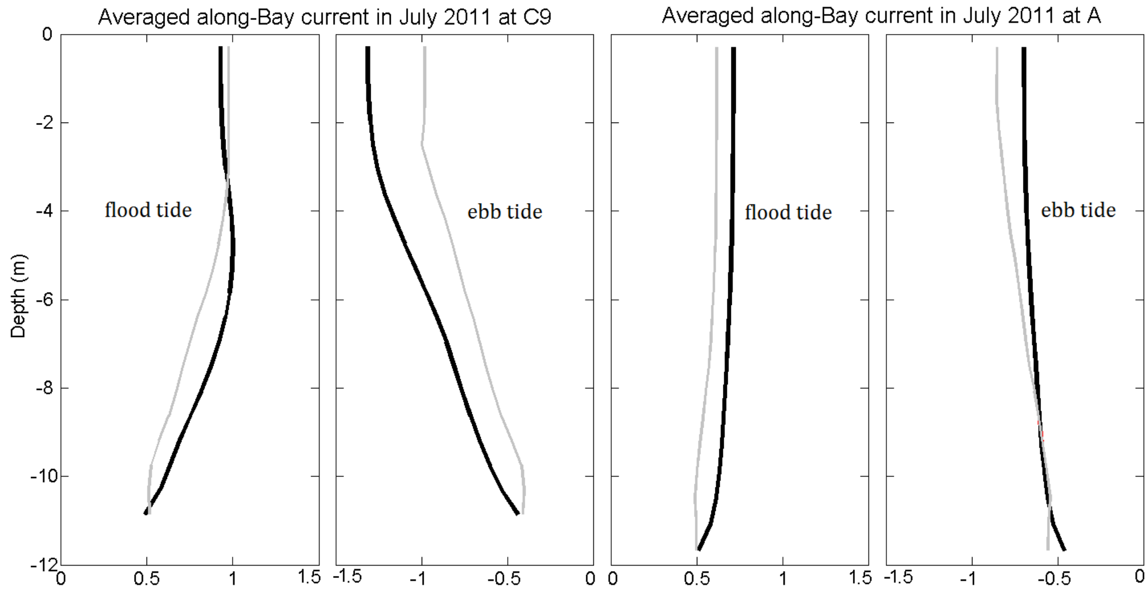

Figure 14. Vertical profile of observed (black) and simulated (grey) along-Bay current average during high / low tide (current goes toward the upper / lower Bay with amplitude bigger than 0.5 m/s), based upon 10-minute data in July 2011 at mooring A and C9.

§2-3-2d. Horizontal structure

The available data permit us to compare the observed and simulated horizontal differences of salinity (Fig. 15a) and temperature (Fig. 15b) at six pairs of moorings with sample sizes 2269-4882 and the horizontal differences of the along-Bay current (Fig. 15c) at four pairs of moorings with sample sizes 709-3025. These data cover three seasons from July 2010 to September 2011 (no data in winter, see Fig. 4c and Tabs. 3 and 4). The horizontal differences of the data are very small in size because of the relatively small distances between the pairs of moorings. For the horizontal difference of salinity, COR=0.44~0.82 with CON = 100%, NSTD = 0.90~1.93, WSK = 60~88%, bias = -0.45~0.47, and rbias = -3.6~3.7%; for the horizontal difference of temperature, COR =

0.28~0.87 with CON = 100%, NSTD = 0.61~1.95, WSK = 47~87%, bias = -0.49~0.51, and rbias = -12.6~13.1%; for the horizontal difference current, COR = 0.54~0.83 with CON = 100%, NSTD = 0.41~1.33, WSK = 51~96%, bias = -0.07~0.06, and rbias = -5.0~4.3% (see Table 5).

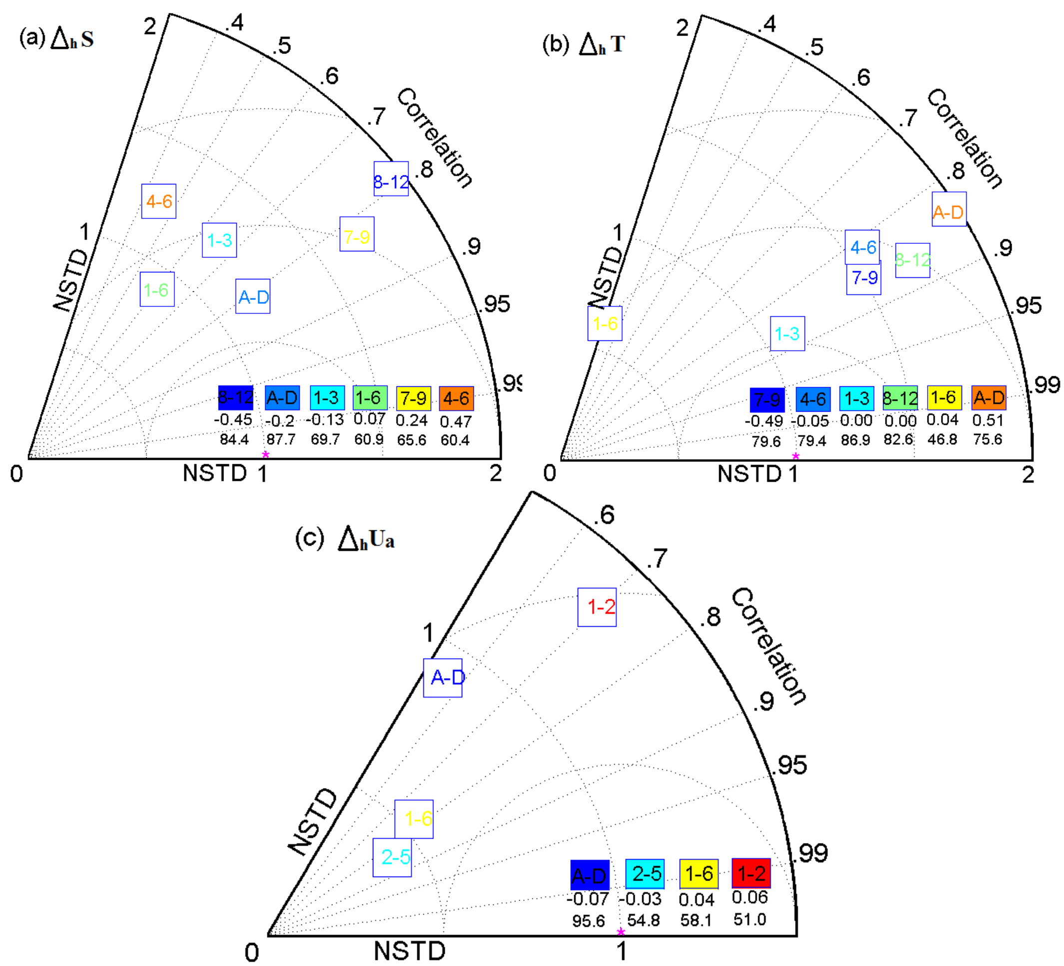

Figure 15. Taylor diagrams for the horizontal differences of (a) salinity and (b) temperature at the six pairs of moorings with sample sizes 2444-4882 and (c) for the horizontal difference of vertically averaged along-Bay current at the four pairs of moorings with sample sizes 709-3025. These data cover three seasons from July 2010 to September 2011 (no data in winter), their detailed locations, temporal coverage, and sample sizes are described in Figure 4c and Tables 3 and 4. The data are provided by Dr. Bob Chant.

§2-3-3. Summary

The Delaware Bay model accurately reproduces temperature, salinity and currents. The simulated properties are accurate to within 1^{o}C in temperature and 1 in salinity, which would be a reasonable tolerance for, e.g., successful reproduction of larval growth and behavior according to the larval individual-based modeling (Narvaez *et al.*, 2012). Multiple statistical evaluations show high simulation scores with small systematic biases, proper standard deviations, accurate amplitudes and phases, etc., as described above and listed in Table 5. All the scores for the horizontal and vertical differences of salinity, temperature and current are lower than those for salinity, temperature and current themselves because all these differences are the secondary quantities in the small Bay. Although their simulations are basically consistent with data in signs and amplitudes, even a small difference in phases will reduce the scores significantly.

The validated model is next applied in two ways. The first is the simulation of the temporal variability of salinity and temperature, and exploration of their relationship to the observed time series of MSXP (Chapter 3). The second is the simulation of potential climate-related changes in temperature, salinity and current (Chapter 4).

§3. Variability in water properties, circulation and MSX

It has been suggested in prior studies (Andrews, 1964; Haskin and Ford, 1982) that MSXP is highly correlated with fluctuations in salinity, and therefore with fresh water inflow. Rather than a single determining factor, we hypothesize that MSXP in the upper Bay locations is related to the co-occurrence of three factors. These are: the availability of high infection prevalence at down-Bay locations *(i.e.,* a source region), a transport mechanism from lower- to upper-Bay locations, and lastly environmental conditions (*i.e.,* temperature and salinity) conducive to *MSX* survival and ability to proliferate in oysters.

Here, we investigate several specific questions related to the observed inter-annual variations in MSXP. How much variability in MSXP can be accounted for purely on the basis of salinity variations, temperature, or both? Is there any evidence for the hypothesized role of upper Bay passive transport? And finally, is there any evidence for limitation due to the absence of a down-Bay source?

To investigate these questions, we have carried out simulations over five multi-year periods (1974-76, 1979-81, 1984-86, 1990-92, and 2006-09) to explore the relationships between environmental conditions and MSXP. During these five periods, the overall properties are: 1974-76 (average/above average river flow, low upper Bay MSXP), 1979-81 (average river flow, low upper Bay MSXP), 1984-86 (average river flow, high upper Bay MSXP [especially 1985-86]), 1990-92 (average river flow, high upper Bay MSXP [especially 1992]), and 2006-09 (average/above average river flow, elevated upper Bay MSXP in 2008). The conditions during each of these periods are described in more detail in section 3-1.

Using model outputs for the tracer and circulation fields, we have applied statistical analysis to explore the relationships among the variations in MSXP and physical conditions in Delaware Bay. To check the combined role of both salinity and temperature, we have also developed a new index, the "salty-warm water area" (SWA), which is defined as the area of the bottom water whose salinity is higher than 17.5 and whose temperature is higher than 12.5^{o}C. These values represent conservative estimates of the lower thresholds for *MSX* proliferation in oysters (Ford and Haskin, 1982; Haskin and Ford, 1982). The results of this statistical analysis are described in section 3-2.

Lastly, particle transports are inferred for the contemporary period 2007-2009 (section 3-2). There are three occurrences of enhanced MSXP at Arnolds in 1985, 1992 and 2008. As will be shown below, particle transport in these simulations is primarily due to the combined effects of riverine and tidal forcing, with wind forcing of secondary importance, although the mean wind is stronger in spring 2008 and varies much in fall 2007-09 (Fig. 16).

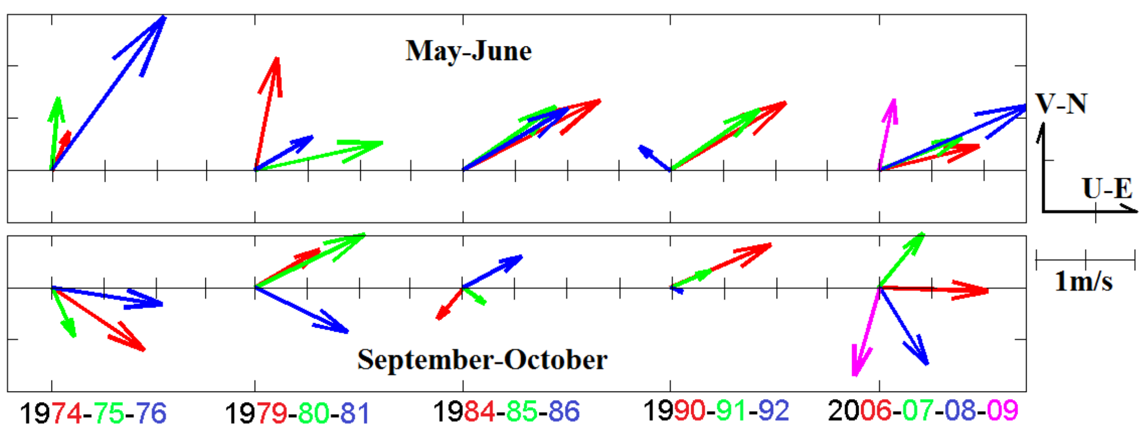

Figure 16. Mean wind vectors in May-June (above) and September-October (below) of the five multi-year periods 1974-76, 1979-81, 1984-86, 1990-92, and 2006-09, based on 6-hourly surface wind in 1974-1976 from the ERA-40 data of European Centre for Medium-Range Weather Forecasting (ECMWF) and 3-hourly surface wind in the other years from the North American Regional Reanalysis (NARR, Mesinger, *et al.*, 2006). Their links are: http://nomads.ncdc.noaa.gov and http://data-portal.ecmwf.int, respectively. Wind data locations are shown in Figure 4a.

§3-1. Variability in MSXP and the physical environment

MSXP displays significant temporal (seasonal and inter-annual) and spatial variability over a 52-year period (1958-2009, Fig. 3). It is higher in the lower Bay, but lower in the upper Bay, making transport from lower to upper Bay an important issue. In the upper Bay, it is higher in the 1960s, 1980s, and 1990s, but lower in the 1970s and 2000s. In the lower Bay, it is persistently higher except in the falls of 1990s and 2000s. MSXP is higher in fall than in spring. Figure 17 displays time series for the five multi-year periods (16 years in total) of the following physical properties: the observed total fresh water inflow of the six river inputs, and the simulated bottom temperature averaged within the Bay and salinity averaged around the beds in the upper, middle and lower Bay as well as their anomalies. Anomalies for temperature and SWA are obtained by removal of a 16-year mean seasonal cycle; anomalies for salinity and river flow are formed by removal of a 16-year mean value (i.e., by removal of a constant from the time series at a given location). Considerable seasonal and inter-annual variation in the physical environment is evident. A brief summary of the inter-annual variations is as follows:

1974-76: MSXP is elevated in the lower Bay but reduced in the upper Bay. River input is the second highest among the five multi-year periods (63 m^3/s above the sixteen-year mean of 463 m^3/s). Salinity is slightly below the 16-year average by -0.5 and -0.3 at up and middle Bay, respectively, but average in the lower Bay. The three-year-mean temperature is close to the sixteen-year mean (-0.2^oC). Salinity and temperature are mostly out of phase. SWA is below average (the sixteen-year mean of

773 km^2) by 13.2 km^2. The warmer 1975 is accompanied by fresher spring and early summer.

1979-81: MSXP is elevated in the lower and middle Bay but reduced in the upper Bay. River flow is the second lowest (63 m^3/s below the sixteen-year mean) for an extended period from May 1980 to January 1981 and from August to October of 1981. Mean conditions in 1979-81 are both the saltiest (upper Bay, +1.5; middle Bay, +1.3; lower Bay, +0.8) and coolest (-1.2 ^oC) of our five time windows. SWA is the smallest of any of the multi-year periods (-43.3 km^2). The saltier 1980-81 is accompanied with colder phases.

1984-86: MSXP is elevated in the lower, middle, and upper Bay. River input in this three-year period is below the 16-year mean by 26 m^3/s. Both salinity and temperature are "spot on" the 16-year mean values, with temperature a bit higher than the mean (+0.3 ^oC). SWA is the second largest (+12.1 km^2). Although the three-year means are near the sixteen-year average, there is an extended period of above-average temperature and salinity from approximately July 1984 to October 1985 corresponding to a period of reduced river inflow. This period of both warmer and saltier conditions was not broken by a significantly cold or fresh condition as they were in the other four multi-year periods, making SWA persistently higher than average with a largest yearly averaged SWA (+ 111 km^2) in 1985.

1990-92: MSXP is the highest in the upper Bay in 1991-92. The river flow input is the lowest (115 m^3/s below the sixteen-year mean). Saltier condition presents in the upper (+0.9), middle (+0.7), and lower (+0.4) Bay. An extended saltier period from early 1991 to early 1992 in the upper Bay is accompanied by a persistently warmer 1991 and above-normal SWA. The significantly colder year 1992 makes the three-year average temperature and SWA (-12.5 km^2) below the sixteen-year mean.

2006-09**:** MSXP is elevated in the upper Bay in fall 2008 to spring 2009 but is the lowest elsewhere. This is the warmest (+1.0 ^oC) but freshest (-0.5~-1.0 below the sixteen-year mean in salinity) period with largest river flow input (73 m^3/s above the sixteen-year mean). The averaged SWA is enhanced above the long-term mean (+42.7 km^2); however, there is no extended period that is longer than 8 months and has both saltier and warmer conditions.

The previous study (Wang *et al.*, 2012) computed the SWA within a larger water area that included some neighbored open ocean. Therefore the previous sixteen-year mean SWA (839 km^2) was larger than the current sixteen-year mean SWA (773 km^2) computed within the major Bay from its mouth to 39.77^{o}N, corresponding to a larger variation: -26.5 km^2 in 1974-76, -72 km^2 in 1979-81, +29.1 km^2 in 1984-86, -10.7 km^2 in 1990-92, and +59.9 km^2 in 2006-2009. However, the variation of SWA in the major Bay, though smaller, does not change the SWA-MSXP correlation compared to the previous SWA-MSXP correlation, implying SWA change in middle-upper Bay matters to MSX because the upper-Bay extending distance of salty-warm water is more sensitive to SWA in the narrower middle-upper Bay where the oyster beds are located.

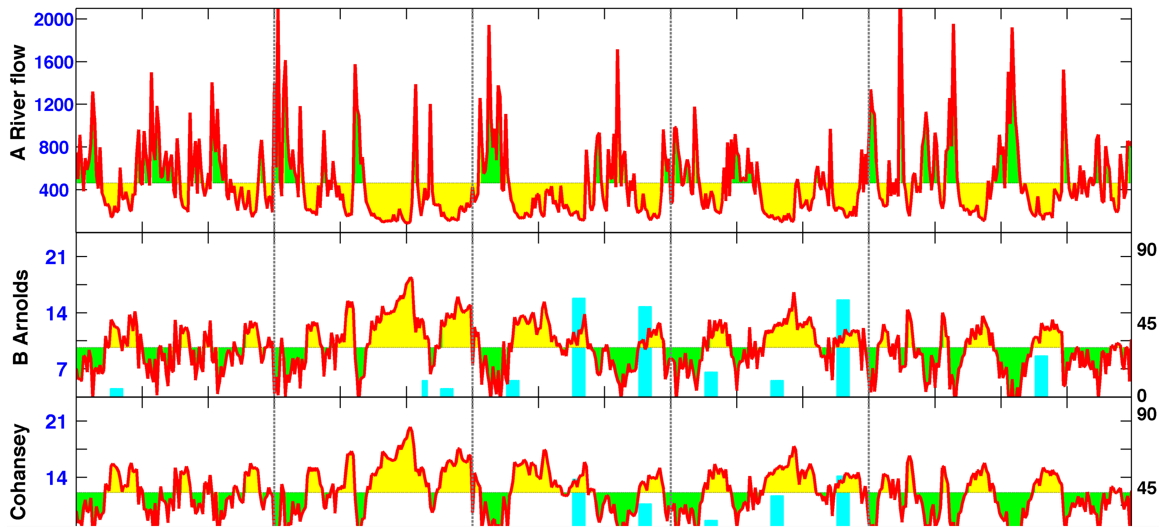

Figure 17. MSXP and ten-day-averaged factors. (**A**) River flow (m^3/s, from USGS). (**B-D**) MSXP (narrow/wide bars in Dec-May/Jun-Nov, right scales,%) and simulated bottom salinity at Arnolds, Cohansey and Egg Island, respectively (bed locations are given in Fig. 16). (**E**) Simulated bottom temperature (^oC, blue line) and its anomaly (red line, 98% correlated with sea surface air temperature plotted with pink line, from the North American Regional Reanalysis). (**F**) SWA anomaly (km^2, each arrow points a phase where SWA-anomaly is continuously below 50 km^2 for 40 days). The anomalies are relative to the means within the sixteen years with seasonality deducted only for the bottom temperature and SWA. During shaded periods the anomaly is positive/negative continuously for over twenty days.

§3-2. Correlation analysis

To examine the quantitative relationships between MSXP and accompanying environmental conditions, we have performed a systematic correlation analysis, seeking significant correlations between factors including: fall (June-November), spring (December-May) and yearly MSXP; monthly, seasonal (DJF, MAM, JJA, and SON), and yearly river discharge and simulated salinity and temperature. Correlations of total river flow integrated from the six rivers whose locations are shown in Figure 4b with MSXP are based upon seasonal observations in 1958-2009, with the sample size being 52. The simulated salinity, temperature and SWA in 1974-76, 1979-81, 1984-86, 1990-92, and 2006-09 are used to correlate with each other and with river discharge and MSXP with the sample size being 12 in spring and 16 in fall. (Spring samples of MSXP are not available for the 2006-2009 period.). The data availability of MSXP and the rationale for selection of model simulation periods dictate our data sample sizes. For a correlation between two time series x and y with same sample size N, the confidence interval is examined by using the correlation coefficients and the effective degrees of freedom (N*, Emery and Thomson, 2004) computed by the formula given by Chelton (1983), as below,

$$N^* = NC_{xx}(0)C_{yy}(0)/\sum_{\tau=-P}^{\tau=p}[\,C_{xx}(\tau)C_{yy}(\tau) + C_{xy}(\tau)C_{yx}(\tau)] \qquad (3)$$

where, the auto-covariance function of z (z=x or y) and the cross-covariances between x and y are expressed, respectively, as below,

$$C_{zz}(\tau) = (N_2 - N_1 + 1)^{-1}\sum_{i=N_1}^{i=N_2}(\,z_i - \bar{z})(z_{\tau+i} - \bar{z}) \qquad (4)$$

$$C_{xy}(\tau) = (N_2 - N_1 + 1)^{-1} \sum_{i=N_1}^{i=N_2} (x_i - \bar{x})(y_{\tau+i} - \bar{y}) \quad (5)$$

$$C_{yx}(\tau) = (N_2 - N_1 + 1)^{-1} \sum_{i=N_1}^{i=N_2} (y_i - \bar{y})(x_{\tau+i} - \bar{x}) \quad (6)$$

For the finite sample size N, $p = (N-1)/2$ if N is odd number, $p = N/2 - 1$, if N is even number. τ is the lag time. If $\tau \geq 0, N_1 = 1$, $N_2 = N - \tau$; if $\tau < 0, N_1 = 1 - \tau$, $N_2 = N$. $A_i = A(t_i)$, the value of A at time t_i, $\bar{A}$ is the mean of A ($A = x, y,$ or, z).

The true skill (Emery and Thomson, 2004; Davis, 1976 and 1978) defined as the fraction of the true parameter variance explained by linear statistical estimator is, as below,

$$S_{ed} = corr^2 - 1/N^* \quad (7)$$

where, *corr* is the correlation coefficient between series x and y, $1/N^*$ is the artificial skill decided by the effective degrees of freedom.

§3-2-1. **Correlations among physical properties** (Tab. 6a)

The seasonal signals have been removed from the bottom temperature and SWA that are dominated by seasonal cycles. River flow is stronger in spring than in fall. Salinity and temperature are lower (do not always favor MSX) in spring than in fall. Salinity has bigger variation in spring in the upper Bay than in fall in the lower Bay.

As expected, river flow and simulated salinity are highly negatively correlated at all locations (up to -0.87, higher in the upper Bay or in spring). Water temperature of the shallow Delaware Bay represents the air temperature (bottom temperature and surface air temperature are 98% correlated, Fig. 17E). A positive yearly correlation exists between river flow and bottom temperature (up to 43% correlated). In February and November when the annual air temperature variation is the largest, the correlation becomes statistically significant (up to 68% correlated). The river flow-temperature correlation presumably indicates a positive relationship between temperature and winter/spring snow melt and precipitation. The negative river flow/salinity and positive river flow/temperature correlations are consistent with a negative temperature/salinity correlation (up to 71% correlated). Therefore, temperature plays a complicated role in influencing MSXP by negatively influencing salinity, although elevated temperatures, by themselves, are generally conducive to MSXP for the prevailing spring and summer temperature ranges in Delaware Bay (Ford and Haskin, 1982).

§3-2-2. Correlations between MSXP and physical properties (Tab. 6b)

Salinity is positively correlated with MSXP, significantly (up to 71% correlated) in spring in the upper Bay where salinity is not always salty enough to favor MSX and undergoes large variations. River flow is negatively correlated with MSXP (up to -52% correlated) since river flow changes salinity with a significant negative correlation (up to -87% correlated).

In spring, temperature by itself correlates with MSXP negatively (up to -64%) in the upper-most Bay but positively (up to 60%) elsewhere. Only in the lower Bay has the negative correlation between the fall MSXP and prior spring temperature. As mentioned above, temperature presents a complicated role in influencing MSX by negatively influencing salinity.

SWA helps to better understand the complicated role of temperature in MSX since it reflects the combined effects of temperature and salinity. SWA is highly correlated with MSXP in Cohansey (0.91), New-Bennies (0.92) and Egg Island (0.63), showing that MSX prefers warmer and saltier water. The elevated correlation with SWA at mid-Bay locations is due to the fact that variations in salinity about the value 17.5 are greatest at mid-Bay. The SWA metric has essentially zero explanatory power at upper-Bay sites such as Arnolds because salinity values rarely, if ever, exceed 17.5 at these locations. Likewise, the SWA metric is reduced at the most down-Bay locations such as Leased Grounds where the water is always salty enough for proliferation.

The co-occurrence of warmer temperatures with more saline conditions is relatively rare since salinity and temperature are mostly out of phase. Higher temperatures tend to bring more river flow via snow-ice melt and precipitation and therefore reduces salinity as, e.g., in 1974-1976 and 1993-2009. This pattern of physical conditions is beneficial to the Bay in controlling MSX.

However, when the Bay gets both warmer and saltier with large SWA, as it did in 1984-1986, the environment is especially conducive to elevated MSXP. A warming climate together with less river flow input due to, e.g., less precipitation and snow-ice melt, would lead to elevated MSXP.

MSX resistance of oysters after the late 1990s (Ford *et al.*, 2012) does not change the correlation analysis below (Tab. 6). Without the contribution from the covariance between river flow and MSXP after the late 1990s, the correlation between the 52-year river flow and fall MSXP increases a little bit, e.g., from -0.29 to -0.33, -0.39 to -0.42, from -0.29 to -0.30 at Arnolds, Cohansey, New-Bennies, respectively. However, the reduced MSXP and intensified river flow coincide with the intensified warming period 1993-2009 with MSXP and river flow being approximately -33.7, -43.9, and -38.8% correlated with confidence 81, 92, and 88% at Arnolds, Cohansey, New-Bennies, respectively. The intensified warming climate might partially constrain MSX infection via intensified river flow input.

Table 6. Correlations (a) among water properties and (b) between MSXP and water properties. The bold black, grey-shade black, and italic grey numbers and correlation coefficients with confidence≥95%, 90~95%, and <90%, respectively, based on confidence-intervals examineination using the correlation coefficients and effective degrees of freedom (numbers following the correlation coefficients, Emery and Thomson, 2004) computed by the formula given by Chelton (1983). MSXP is defined as 100×number of infected oysters / number of oysters sampled, assessed using tissue-section histology for 1974-76, 1979-81, 1984-86 and 1990-92 and using both histology and polymerase chain reaction for 2006-09 (Ford *et al.*, 2012). Correlations between river flow and MSXP are for 1958-09 yearly observations, others for 1974-76, 1979-81, 1984-86, 1990-92 and 2006-09. Seasonal signals have been removed from temperature and SWA. Bottom salinity is averaged within two-by-two kilometer square around the beds whose locations are given in Figure 18.

a, Water properties **Beds**	River flow - Salinity			River flow-Temperature			Salinity - Temperature		
	yearly	Spring	Fall	yearly	Feb	Nov	yearly	DJF	Spring
Arnolds	**-0.86**,6	**-0.86**,8	**-0.87**,6	*0.41*	**0.58**,13	0.43,14	-0.58,9	**-0.68**,8	**-0.60**,9
Cohansey	**-0.86**,6	**-0.86**,8	**-0.86**,6	*0.43*	**0.65**,11	**0.53**,13	-0.60,9	**-0.68**,9	**-0.61**,10
New bed+Bennies	**-0.81**,6	**-0.83**,8	**-0.80**,7	*0.36*	**0.59**,13	0.50,14	-0.58,8	**-0.71**,8	**-0.64**,9
Egg Island	**-0.77**,7	**-0.81**,8	**-0.73**,8	*0.39*	**0.63**,12	**0.53**,13	-0.59,8	**-0.71**,8	**-0.65**,9
Leased Grounds	**-0.68**,8	**-0.75**,8	**-0.59**,10	*0.43*	**0.68**,10	**0.54**,13	-0.55,9	-0.63,8	**-0.66**,9

b, Water properties **MSXP & Bed**		River flow		Salinity		Temperature		SWA	
		Dec-May	Jun-Nov	Dec-May	Jun-Nov	Dec-May	Jun-Nov	Dec-May	Jun-Nov
Dec-May MSXP	Arnolds	*-0.31*,16	-0.46,12	**0.71**,7	*0.43*	-0.64,6	**-0.40**, 39	*0.03*	*0.04*
	Cohansey	-0.46,14	*-0.18*	*0.47*	*0.01*	*0.29*	**0.46**, 33	**0.82**,5	**0.91**,6
	New bed+Bennies	-0.52,10	*-0.26*	*0.57*	*0.15*	*0.11*	**0.60**,10	**0.69**,7	**0.92**,5
	Egg Island	*-0.48*,8	*-0.32*	*0.46*	*0.02*	*0.06*	**0.47**,16	*0.48*	**0.63**,8
	Leased Grounds	*-0.27*	*-0.18*	*0.36*	*0.05*	*0.11*	*0.20*	*0.48*	*0.42*
Jun-Nov MSXP	Arnolds	-0.28,32	*-0.18*	*0.12*	*0.06*	*-0.05*	*0.11*	*0.12*	*0.40*
	Cohansey	**-0.37**,29	*-0.25*	*0.35*	*0.16*	*-0.09*	*0.01*	*0.01*	*0.41*
	New bed+Bennies	-0.28,35	*-0.24*	*0.39*	*0.28*	*-0.39*	*-0.11*	*-0.20*	*0.12*
	Egg Island	*-0.16*	*-0.15*	*0.29*	*0.11*	*-0.41*	*-0.18*	*-0.28*	*0.05*
	Leased Grounds	*-0.07*	*-0.15*	*0.27*	*0.06*	*-0.60*[1]	*-0.36*	*-0.46*[2]	*-0.30*

§3-3. Particle transport between the lower and upper Bay

Spatial variability in MSXP follows a typical gradient from lower Bay to upper Bay. The down-Bay gradient provides the pre-conditions for a potential horizontal transport mechanism. Among the fall surveys covered in our 16 years of simulations, there are noticeable year-to-year increases in MSXP in the upper Bay (Arnolds) in years 1985, 1992 and 2008 (Fig. 3). The saltier and persistently warmer water in the upper Bay in 1991-92 and 1985-86 would in principle be suitable to MSX proliferation in 1992 and 1985. However, there are no extended intervals of both saltier and warmer conditions in the upper Bay in fall 2008. Additional mechanisms besides beneficial environmental conditions might have been at work in 2008. In particular, the significantly high MSXP in the upper Bay in the summer of 2008 might be related to the enhanced up-Bay transport of MSX particles.

To examine particle transport, we release passive particles near and at the sea bed at the horizontal locations shown in Figure 16. We do not know if MSX is passive or neutrally buoyant because the infective stage or any free living stages have not been identified. It is plausible that other factors may account for its movement such as buoyancy or perhaps an intermediate host that can migrate to some degree. However, the small size of *H. nelsoni* must move very slowly in the water compared to the current speed, which suggests that we begin by treating it as a passive particle.

The particles are released at five locations within the Bay (labeled 1 through 5), and during each of three years (2007-2009) on nine different days (1, 15 and 29 May; 12 and 26 June; 15 and 29 August; 12 and 26 September; and 10 October). On each of these days, the particles are released five times at three-hour intervals to cover approximately one M2 tidal period. The passive particles are tracked from their release time to 31 October of the year unless they leave the water of the Bay. We are particularly interested in the resulting distribution of particles within the sub-regions labeled A through F.

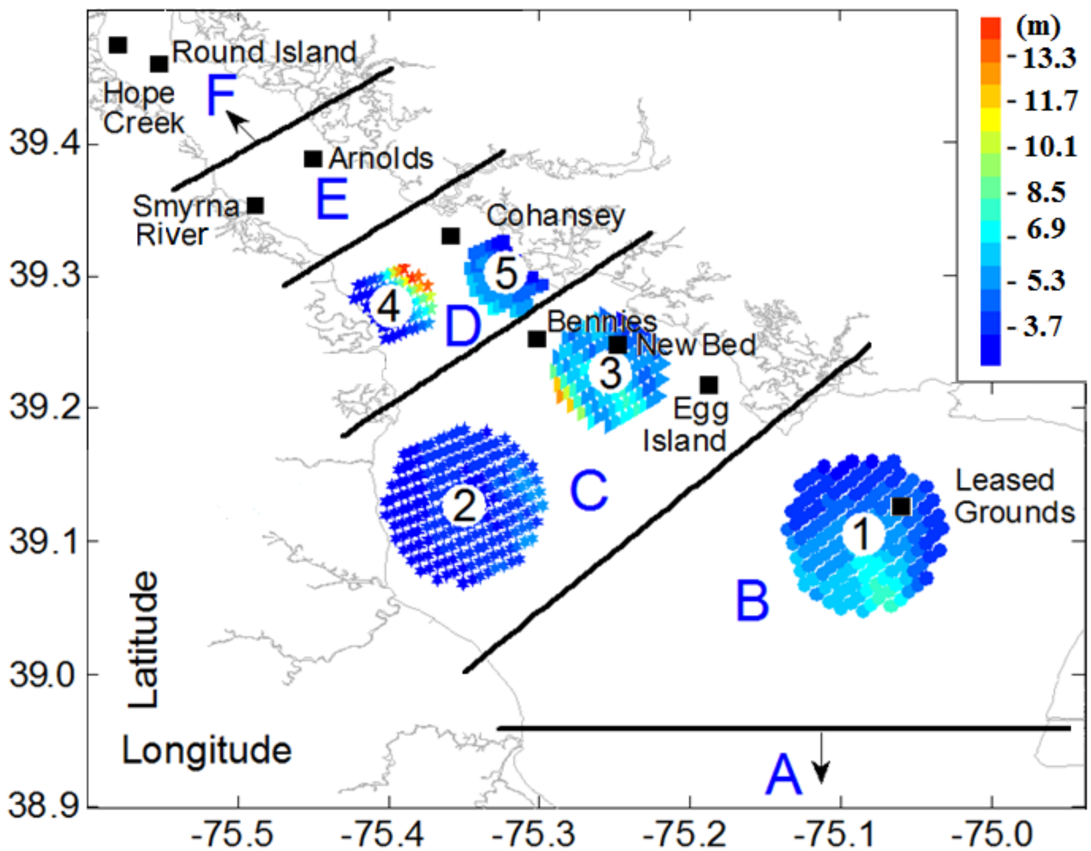

Figure 18. Locations of major oyster collection sites (black squares), released floats (colored shapes), and transport/retention-regions (separated by straight lines). There are 141, 194, 106, 59, and 50 releasing grid points within the five circular areas (1-5, respectively). On each grid point ten floats are released (five at bottom, five near bottom, at three-hour intervals) on each of the release days: 1, 15 and 29 May, 12and 26 June, 15 and 29 August, 12 and 26 September, and 10 October. The color bar indicates the releasing depth (m) averaged between the two releasing layers. Six regions (A, B, C, D, E, and F) are used to locate floats.

§3-3-1 General patterns of passive particle movement

Figure 19 summarizes the general patterns of particle redistribution and current pattern. The two panels display the three-year average (2007-2009) for particles released on 1 May (left) and 29 August (right) and subsequently tracked for 60 days and the currents averaged within May-June (left) and September-October (right). We choose these release dates to represent early- and late-season dates when infective elements might be released during the infection period (~June through early October) for MSX in Delaware Bay (Ford and Haskin, 1982). Three major points can be derived from this Figure:

Particles released in the lower Bay – at site 1 on the New Jersey side, and site 2 on the Delaware side -- are retained to a far greater extent than particles released from more up-Bay sites, ~50% (May-June) and ~40% (September-October) in sites 1 and 2 and ~24% (May-June) and ~18% (September-October) in sites 3, 4, and 5. The increased residence times of passive particles in region B is consistent with the hypothesis, based on elevated infection prevalence in Leased Ground oysters, that MSX infective elements are concentrated in the lower Bay and become diluted in an up-Bay direction (Ford and Haskin, 1982). Particle transport depends on current. Around sites 1 and 2, the Bay is at its widest with convex geometry. As a consequence, the along-Bay current speed and transport efficiency are reduced there.

Particles are more retentive in sites 1 and 2 in May-June than in September-October, 46-55% and 43-36% for retention in sites 1 and 2. More particles are eventually transported to region F and A in September-October than in May-June, 8% and 6% to F and 21% and 13% to A, on average. The river flow input and the down-Bay surface current, and therefore lower Bay (regions A-D) exchange inflow averaged within May-June are stronger than those averaged within September-October.

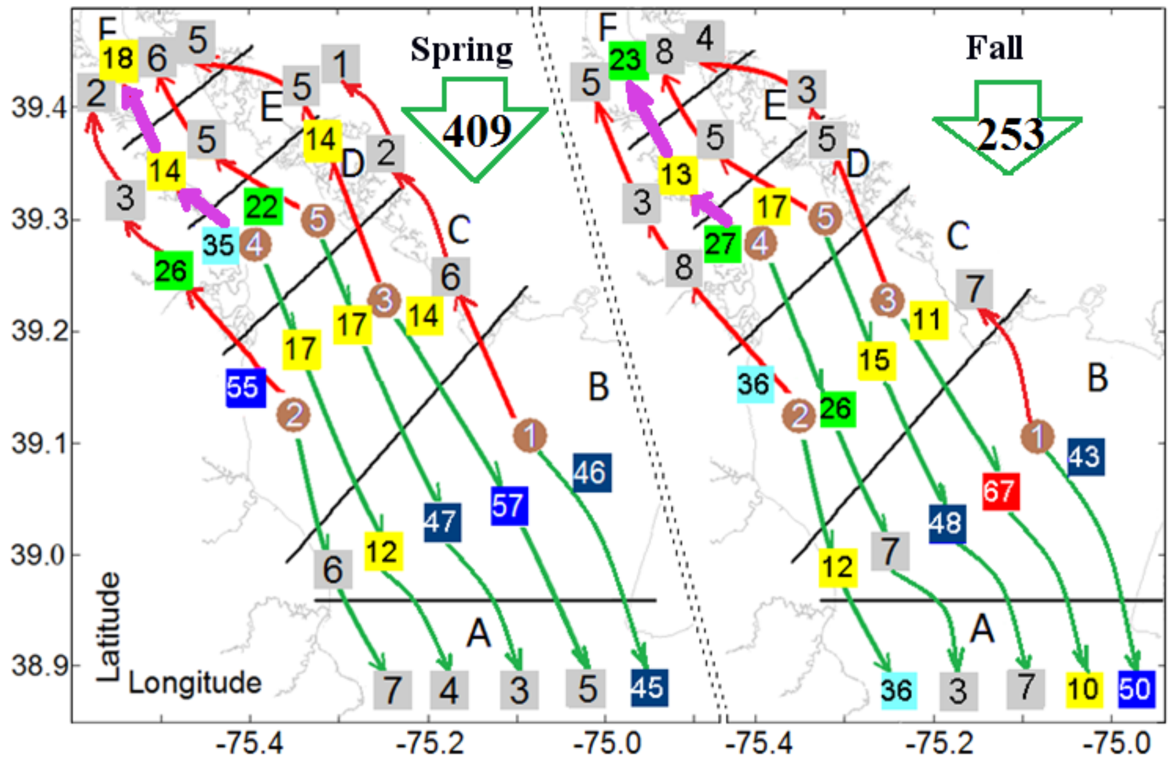

Figure 19: Particle transport pathway in spring and fall. Particle transport and retention percent on the 60th tracking day since release dates 1 May (left) and 29 August (right). The numbers in the squares show the percent of particles released at each of the sites 1-5 that reach each of the 6 sub-regions A-F after 60 days. Arrows with numbers are the 60-day-average river discharge rates (m^3/s) over the same period. Each panel is a three-year average over the years 2007, 2008 and 2009. The colored squares are used to highlight the larger numbers with an interval of 10%: grey 0-10, yellow 11-20, green 21-30, light blue 31-40, dark blue 41-50, blue 51-60, and red 61-70%, respectively.

Delivery of passive particles to the upper-Bay (regions E and F) is primarily from the Delaware side of the Bay at release location 4, with a lesser contribution from release sites 2, 3 and 5. The fact that sites 2 and 5 are closest neighbors to site 4 suggests that passive particles from 2 and 5 that successfully reach upper Bay locations may do so by first passing through the Delaware side of region D near release site 4. This is clearly the efficient upper Bay path for particles released at site 2, immediately down-Bay of site 4. The net transverse circulation matters to the particle communication.

Figure 20 shows the time-mean circulation in July 2011 in the cross-Bay plane at the location of the DBMDP moorings (Fig. 4c). The time-mean circulation in the plane of the mooring array is determined to be in the counter-clockwise sense. This residual circulation is consistent with the primary route for simulated passive transport to the upper Bay. Particles released on the Delaware side of the Bay are preferentially transported across and down into the shipping channel, where transport to the upper Bay is enhanced. It also suggests that particles from both sites 2 and 5 reach upper Bay locations, at least in part, via site 4.

Figure 21 depicted the monthly cross-Bay particle exchange between sites 4 and 5 in region D, showing the percent of particles released at site 5 that successfully transit to the New Jersey side of the Bay, as well as those released at site 4 that arrive on the New Jersey side. There are approximately net 8~15% particles successfully transported from NJ side (site 5) to Delaware side (site 4), which also conduces to transport food from NJ side to Delaware side. The geographic structure of food estimated as the sum of protein labile carbohydrate and lipid (Powell *et al.,* 2012) did show a consistent pattern that food values on oyster beds in NJ side were often depressed relative to the Bay-wide mean.

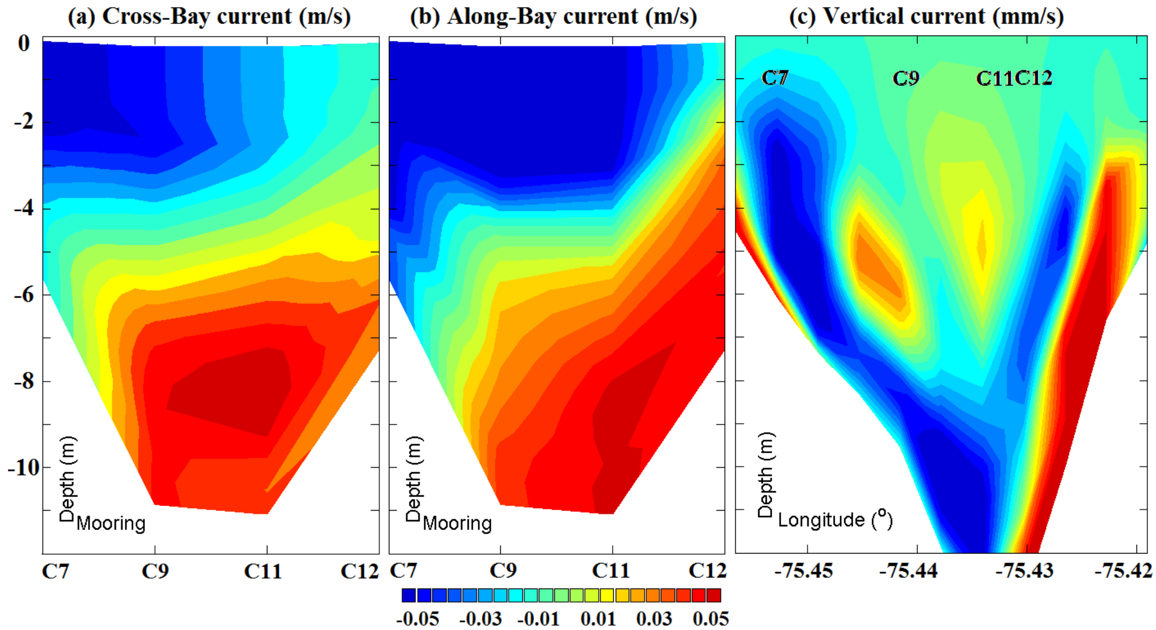

Figure 20. Cross-Bay sections of time-averaged currents for July 2011: a) observed DBMDP cross-Bay component of vector current (m/s), b) observed DBMDP along-Bay component of vector current (m/s), and c) simulated vertical current (mm/s).The location of section C7-C12 is indicated in Figure 3c. Positive values of the color-bar correspond to transport from Delaware towards New Jersey [in (a)], upper Bay transport (b), and upwards transport (c).

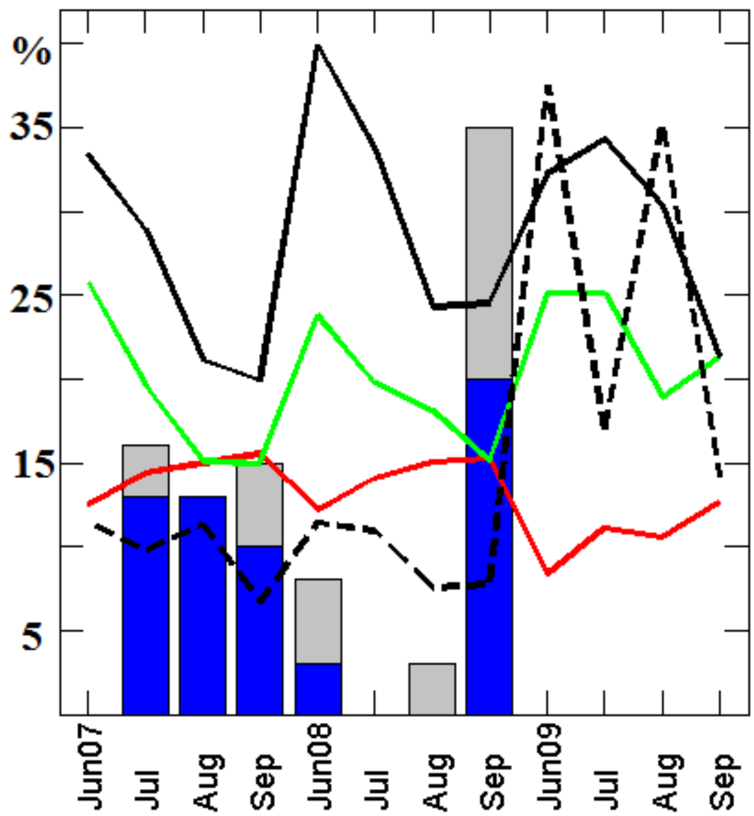

Figure 21. Monthly cross-Bay particle exchange in region D (%, green and black lines), *Haplosporidium nelsoni prevalence* (MSXP, %, bars), bottom salinity averaged in region E (red line), and river flow input from upper Bay (X 20 m^3/s, dashed line). Green (black) line shows the percent of particles released at site number 4 (5) that successfully transit to the NJ (DE) side of the shipping channel. Blue (grey) bars shows MSXP averaged in region E (Arnolds Bed and Smyrna River) and F (Round Island and Hope Creek)

§3-3-2 Inter-annual variability in particle redistribution

Figure 22 compactly summarizes the location probability matrix (LPM) in which the probability that particles released at each of the five sites (1 through 5) will terminate in one of the six Delaware Bay sub-domains (A through F) is tabulated in a 5-by-6 matrix. It indicates a temporal dependence in the effectiveness for passive particles to reach upper Bay regions (E and F) primarily via release site 4. Particles are transported to up-Bay regions most effectively in fall (September-October) for 2007 and 2009, but (anomalously) in spring (May-June) for 2008. For example, 30-60 days after release approximately 56-41%, 33-25% and 51-43% of particles in fall, while approximately 27-35%, 37-38%, and 40-21% particles in spring are transported through the primary route via site 4 to regions E and F, in 2007, 2008 and 2009, respectively.

Fewer than 0.5% of particles released at site 1 are directly transported to regions E and F except in June 2008 when approximately 2% of them are transported to the upper Bay. Finally, we note that summer 2008 is also a period of strong cross-Bay particle exchange in region D with approximately net 15% particles successfully transported from the NJ side (site 5) to the Delaware side (site 4) in June 2008 (Fig. 22). In the other months of 2007-09, the net percent is below 10%. The anomalous period of high up-Bay MSXP in Fall 2008 therefore does correspond to a year in which both cross-Bay and up-Bay transport of passive particles was enhanced in May and June when river freshwater input from the upper Bay is relatively low while tide induced salt-intrusion from the lower Bay is relatively strong with relatively high salinity (notes: salinity in 2006-09 is lower compared to other periods, as mentioned above and depicted in Fig. 17), implying that tidal-intrusion and river flow contributes to the up-Bay transport.

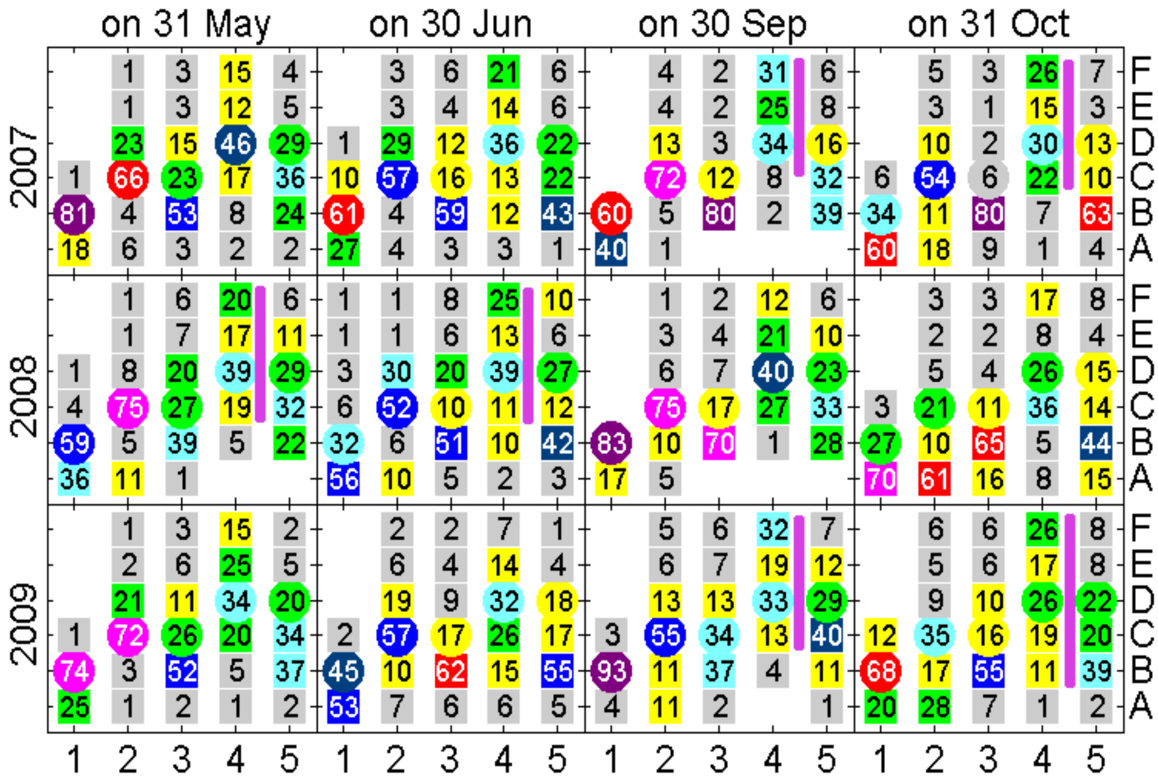

Figure 22. Percent of particles that are released at each of the sites 1-5 (x-axis) and reach in each of the 6 sub-regions A-F (y-axis) after 30 (columns 1 and 3) or 60 (columns 2 and 4) days. The years labeled 2008A and 2008B are the no-wind and increased bottom stress cases, respectively. Particles were released on 1 May, 1 May, 29 August and 29 August for the columns labeled 31 May, 30 June, 30 September and 31 October, respectively. Circled numbers correspond to the regions within which the particles of the respective groups were released, *i.e.,* to retention percentages.

The sensitivity experiments 2008A and 2008B are both instructive. With the wind forcing removed (2008A), the anomalous direct communication from release site 1 to the upper-Bay in May/June 2008 is lost. Although not the dominant mechanism for particle redistribution, the wind was apparently consequential in enhancing upper Bay transport in May/June 2008. The mean spring 2008 winds are directed cross-Bay from the southwest and were particularly strong (Fig. 16). Although balanced by Ekman transport toward lower Bay, the a little enhanced upper Bay communication of particles in spring 2008 is consistent with upper Bay geostrophic flow arising from an enhanced wind-induced sea surface tilt. In fall 2008, wind is from the northwest but much weaker (Fig. 16). A bottom stress coefficient enhanced by 50% (2008B) reduces the amplitude of the tidal circulation (section 2-2-2) and thereby reduces up-Bay transport of passive particles. For both sensitivity experiments, transport via site 4 remains the primary transport route.

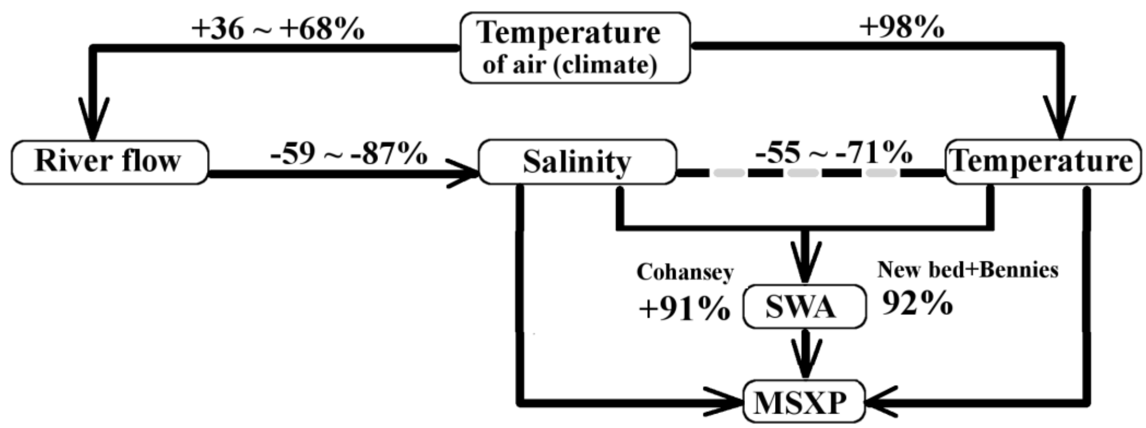

Figure 23. Diagram for the feedbacks evaluated with significant correlation (%) whose confidence is higher than 95%, summarized from Table 6, with correlations done on monthly-seasonal scales.

§3-4 Summary

The validated Delaware Bay model has been applied to quantify the relationship between observed *H. nelsoni* infection prevalence (MSXP) and concurrent physical conditions in Delaware Bay after simulations of passive particle transport in 2007-2009 and environmental conditions in 1974-76, 1979-81, 1984-86, 1990-92 and 2006-09. A new index, the salty-warm water area (SWA) was developed to help understand the complex role of temperature in MSXP. Statistical analysis methods were used to validate the model and explore the relationship with the hypothesis that elevated levels of MSXP depend upon a source of infective stages, an effective means of upper Bay transport, and environmental conditions hospitable to the parasite.

An effective upper Bay transport mechanism might have contributed to MSXP in the upper Bay in 2008. This transport was anomalously effective in spring (May-June) for 2008, not as it usually is in fall (September-October) for 2007 and 2009.

Results from the correlation analysis suggest that MSXP may be related to multiple physical factors, depending on location and time of year. MSXP is significantly correlated with river flow and salinity, especially in the upper Bay locations where salinity is not always automatically hospitable to the parasite. When the Bay gets both warmer and saltier with large SWA, as it did in 1984-1986, the environment is especially conducive to elevated MSXP, about 70-75% of the oysters in the upper Bay died over a two-year period in 1985 and 1986 when MSX was most prevalent in Delaware Bay (Powell *et al.* 2008; Hofmann *et al.*, 2009).

Fortunately, the negative river flow/salinity and positive river flow/temperature correlations dictate a negative temperature/salinity correlation to make the salinity and temperature in the Bay mostly out of phase on week-to-month temporal scale. An intensified warming climate might partially constrain MSX infection via replacing the Bay with fresher water from intensified river flow input. Higher temperature timely reduces salinity via more river flow as, e.g., in 1974-1976 and 1993-2009. This pattern of physical conditions is helpful to the Bay in controlling MSX infection. To keep this pattern, there are two important conditions (Fig. 23): One, a regular precipitation or snow/ice melting produces a river flow that positively responds to air temperature to make a warmer/colder weather bring more/less river discharge input into the Bay. This needs sufficient ice and snow to be available. Two, the small Bay and regular river flow and the limit salt intrusion make salinity in the Bay sensitively change with river flow and the temperature in the Bay positively respond to air temperature on a week-to-month temporal scale. This requires the Bay to be shallow, small in size and not too saline in its water.

Future changes to the thermal and hydrologic conditions may be expected to have a profound influence on MSXP in Delaware Bay. A warming climate is expected to be accompanied by changes in both precipitation patterns and ice and snow cover (Rudolf *et al.*, 1994; Lemke *et al.*, 2007). All of these effects will mutually combine to establish future levels and distributions of MSXP. A natural next step is to inquire into the potential impacts of future climate variability on circulation, tracer fields, and MSXP in Delaware Bay using the modeling tools developed here. A sequence of climate sensitivity studies addressing these issues is carried out in section 4.

§4. Climate sensitivity studies

This chapter addresses three primary questions: First, what alterations in the physical environment in Delaware Bay may be expected from projected climate change? Second, what dynamical mechanisms account for these alterations? And lastly, do climate-related changes in the physical environment have the potential to significantly impact the oyster population in Delaware Bay? To answer these questions, we conduct a series of climate sensitivity studies, described in detail below.

In Chapter three, we explored the relationships between the principal environmental variables (river flow, salinity, temperature, and circulation) and the observed prevalence of the oyster disease MSX (MSXP). The results indicate several statistically significant correlations. The most striking of these is the occurrence of elevated levels of MSX with the anomalous co-occurrence of warmer and more saline water, with the so-called "salty-warm water area" (SWA) highly correlated with MSXP at two mid-Bay locations, Cohansey and New Bennies. The passive-release studies further implicate the circulation patterns in Delaware Bay in the potential transport and redistribution of MSX. Preferential up-Bay transport pathways, the principal one of which connects the Delaware side of the Bay with the up-Bay oyster beds, were identified and proved to be consistent with concurrent studies of the observed food distributions (Powell *et al.*, 2012).

In summary, both the physical tracer fields and circulation patterns jointly play a role in determining the observed levels of MSX. In future years, as climate-change-related variations in atmospheric and hydrologic forcing induce changes in environmental conditions in Delaware Bay, it is important to consider whether conditions will be more or less favorable to the proliferation of oyster diseases such as MSX and Dermo.

§4-1. Questions to be answered

The climate sensitivity studies described below have been designed to explore the following questions.

How might the evolving climate over the next 50 to 100 years influence the salinity and temperature fields in Delaware Bay? Specifically:

Is the Bay likely to become more saline, by how much, and which climate changes will be most influential? How might the salinity structure, e.g., salt wedge, change with time? How might the response of salinity to freshwater input be modified? How much warmer might the shallow and thermally sensitive Bay get in response to the higher surface air temperature associated with global warming? How might the distribution and occurrence of salty-warm water change, and what might be the implications for the conditions at the locations of present-day oyster beds?

How might the evolving climate over the next 50 to 100 years influence the circulation and transport in Delaware Bay? Specifically:

How might the transport pathways in Delaware Bay be modified in response to climate-induced changes in forcing? How might the efficiency of up-Bay exchange, and the principal transport pathways, be changed? How are the simulated changes in circulation and mixing related to the simulated modifications salinity patterns?

In the reminder of this chapter: we summarize the projected future climate changes in sea level, sea surface air temperature, winds and hydrology based upon observations and existing climate impact modeling studies (**§4-2**), conduct a suite of climate sensitivity studies (**§4-3**), exhibit and analyze our experiment results (**§4-4**, **§4-5**), and consider theoretical and analytical methods to summarize our experimental results (**§4-6, §4-7**).

§4-2. Climate-related changes in sea level, sea surface air, and hydrology

§4-2-1. Sea-level rise (SLR)

Global average sea level has risen at a rate of about 1.8 mm/yr (Najjar *et al.*, 2010; Church and White, 2006). Modern sea-level trends are found to be consistently 1-1.8 mm/yr higher than those derived from long-term geologic data, implying a recent acceleration of sea-level rise relative to the last few thousand years. The 20th century sea-level rise for the U.S. Atlantic coast is 1.94±0.6 mm/yr monitored by ^{14}C-dated relative sea-level histories (Peltier, 1996) and 2–4 mm/yr from tide-gauge data, or 1.26 ± 0.78 mm/yr after subtracting the late Holocene trend (Gornitz and Seeber, 1990). Model-based studies predict that sea-level in Delaware Bay could rise 40 to 65 cm by the year 2100 due to climate warming (Gornitz, 1995). The average Delaware-marsh accretion rate is 3 mm/yr for the last 100 yr (Nikitina *et al.*, 2000). Dredging activities (DiLorenzo *et al.*, 1994) and the opposite process of sediment-sinking (Davis, 1987) in Delaware Bay might also influence overall sea level change.

Recently (1992-2009), the mean sea level and its range in Delaware Bay increased by 4.92 and 4.82 mm/yr (Fig. 24b and c), respectively, as global mean sea level rose with a mean rate of 1.2 mm/yr (Fig. 24a). After 1995, the time periods for mean sea level above its medium value lasted significantly longer than those for mean sea level below its medium value, 113 and 53 months, coincident with the warmest years 1995 to 2006 on record since 1850.

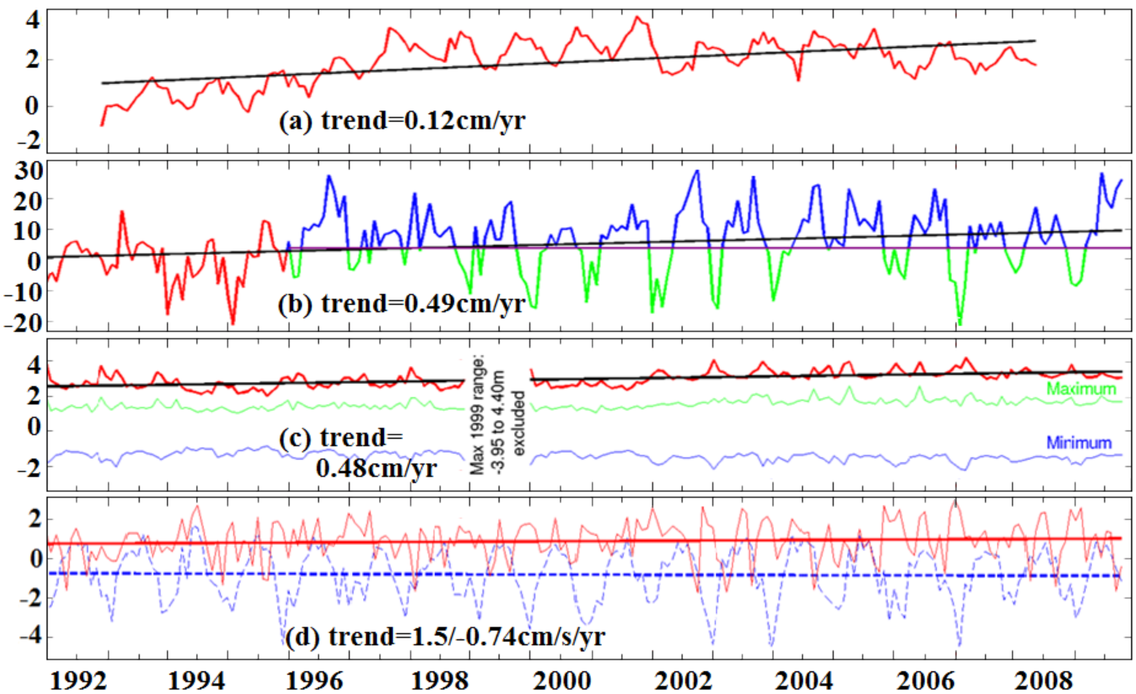

Figure 24. Recent changes in mean sea-level (MSL) and winds: (a) MSL (cm) of global oceans (global Jason and Topex sea-level anomaly) and (b) Delaware Bay (NWLP hourly mean sea-level), (c) MSL range (m) and (d) the cross-/along-Bay winds (m/s, red/blue lines, NARR reanalysis).

§4-2-2. Sea surface air temperature and winds

The future temperature and wind over Delaware Bay will also be influenced by changing climatic conditions. Over the last 100 / 50 years (1906–2005 / 1956-2005), global mean surface temperature has risen by 0.07°C±0.02°C / 0.13°C±0.03°C per decade and has been further enhanced since about 1994 (Fig. 25; Trenberth *et al.*, 2007). By 2070-2099 with a CO_2 level of about 850 ppm for a medium-high emission, a 4.9°C±1.8°C increment of the sea surface air temperature over Delaware Bay has been predicted by seven global climate models (Najjar *et al.*, 2009). Higher surface air temperature will increase the ocean temperature of the shallow Delaware Bay through heat exchange between surface air and water. Given its shallow bathymetry and rapid vertical mixing, even the bottom sea temperature in the Delaware Bay also consistently increases with surface air temperature (see, e.g., Fig. 17e).

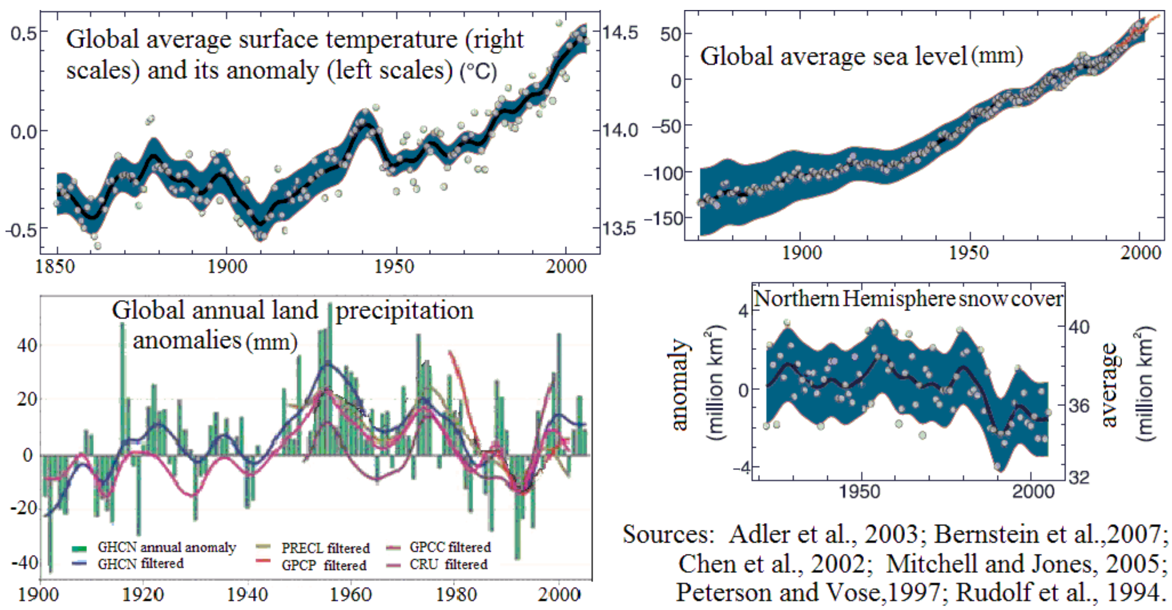

Figure 25. Changes of temperature, precipitation, sea level, and snow cover. Smoothed curves represent decadal averaged values while circles show yearly values. The shaded areas are the uncertainty intervals estimated. Precipitation anomalies are relative to the climatology for period 1981 to 2000 while other anomalies are respect to 1961 to 1990 base period.

Global warming will likewise alter the atmospheric circulation. For the period 1992 to 2009 in Delaware Bay, the cross-Bay wind increased with a mean rate of 150 mm/s per decade while along-Bay wind decreased with a mean rate of -74 mm/s per decade (Fig. 23d). By the year 2100, cross-Bay wind would increase by 1.5 m/s (or about 30% to a 5 m/s variation in cross-Bay wind, even bigger relative to the size of the average cross-Bay wind) and along-Bay wind would decrease by 0.75 m/s (or about 15% to a 5 m/s variation in along-Bay wind, even bigger relative to the size of the average along-Bay wind). The changes in amplitude and direction of the wind can be expected to produce changes in the circulation and shear in Delaware Bay through alterations in wind-driven currents, Ekman transport, draining, and mixing (Chen and Sanford, 2009).

§4-2-3. Hydrologic conditions

River flow changes with precipitation that has generally increased over land north of 30°N over the period 1900 to 2005 (Rudolf *et al.*, 1994; Chen *et al.*, 2002; Adler *et al.*, 2003). By 2070-2099 with an expected CO_2 level of about 850 ppm for a medium-high emission, a 4%±7% increment of precipitation over Delaware Bay has been predicted by seven global climate models (Najjar *et al.*, 2009). Over the period 1974 to 2011, the river flow input into Delaware Bay increased at a rate of 3.6 m^3/s/yr. Linearly extrapolated, the river flow input would increase by approximately 360 m^3/s in 100 years. A relative change in run off in each month (prepared by Pollard, pollard@essc.psu.edu) shows a significant summer and autumn increase in run-off (Fig. 26). However, earlier predictions (e.g., McCabe and Ayers, 1989) give a decreased annual stream flow, -39 to 9%, over the Delaware River Basin by 2070-2099 with a doubled CO_2 level.

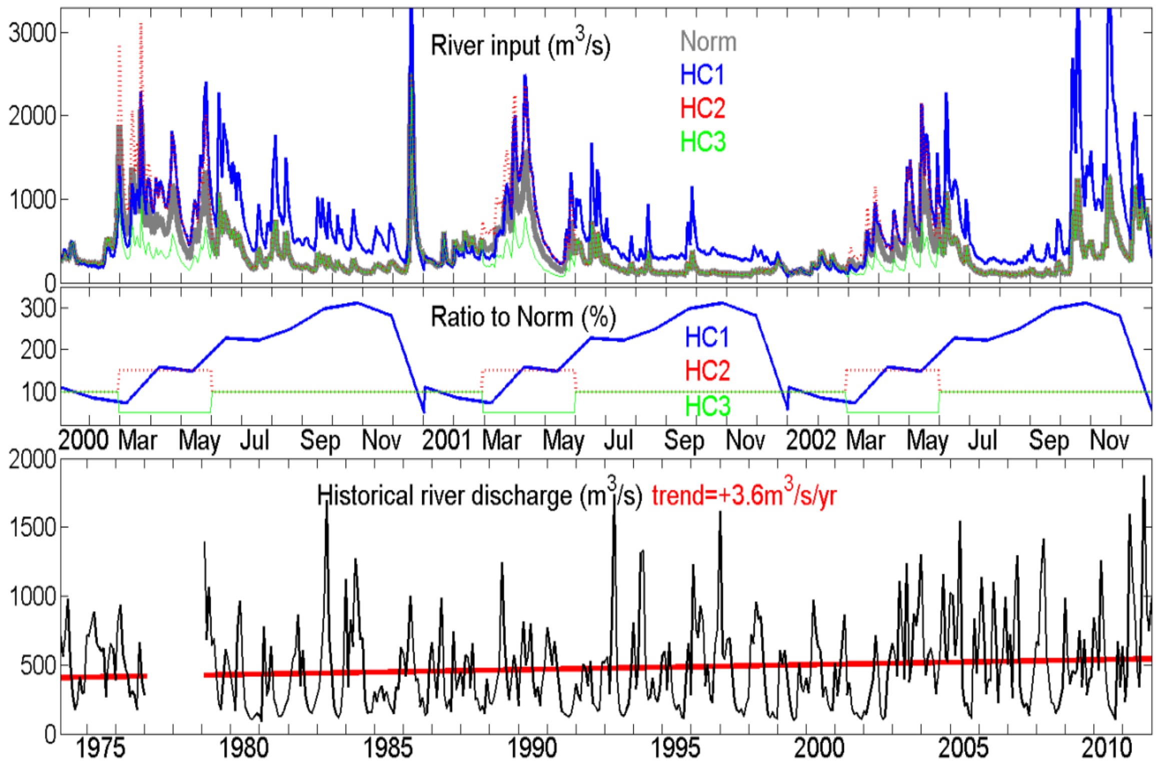

Figure 26. (Above) Daily river flow (m^3/s) input into Delaware Bay under different conditions: modern river flow (grey: Norm), predicted river flow future (Pollard, pollard@essc.psu.edu, blue: HC1), 50% increment in March-May of modern river flow (red, HC2), and 50% reduction in March-May of modern river flow (green, HC3) .(Middle) Ratio (%) of HC1, HC2 and Hc3 to Norm.(Below) Monthly historical river flow (m^3/s, USGS) .

§4-3. Numerical sensitivity studies

In view of the historical trends and future predictions described above, a suite of climate sensitivity simulations has been designed and conducted, as described in Table 7, by using the validated model (section 2-3). 2000-02, the beginning of the 21st century between La Niña and El Niño phases during an ENSO cycle, was set as the normal case (Norm). Based on Norm, cases for climate warming, sea level rise (SLR) and hydrology change are designed as follows:

Case Warm was conducted with surface air warming by 5 ^{o}C (relative to 2000-2002) and with other conditions the same as Norm.

Cases SLR1 and SLR2 were conducted for 50 cm and 100 cm sea-level rise (SLR, maintaining a 2 m minimum depth as required to avoid wetting/drying of land areas). Case SLR3, a companion experiment to case SLR1 but with the coastline fixed, was run to assess the effect of the horizontally enlarged Bay geometry as compared with case SLR1. Conditions other than the bathymetry and/or geometry of SLR1, SLR2 and SLR3 are the same as Norm.

Three numerical experiments (HC1, HC2 and HC3) were conducted to examine the effects from predicted changes in hydrologic forcing, corresponding to river flow increases by 20-200% from April to November, from higher spring river flow, and from lower spring river flow. Other conditions are same as Norm.

Two experiments (Wind1 and Wind2) were designed to examine the effects from changed cross-Bay and along-Bay winds. Other conditions are the same as Norm.

Table 7. Simulations conducted for climate sensitivity studies with climate changes in 50-100 years (In modeling, 2-m minimum depth is required for all cases including the validated Norm)

Case	Definition	Object
Norm	Normal case in 2000-2002	for comparison with other cases
SLR1	1-meter sea level rise (SLR)	effect from extreme SLR
SLR2	0.5-meter SLR	effect from medium SLR
SLR3	1-meter SLR with coastline fixed	effect from extreme SLR & fixed coastline
Warm	Surface air warmer by 5°C	warm effect
HC1	Predicted river flow	effect from predicted hydrology
HC2	March-May river flow increases by 50%	effect from higher spring river flow
HC3	March-May river flow decreases by 50%	effect from lower spring river flow
Wind1	Cross/along-Bay wind increase/decrease by 30%	effect from enhanced zonal wind
Wind2	Cross/along-Bay wind decrease/increase by 30%	effect from enhanced meridional wind
Comb1	SLR1+Warm+HC1	combined effect from SLR1+Warm+HC1
Comb2	SLR2+Warm+HC1	combined effect from SLR2+Warm+HC1
Comb3	SLR3+Warm+HC1	combined effect from SLR3+Warm+HC1
Further diagnostic cases		
SLR2C	SLR2 without Coriolis force to test the effect of Coriolis force, compared to SLR2	
SLR2I	SLR2 with zero initial salinity for new water to test the effect of fresher initial condition	
SLR2W	Same water area as SLR2 but without SLR to test the effect of purely widened geometry	

SLR1 (SLR2), Warm and intensified river flow (HC1) induced by the warming are all potentially significant factors and of high likelihood in the future. Experiments Comb1 (SLR1+Warm+HC1) and Comb2 (SLR2+Warm+HC1) were conducted to examine their comprehensive effect. Experiments Comb3 (SLR3+Warm+HC1) and Comb1 were

conducted to examine the effect from horizontally enlarged geometry under comprehensive conditions. Three other diagnostic cases were also carried out. They are defined, as follows: SLR2C to test the influence of the Coriolis force by turning off the Coriolis force in case SLR2, SLR2I to check if a fresher initial condition may eventually reduce the salinity in SLR2 by removing the salt in the new water area induced by SLR from the initial conditions of SLR2, and SLR2W to enhance our analysis on the salinity effect from a widened geometry by keeping the normal bathymetry intact but using the same land-sea mask as SLR2 (the Bay is enlarged as in SLR2, but with no increase in water depth).

The model was run for three years for each of the cases. We leave one year for model adjustment for each of the cases. (Case SLR1 adjusts the slowest and reaches an equilibrium state after about 8 months. One year is therefore sufficient for model adjustment.) In the following text, the first year covering adjustment phase is simply called year 1, while the second year when modeling reached the equilibrium phase is simply called year 2. All the comparisons between the normal case and a specific case were done within year 2. The third year was run for some special comparisons and for making sure that the model has reached the equilibrium state for all the cases in year 2.

§4-4. Experiment results and analysis

As compared to the case Norm during its equilibrium phase (year 2), a significant temperature change is caused by warmer sea surface air as will be displayed in case Warm and its comprehensive cases (i.e., Comb1, Comb2 and Comb3); salinity changes radically in the cases that widen the geometry as will be displayed in cases SLR1, SLR2, Comb1, Comb2, SLR2C, SLR2I and SLR2W. A 50% changed spring river flow (HC2/HC3) and a 30% changed cross-/along- Bay winds (Wind1/Wind2) produce minor effects (listed in Tab. 8 and plotted in Fig. 27E and G and Fig. 31).

§4-4-1. Salinity and its stratification

With 50-100 cm SLR the mean salinity is increased by ~8.0-8.2 (~1 to 19 from mouth to the upper Bay). The salinity difference between bottom and surface, used as a measure of salinity stratification, is reduced by ~0.6 yearly averaged, ~0.8-0.9 averaged in the spring and summer, and ~0.3-0.4 averaged in the winter and fall (Fig. 27A and B, Tab. 8). Salinity departure relative to Norm can reach 18 at the upper Bay in Comb2. In the middle Bay at the contemporary salt wedge location (30-80km from the mouth), salinity departure relative to Norm is ~5-17 (larger in the spring and summer when river flow is seasonally stronger than in winter and fall, Fig. 28). The salt wedge disappears in SLR1 and SLR2 from its regular location in Norm with the along-Bay salinity gradient reduced from ~31.9 in Norm to ~7.2 in SLR1 and SLR2 ($\times 10^{-5} m^{-1}$, Fig. 32A). HC1 can reduce salinity by 1.6 and enhance salinity stratification by ~0.5 in summer and fall (Fig. 27A and B; Tab. 8).

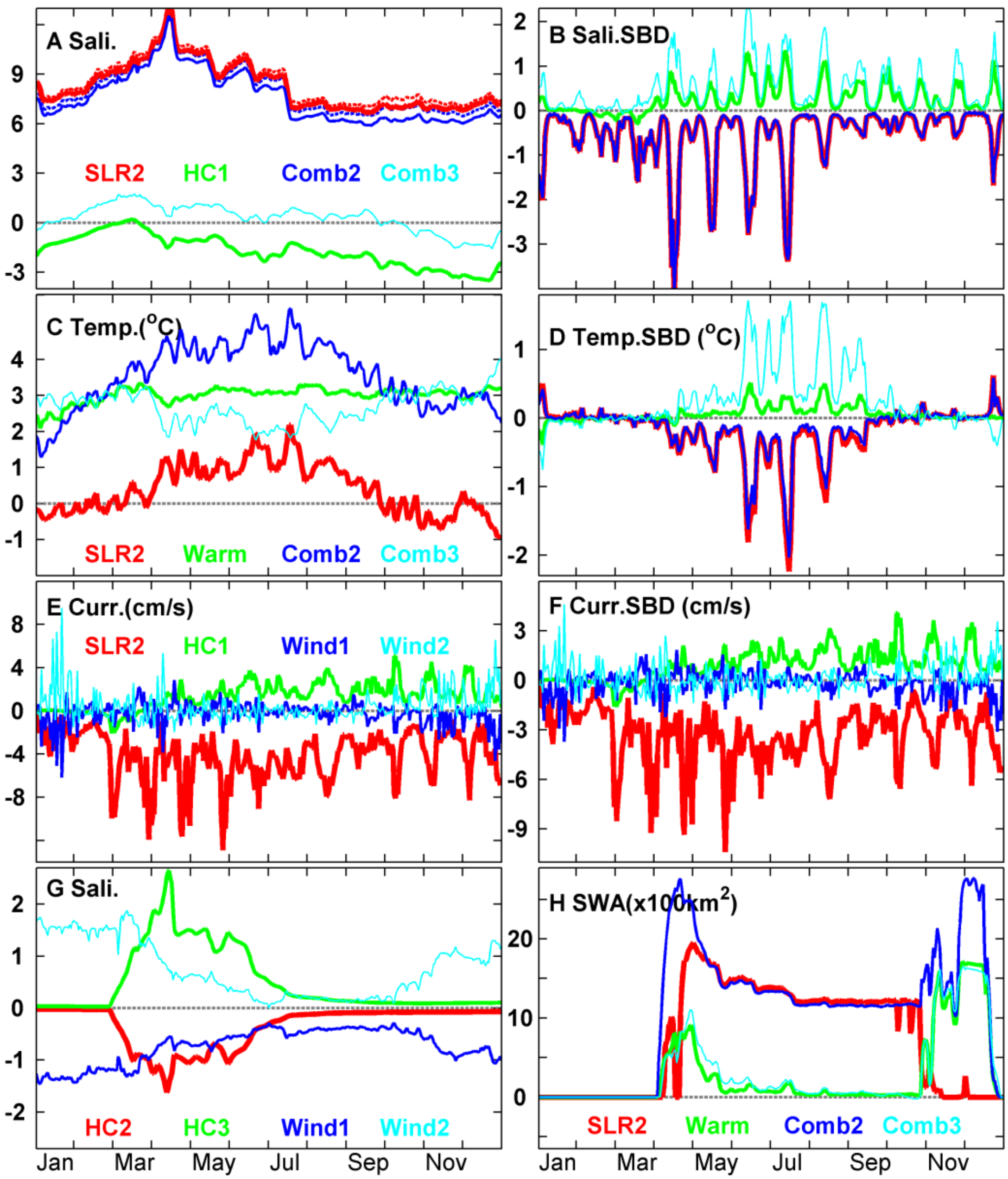

Figure 27. Departures of bottom salinity (A) and salinity SBD (B), bottom temperature (°C, C) and temperature SBD (D), surface current (cm/s, E) and current SBD (F), and salty-warm water area (SWA, x100 km^2, H), based on simulation in one year after the model runs through the first year for full adjustment. Salinity, temperature, current and their SBD are all averaged within the Bay with/without sea level rise. The dashed lines in A indicate the salinity and its SBD for SLR2 and Comb2 are averaged within the bathymetry without sea level rise. SBD is bottom minus surface salinity, surface minus bottom temperature or current. Cases are as described in Table 7.

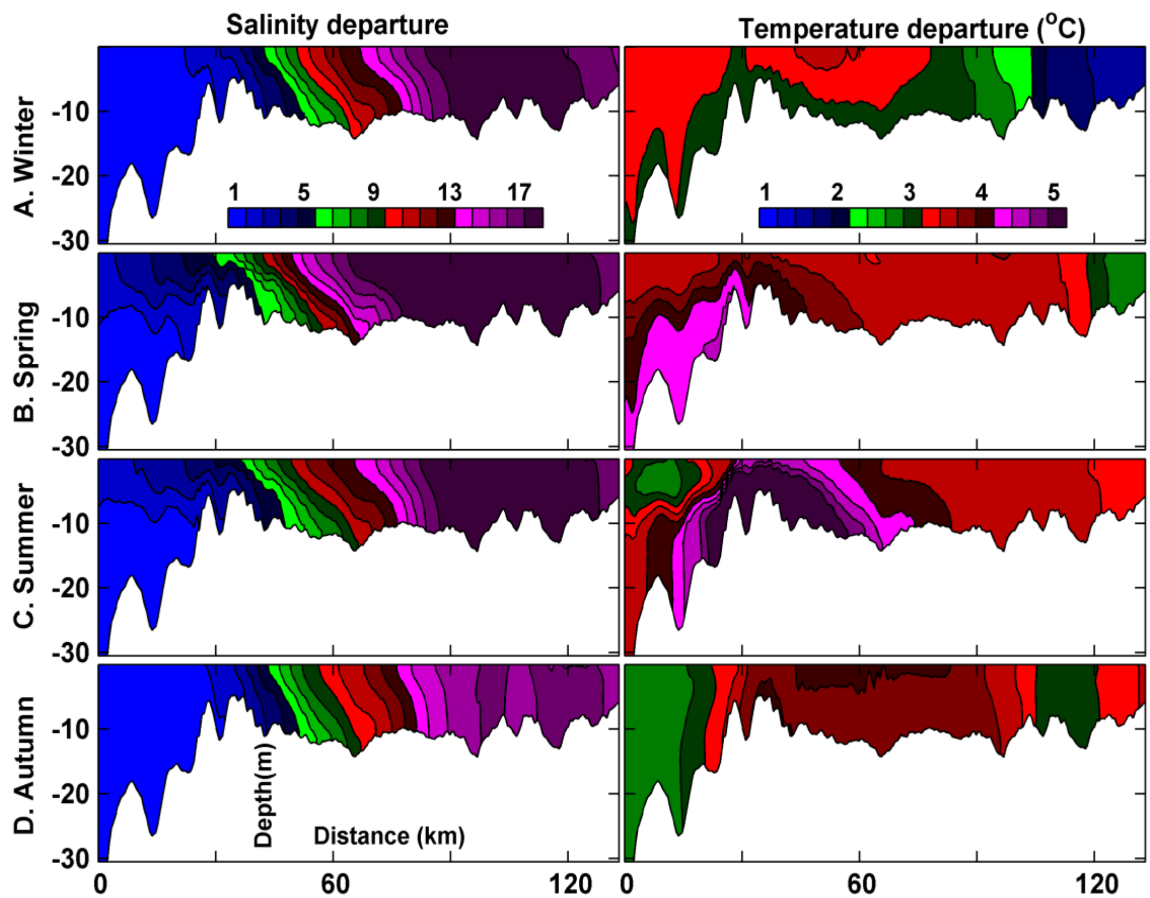

Figure 28. Seasonal salinity (left) and temperature (°C, right) departures from Norm for case Comb2 along Delaware Bay. Comb2 is described in Table 7.

Salinity is usually sensitive to the freshwater input rate (Q_{riv}, m^3/s), as studied by, e.g., Hansen and Rattray (1965), with a relationship between salt intrusion distance (SID) and river flow input rate defined as follows,

$$SID = B\, Q_{riv}{}^{q} \tag{8}$$

According to the theory of Hansen and Rattray (1965), MacCready and Geyer (2010), and Monismith *et al.* (2002), $q = -1/3$, implying that salinity (salt intrusion) is relatively sensitive to river discharge input.

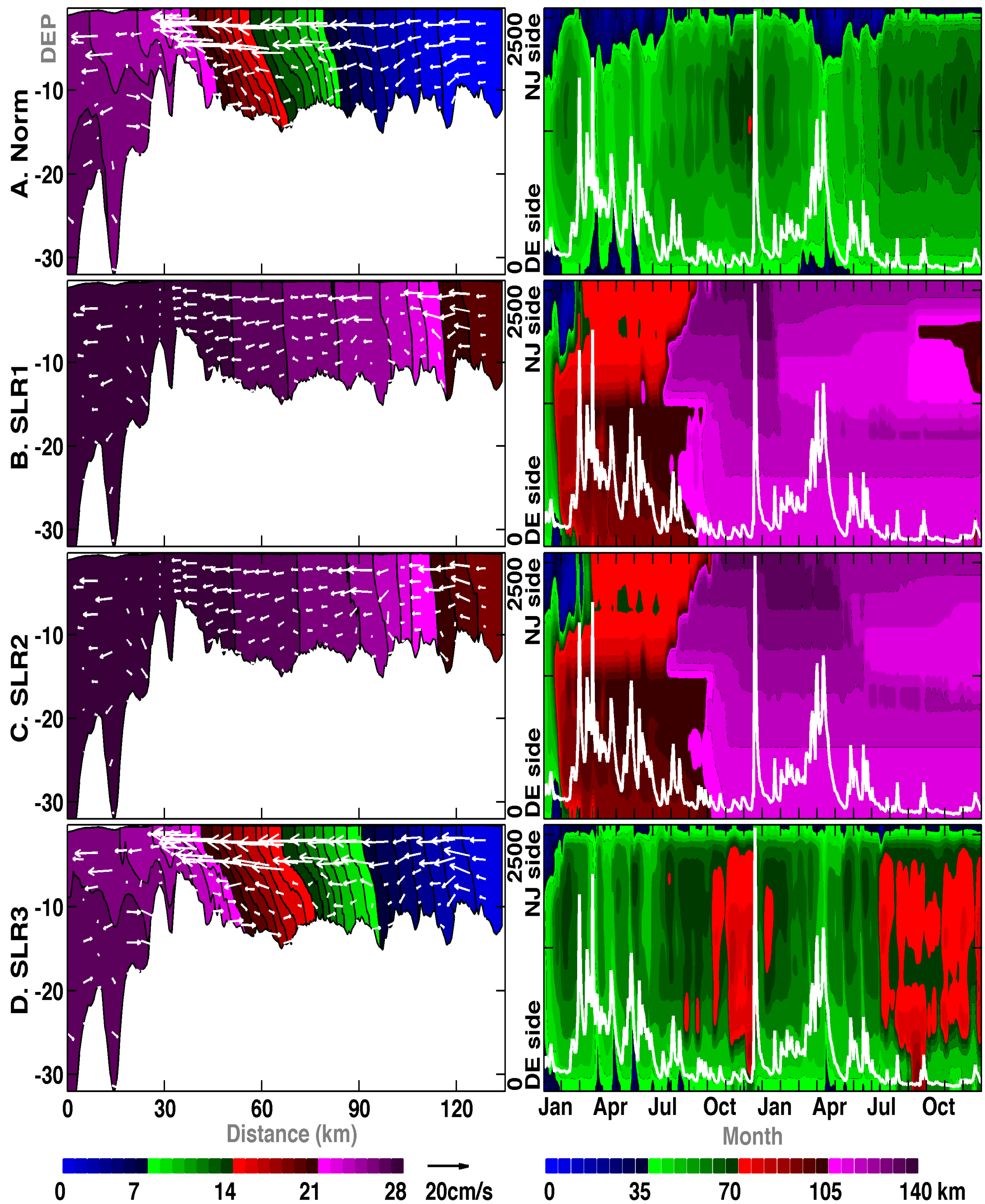

Figure 29. Along-Bay salinity, current and salt-intrusion distance of cases Norm and sea level rises. Left: salinity (contour) and current (m/s, white arrow) averaged within year 2. Right: salt intrusion distance for 17.5-isohaline (km, contour, from Delaware to New Jersey sides) and river flow input rate (m^3/s, white curve) against time (year 1-year 2), for cases Norm, SLR1, SLR2 and SLR3, at **A, B, C,** and **D** respectively. Cases are as described in Table 7.

In Delaware Bay, Aristizabal and Chant (2013) determined q to be approximately −0.1 to −0.16 and B to be 114 to 206 km, depending upon the isohalines, based upon idealized ROMS simulations using constant river flow and M_2 and S_2 tidal constituents. Salinity (salt intrusion) is therefore less sensitive to river discharge input in these prior simulations.

In this study, using the real river flow input from all six rivers from the upper Bay and seven tidal constituents (M_2, N_2, S_2, K_1, O_1, M_4, and M_6), a similar result is produced with q = −0.119, −0.107, −0.114, −0.167, and −0.279, and B = 137.60 km, 107.51 km, 91.58 km, 91.03 km, and 95.80 km, for isohalines 10, 14, 18, 22, and 26, respectively. However, if we apply Equation 8 to cases SLR1 and SLR2, the parameters are determined to be: q = −0.001, −0.001, −0.001, −0.002, and −0.001 and B = 107.59 km, 110.97 km, 119.87 km, 122.91 km, and 62.98 km, for isohalines 10, 14, 18, 22, and 26, respectively. B, as a fitting coefficient, depends upon all the factors that influence the resultant SID in the cases Norm and SLR2. The parameter q, however is determined by the extent to which SID depends upon river flow rate in the least square regression. That q is much smaller in size indicates that the SID is much less sensitive to river flow input rate in the new enlarged and salinized Bay that is basically always flooded with salty water, independent of river flow rate.

The SID and river flow input rate is depicted in Figure 29. For the regular Delaware Bay that is small in size, narrow in mouth and in middle-upper body, shallow in depth and has medium salinity, the SID and therefore the salinity are sensitive to river flow input, with the SID delaying the river flow input by a few weeks (Fig. 29A and D). The intensified river flow input decreases the mean salinity (18.2) by ~1.6 (~ -8.8%, case

HC1, Tab. 8). However, with a 50-100 cm SLR, the SID and therefore the salinity are less sensitive to river flow input. In other words, for a given river flow input rate, the salinity of the enlarged and saltier Bay changes much less than it does under contemporary conditions (Fig. 29 B and C). The intensified river flow input decreases the mean salinity (26.2) by ~0.5 (~ -1.9%, cases SLR2 and Comb2, Tab. 8). In mid-April the strong river flow reduces salinity more in Norm than in SLR2 and induces the largest salinity departure between SLR2 and Norm (Fig. 27A).

Under contemporary conditions, Delaware Bay provides a large habitat for aquatic life (e.g., oysters) and freshwater area because of its two important properties: first, the salinity over much of the Bay is lower than the oceanic salinity, and second, its salinity field responds significantly to river flow input with a salt wedge localized at mid-Bay, arising from the balance between river flow input and oceanic salt intrusion. However, 50-100 cm SLR incurs a Bay of much higher and insensitive salinity with the salt wedge disappearing from the middle Bay due to intensified mixing and salt-intrusion. The contemporary Bay contains some 234.9 million tons of salt, while the enlarged Bay contains some 392.1/419.2 million tons of salt for SLR2/SLR1, with ~157.2-184.2 million tons of more salt intruding into the enlarged Bay. As a result, the Bay is “salinized”. A new experimental index “estuarine salinization index (ESI, %)” is used to quantitatively evaluate estuarine salinization, with ESI defined as,

$$ESI \equiv 100 \times \frac{\Delta A_S - \Delta A}{A} \tag{9}$$

where, ΔA_S is the increment of salty-water area (m^2, i.e., the area of the bottom water whose salinity is higher than 17.5), ΔA is the increment of water area (A, m^2). If ΔA_s is computed from an unchanged water area, ΔA=0. ESI>0 / <0 indicates salinization /

desalinization with salty-water area increasing faster / slower than the water area. The larger the ESI, the more an estuary is salinized. As listed in Table 8 below, ESI displays a high degree of salinization with the net salty area increasing ~26% (ESI=~26%). With the HC1 (intensified hydrology), a slight desalination is induced in April to November, with ESI = -8%, and bottom salinity -1.6. Experiments were further carried out to check the comprehensive effects from the SLR1 and SLR2 plus the warmer surface air and the intensified hydrology in cases Comb1 and Comb2. The intensified river flow included in the cases Comb1 and Comb2 will not help reduce the salinization induced by SLR1 and SLR2, with ESI = +22~+25%, and bottom salinity +7.5 in Comb1, with ESI = +21~+24%, and bottom salinity +7.3 in Comb2.

If the coastline were fixed (as shown in cases SLR3 and Comb3), 100 cm SLR would not cause serious salinization with ESI = 7%, and bottom salinity +1.7 in SLR3, ESI = 4%, and bottom salinity +0.5 in Comb3.

§4-4-2. Temperature and its stratification

Warm and SLR as well as their combinations (Comb1-3) are the major cases that influence the temperature and temperature stratification (evaluated with temperature difference between surface and bottom, Fig. 27 C and D).

A 5 ^{o}C warmer surface air (Warm) significantly warms the shallow and thermally sensitive Bay mainly via increasing sensible heat flux by ~10-20W/m^2 into the shallow ocean. The bottom temperature increases by approximately 3.0 ^{o}C: 1-3.5 ^{o}C in winter and fall, and 2-5 ^{o}C in spring and summer (4-5 ^{o}C warming occurring locally in the subsurface in the lower Bay). With a 50 cm SLR, the newly formed water area will become warmer by ~0.4 ^{o}C totally, ~0.5-1.2 ^{o}C in spring and summer, but becomes colder by ~0.2 ^{o}C in winter and fall. Temperature stratification increases a little, by ~0.1 ^{o}C, with a 5 ^{o}C warmer surface air, but decreases by ~-0.2 ^{o}C with SLR1 and SLR2. Comb2 (Comb1 similarly) warms the Bay by ~3.6 ^{o}C and decreases temperature stratification by ~-0.2 ^{o}C (Fig. 26C, right of Fig. 27 and Tab. 8). A 5 ^{o}C warmer surface air plus 50 cm SLR with the coastline fixed (Comb3) results in ~1-3 ^{o}C warmer bottom and ~0.3 ^{o}C stratified water column (Fig. 27C, D and Tab. 8).

§4-4-3. Circulation and current shear

Circulation and current shear are mainly influenced by changes in SLR, wind and river flow. Simulations in year 2 (equilibrium phase) are used here for comparison between case Norm and the other cases.

SLR enlarges the cross-sectional area and reduces the along-Bay current speed for a given river flow input rate. With SLR1 and SLR2, the along-Bay current is reduced via the enlarged cross-sectional area of the Bay. Currents become weaker by ~4 cm/s (averaged at surface) with a range of 0 to -9 cm/s. Current shear becomes weaker (~3-4 cm/s reduced in current difference between surface and bottom, with a range of 0 to -9 cm/s; Fig. 27E and F). The changed current field in SLR (e.g., SLR2) changes the particle pathway. For instance, the major up-Bay transport pathway in case Norm is via site 4 near the Delaware side, but, compared to Norm, this pathway disappears in SLR2 and the particles released in sites 1-5 are generally more retentive (Fig. 30). The communication between the oyster beds in the lower and upper Bay is limited.

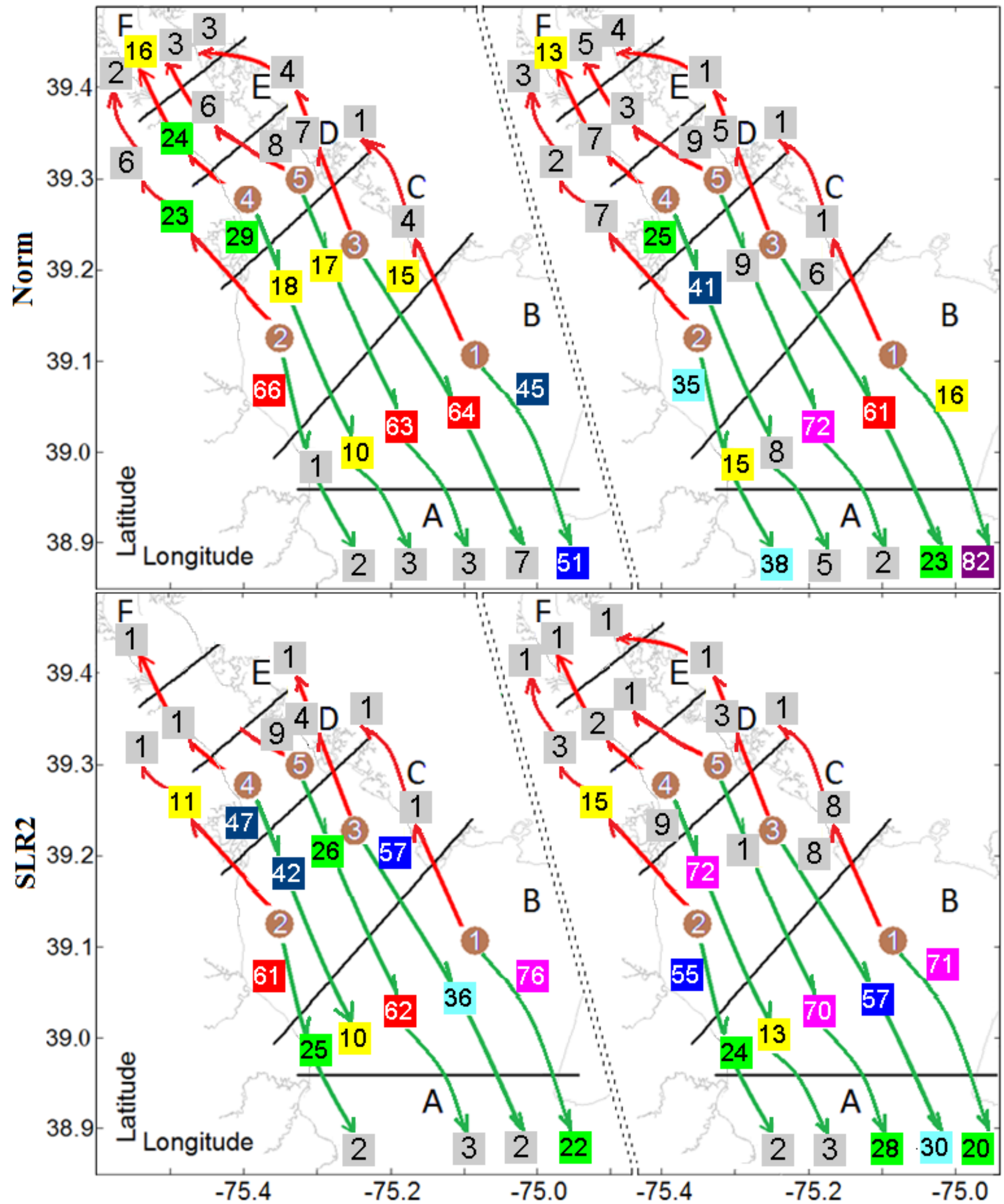

Figure 30. Particle transport pathway for cases Norm and SLR2. Particle transport and retention percent on the 60th tracking day since release dates 1 May (left) and 29 August (right) for cases Norm (above) and SLR2 (below). The numbers in the squares show the percent of particles released at each of the sites 1-5 that reach each of the 6 sub-regions A-F after 60 days. The colored squares are used to highlight the larger numbers with an interval of 10%: grey 0-10, yellow 11-20, green 21-30, light blue 31-40, dark blue 41-50, blue 51-60, and red 61-70%, respectively.

Table 8. Departures of different cases from Norm in SWA (km^2), ESI (%, Eq.9), salinity, temperature (^oC) and current (cm/s) averaged within one year after the model runs through the first year for full adjustment. SBD=bottom-surface for salinity, SBD=surface-bottom for temperature and current.

Case	SWA	ESI	Salinity		Temperature		Current	
			BOT	SBD	BOT	SBD	SUR	SBD
Norm	770	0	17.9	0.6	13.3	0.3	10.0	6.7
SLR1	+765	+24	+8.2	-0.6	+0.4	-0.2	-3.9	-3.1
SLR2	+723	+23	+8.0	-0.6	+0.5	-0.2	-4.2	-3.3
SLR3	+74	+7	+1.7	+0.1	-0.2	+0.1	+0.9	+0.7
Warm	+284	+1	+0.3	+.03	+3.0	+0.1	+.03	+0.1
HC1	-91	-8	-1.6	+0.3	-0.1	+0.1	+1.3	+0.9
HC2	-26	-2	-0.3	+.08	-.04	+.02	+0.4	+0.2
HC3	+46	+3	+0.5	-0.1	+0.1	-.03	-0.5	-0.3
Wind1	-8	-4	-0.7	-.01	+0.3	-.04	-0.3	-0.2
Wind2	+5	+3	+0.7	-.00	-0.2	+.01	+0.4	+0.2
Comb1	+1160	+22	+7.5	-0.6	+3.6	-0.2	-3.7	-3.0
Comb2	+1093	+21	+7.3	-0.6	+3.6	-0.2	-4.0	-3.1
Comb3	+314	+4	+0.6	+0.5	+2.6	+0.3	+2.5	+2.0

§4-5. Potential impact of the new physical conditions on oyster abundance

Environmental fluctuations and diseases are a crucial influence on oyster population abundance (e.g., Haskin and Ford, 1982; Powell *et al.*, 2008; Hofmann *et al.*, 2009; Mann *et al.*, 2009). The two fatal diseases, MSX and Dermo, multiply fast at higher temperature (above 18-20^{o}C) and higher salinity (above approximately 12) (reviewed in Ford and Tripp, 1996; Cook *et al.*, 1998). A warm and salty environment is highly positively correlated to MSX prevalence (Wang *et al.*, 2012). Dermo has influenced oyster abundance more and more since the late 1980s when oysters developed MSX-resistance (Ford and Bushek, 2012) and since 1990s when more river discharge has been input into the Bay to produce out-of-phase salinity and temperature (Wang *et al.,* 2012).

Unfortunately, a warming climate and SLR incur a warm and salty Delaware Bay. The major contribution to SWA is salinity in spring-summer-fall when the Bay is warmer than 12.5^{o}C and is temperature in spring and fall when temperature can be lower than 12.5^{o}C. Therefore cases SLR1 and SLR2 that change salinity the most and case Warm that changes temperature the most, as well as their combinations (Comb1, Comb2 and Comb3), will mainly influence SWA (Fig. 27H, SLR1 and SLR2, Comb1 and Comb2 have similar effects). As summarized in Table 8 and depicted in Figure 31, with SLR1 and SLR2, the SWA (normally ~770 km^2) will increase by 38% in SLR2 and 75% in Comb2. Case Warm increases SWA by 284 km^2 (or 37%) with the bottom water temperature increasing by ~3.0 ^{o}C.

On average, the oyster beds in the middle Bay located around the border of the salty-warm water in all the cases except the SLR associated cases (SLR1, SLR2, Comb1 and Comb2), as shown with the contours in Figure 31A. SLR or SLR plus warmer surface air will make the salty-warm water cover all oyster beds. In the regular case, the spring salinity around Egg Island, New Bed, and Bennies is below 17.5, the salinity around Cohansey and Arnolds is always below 17.5, and the spring temperature around all the oyster beds is below 12.5°C. However, SLR2 makes the salinity around all the oyster beds higher than 17.5 and makes the summer-fall temperature around all the oyster beds higher than 12.5°C. SLR2 plus Warm will make the temperature around all the oyster beds always higher than 12.5°C (Fig. 31B and C).

The contemporary Delaware Bay provides a particle (representing MSX and Dermo) transport mechanism from the lower Bay (e.g., at Leased Grounds) where the salinity and MSX prevalence are both high to the upper Bay (e.g., at Arnolds) where the salinity and MSX prevalence are both low (Wang *et al.*, 2012). SLR changes this circulation pattern. The communication between the oyster beds in the lower and upper Bay is limited.

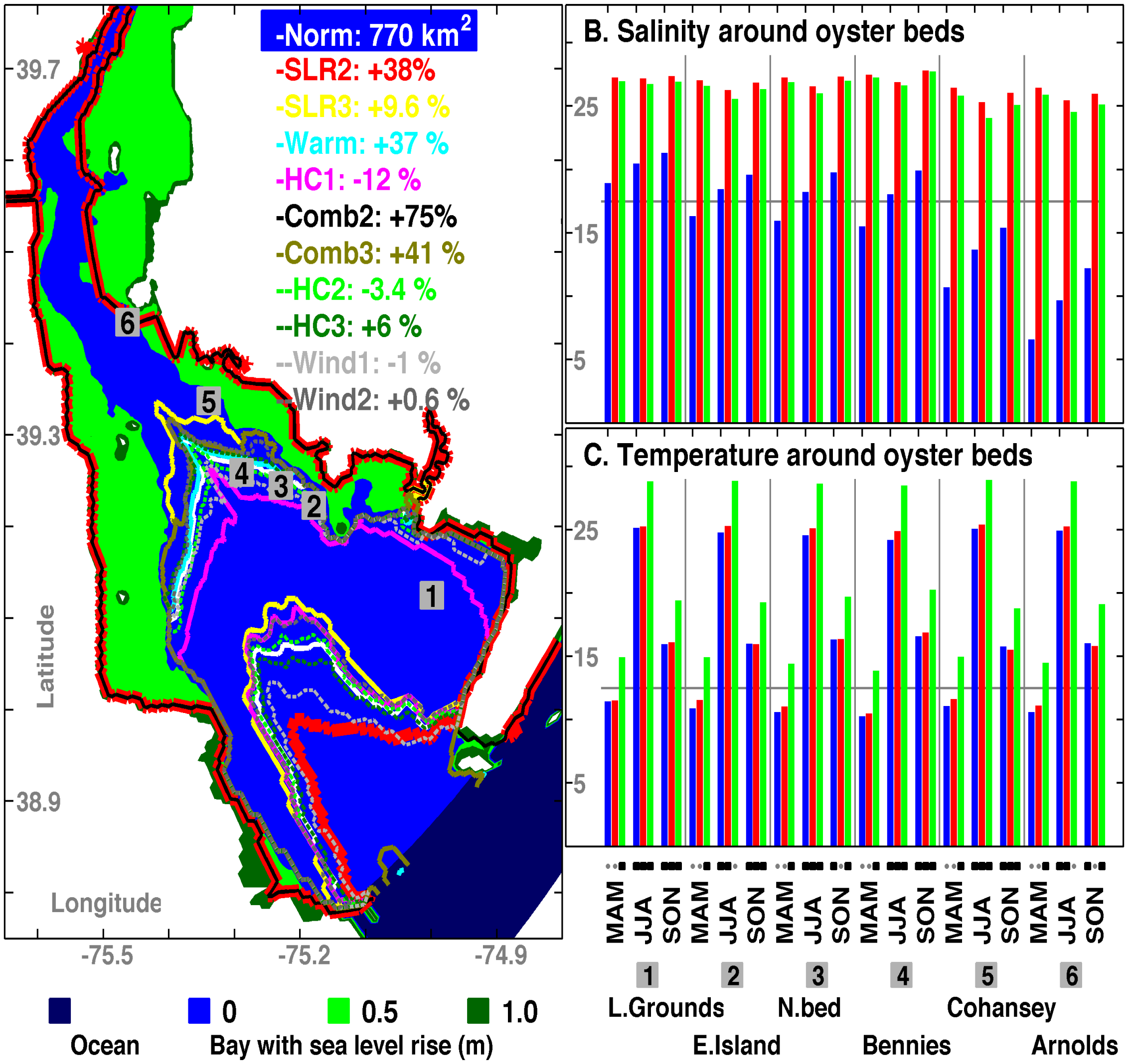

Figure 31. Simulated SWA, salinity and temperature averaged within year 2. **A**: SWA (km^2) for cases circled by color contours. For SLR2 and Comb2, the listed small/large SWA increment excludes/includes the SWA within the newly formed water. The gray squares with numbers indicate oyster beds. The dark blue, blue, green and dark green regions indicate ocean, Bay with 0, 0.5 and 1 meter SLRs, respectively. **B** and **C:** Seasonally averaged bottom salinity and temperature around the oyster beds for cases Norm (blue bars), SLR2 (red bars) and Comb2 (green bars). The gray dots/black squares below **C** indicate non-warm-salty/warm-salty seasons. Cases are as described in Table 7.

§4-6. Theoretical considerations

The biggest event in our experiment results is the SLR-induced estuary salinization, with the salinity being much higher in SLR (e.g., SLR2) than in Norm. This result simulated from a 3D nonlinear model can't be fully reproduced by simple theories. However, we expect that the current theoretical framework, though incomplete, e.g., using simple bathymetry and other idealized treatments, can partially explain our experiment results. For the changed and complicated geometry and bathymetry, our diagnostic numerical experiments are also indispensable to suggest the underlying mechanisms. As compared to Norm, SLR deepens the bathymetry and especially widens the geometry in the middle Bay that is changed from a narrow "pipe" into a wider "pool". The changed geometry and bathymetry in turn modify the salinity field.

§4-6-1. Theoretical explanation: SLR induced stronger SID

Assuming that the only mechanism responsible for the down-gradient salt flux is steady shear dispersion, the theory of Hansen and Rattray (1965), MacCready and Geyer (2010), and Monismith *et al.* (2002) gives the salt intrusion distance (SID), as follows:

$$SID = 0.024H^{8/3}\times\sqrt[3]{\frac{A\,g^2\,\beta^2\,S_{in}^2}{Q_{riv}\,K_M^2\,K_q}} \tag{10}$$

where, H and A are the depth (m) and cross-sectional area (m^2) at the estuary mouth, respectively. Q_{riv} is river input rate (m^3/s); S_{in} is the salinity of inflow from ocean; g$\approx 9.8m/s^2$, the Earth's gravitational constant; $\beta \approx 7.7\times10^{-4}$, the density-change rate with salinity; K_M/K_q the eddy viscosity/diffusivity (m^2 s^{-1}).

Giving the general and simplified relationships, Equation 10 may partially explain the intensified SID induced by SLR in that the SID increases sensitively with the water depth, cross-sectional area and salinity at the mouth, but decreases with the eddy viscosity and diffusivity at the mouth. SLR1 increases the depth/cross-sectional area of Delaware Bay by approximately 10%/14% (if the depth is the one for deep canal) at the mouth and should increase the SID by approximately 35% according to Equation 10 with other parameters fixed. However, this estimation is much smaller than our modeling results. By the numerical experiments (Fig. 29), the 18-isohaline intrudes approximately 60 and 130 km from the mouth for cases Norm and SLR1, respectively. SLR1 increases the SID by approximately 117% relative to that in Norm. Equation 10 explains approximately 30% SID. The left SID difference between Equation 10 and modeling of Delaware Bay is due to the following reasons.

One, Equation 10 is based upon steady shear dispersion that contributes approximately 20% (in Norm) to 49% (in SLR2) to salt flux on average (Fig.33), but for Delaware Bay with SLR, steady shear dispersion is not the major term for salt flux, advective salt flux dominates and tidal oscillatory salt flux also makes difference.

Two, Equation 10 is for estuaries of simple bathymetry and geometry, while the bathymetry and geometry of Delaware Bay vary spatially. SLR mainly enlarges the depth and cross-sectional area in the middle and upper Bay where their original values are very small, which should enlarge salt-intrusion further from the view implied in Equation 10. If the "mouth" is located at an upper place, e.g., 30 km from the mouth, where the depth and the cross-sectional area are enlarged more, the theoretical estimation will be larger: SID = 30km+SID1 (SID1 computed from Eq.10 at the upper place where the depth and cross-sectional area are close to those at the mouth). The depth used in Equation 10 should be for a rectangle mouth. But for Delaware Bay, SLR does not necessarily increase the "depth" used for Equation 10 if the depth is the averaged one.

Finally, in Equation 10 the SID decreases with the eddy viscosity and diffusivity at the mouth. SLR enhances mixing (see below for details) with increased eddy viscosity and diffusivity, which should reduce the SID. However, the enhanced mixing further changes the structure of salinity and induces higher salinity in the upper Bay. If the "mouth" is located at an upper place where the S_{in} is higher due to SLR, the theoretical estimation will be larger.

§4-6-2. Widened Bay enhances mixing, changing salinity structure and salt flux

Our model applies Mellor-Yamada level 2.5 scheme and k-kl parameters (Mello and Yamada, 1974, 1982; Warner *et al.*, 2005a.). Mixing intensity can be scaled by using the turbulent kinetic energy (TKE[2], Umlauf and Burchard, 2003).

We noticed that SLR1 and SLR2 produce identical effects on salinity structure (Fig. 29) and TKE (Figure omitted), with nearly the same geometry but different bathymetry. Norm and SLR3 do similarly. This implies that the width of the Bay matters most importantly to the salinity field in the middle Bay where its width is narrow in Norm but is widened substantially in SLR2. The stronger current difference between bottom and surface, representing current shear, in Norm than in SLR2 does not correspond to stronger TKE that, instead, is smaller in Norm than in SLR2 (Fig. 32A and B). The TKE-difference is from the width difference between the geometries of Norm and SLR2

---

[2] Equations of TKE, $E = \frac{1}{2}(\overline{u'^2} + \overline{v'^2} + \overline{w'^2})$ (m^2/s^2, per unit mass), driven by shear production, buoyancy production and dissipation (item 1, 2 and 3 in the right hand, respectively) is summarized as

$$\frac{\partial E}{\partial t} + u\frac{\partial E}{\partial x} + v\frac{\partial E}{\partial y} - \frac{\partial}{\partial z}\left(K_h\frac{\partial E}{\partial z}\right) = K_M\left[\left(\frac{\partial u}{\partial z}\right)^2 + \left(\frac{\partial v}{\partial z}\right)^2\right] + K_q\frac{g}{\rho_o}\frac{\partial \rho}{\partial z} - \frac{16.19431}{l}E^{3/2}$$

$where, u', v'$ and w' are components of turbulent fluctuations about the mean velocity (u, v, w along x-, y- and z-axes). ρ is sea water density (kg/m^3), ρ_o is the mean of ρ. g=9.8 m/s^2, the gravity constant.

in the middle Bay. The sea level rise cases, e.g., SLR2 increases the width in the middle Bay (30-80km from the mouth) substantially (by ~40-200%, Figs.32B). Consequently, the original middle Bay is not a narrow "pipe", but becomes a wider "pool". The TKE increases by ~5-50% in the middle Bay. The TKE difference significantly (confidence >= 95%) correlates to the width difference between cases SLR2 and Norm along the whole Bay with correlation coefficient = 0.68 (if only middle bad considered, 0.82 with 162 sample size) within year 1 and 2. Due to this increased mixing, the along-Bay salinity gradient reduced from ~31.9 in Norm to ~7.2 in SLR1 and SLR2 ($\times 10^{-5} m^{-1}$, Fig. 32A) and current shear (surface minus bottom current) are much smaller in SLR2 (~0.05 m/s) than in Norm (~0.2 m/s, Fig. 32A).

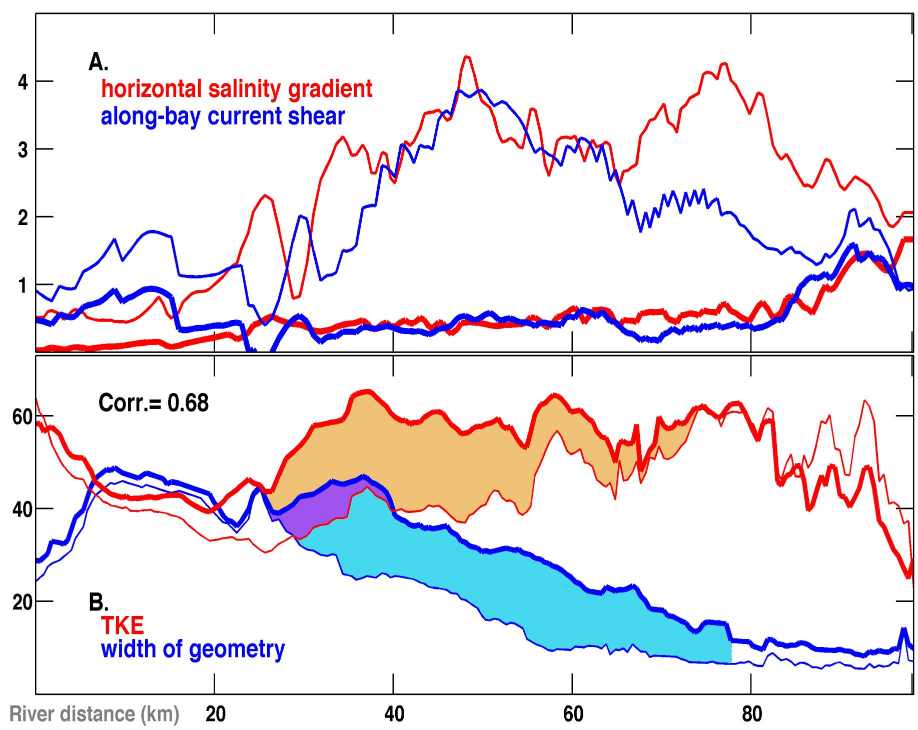

Figure 32. Widened geometry and mixing averaged across the Bay and within year 2. **A**. Along-Bay current shear expressed with current difference between bottom and surface (×0.1 m/s, blue) and horizontal salinity gradient (red). **B**. Along-Bay width (km, blue) and turbulent kinetic energy per unit mass (TKE, red) averaged within entire Bay and year 2. Thick/thin curves are for SLR2/Norm. Correlation is between TKE

and width in their SLR2-Norm differences along the Bay.

At a cross-section on *x-z* plane with a total cross-sectional area *A* (m^2, its tidally averaged value is A_o=<A>, d*A*=d*x* d*z* for a cell), the along-channel current (*V*, m/s) is decomposed into estuarine exchange flow (V_e, defined in Eq. 11), the net outflow ($V_0 = \frac{1}{A_o} < \iint vdA >$) due to river input and tidal current (V_t): $V = V_o + V_e + V_t$; and the salinity (*S*) is decomposed into the salinity for these current components as: $S = S_o + S_e + S_t$ ($S_0 = \frac{1}{A_o} < \iint SdA, S_e = \frac{<SdA>}{<dA>} - S_o$). The along-channel salt flux (F_s, kg/s) integrated at a cross-section is correspondingly decomposed into a steady shear dispersion (F_e) associated with the exchange flow that brings salt into the Bay, an advective term associated with the river outflow that brings salt out of the Bay, and a tidal oscillatory salt flux (F_t) that tends to bring salt into the Bay due to the out-of-quadrature salinity and velocity fields. These quantities are computed as below (Lerczak *et al.*, 2006; MacCready 2011; Aristizabal and Chant, 2013),

$$V_e(x,z,t) = \frac{<VdA>}{<dA>} - V_o \quad (11)$$

$$F_s(t) = \frac{\rho}{1000} < \iint_0^A V\, S\, dA >$$

(after omitting the small cross terms, MacCready 2011; Aristizabal and Chant, 2013)

$$\approx \frac{\rho}{1000} < \iint_0^A (V_o S_o + V_e S_e + V_t S_t)\, dA >$$

$$= F_o + F_e + F_t \quad (12)$$

where, changing with time (*t*) and location on *x-z* plane *V*, *S*, and ρ are the hourly-averaged simulated along-Bay speed (m/s), salinity (‰) and density (kg m^{-3}) at a cross-section, respectively. $F_o = \frac{-\rho}{1000} Q_{riv}\, S_o$ the net outflow due to river input. The brackets are sub-tidal low-pass filter (here Lanczos filter applied with a 32-hour cut-off period). The advective salt flux at a cross-section is influenced the along-estuary salinity gradient as shown in the one-dimensional, along-estuary salt conservation equation (Harleman and Thatcher 1974; Kranenburg 1986; Monismith et al. 2002; Lerczak, 2006):

$$A_o(y)\frac{\partial S_o}{\partial t} = \frac{\partial}{\partial y}[Q_{riv}\ \ S_o + A_o(y)K(y)\frac{\partial S_o}{\partial y}] \tag{13}$$

where, y is the along-estuary distance increasing in the upstream direction , S_o is the cross-sectional average salinity, and K is the along-estuary dispersion rate.

The advective term is the largest one in salt flux balance, as displayed in Figure 33 that depicts the exchange flow, salinity and salt fluxes in year2 where net total salt flux is approximately balanced: ~ -398 and 1021 kg/s in Norm and SLR2 (changing the mean salinity by ~ -0.9 and +2.1 within one year). The salt flux (Fig.33A) gains mainly through the flanks (much larger in Delaware Bay side than in New Jersey side) and loses mainly through area between the two flanks in Norm, but gains less in Delaware Bay side, more in New Jersey side, and loses less in a narrowed area between the two flanks in SLR2, with a narrowed salt-losing area but extended a salt-gaining area (Fig.33A). These patterns are mainly determined by the largest advective salt flux (Fig.33B) that is ~90% correlated with the total salt flux. With the weakened along-bay gradient in SLR2 (Fig. 32A; Eq. 13), the advective salt flux is lager in Norm (approximately -16182 kg/s integrated along the whole cross-section) than that in SLR2 (approximately -2153 kg/s). The smaller steady shear-dispersive salt flux in SLR2 is (Fig.33 C) is associated with the weakened shear in SLR2 (Fig. 32 A and Fig.33 E and F). The negative advective salt flux is approximately balanced by the positive steady shear dispersion and tidal oscillation of salt flux on average.

Intensified mixing reduces the salinity difference between inflow and outflow (i.e.,

S_{in}-S_{out}, where, S_{out} and S_{in} are the salinity of outflow and inflow at the mouth (Fig.33E). On average, there is a salinity-gradient on the cross-section at mouth with salinity changing from approximately 27.6/27.4 to 24/24.8 in Norm for year 1/year 2, but in SLR2 this gradient is weakened with higher salinity from approximately 28 to 25.6 for year 1, and further weakened in year 2 as from approximately 28.4 to 27.4. In the usually (in Norm) stratified Bay, the outflow is located at upper layer near the middle point between two flanks while the inflow takes lower layer. This cross-sectional structure of salinity and exchange flow in Norm maintains a regular salt exchange and salinity with, e.g., the inflow in Delaware side carrying fresher water into the Bay. In the well-mixed Bay with, e.g., SLR2, the cross-sectional structure of exchange flow is changed. Inflow in New Jersey side with higher salinity increases and outflow in Delaware side with lower salinity decreases, bringing more salt into the Bay during the adjustment phase. The salinity difference between inflow and outflow decreases and is much smaller in SLR2 than in Norm (0.77 and 0.26 in year1 and 0.50 and 0.05 on average). The salinity difference permits a significant exchange salt flux in year 1 where the net salt flux into the Bay is about 8000 kg/s (or ~250 million of tons per year) if averaged within year 1, but is too small to make a difference in salt exchange in year 2, limiting the salt flux across the mouth.

§4-6-3. A wider Bay facilitates exchange salt flux

There is an asymmetry in SID (Fig. 29), cross-Bay salinity and exchange flow (Fig.33F and Fig.34), with higher salinity, larger SID and stronger inflow in the New Jersey side than on the Delaware side. This asymmetry can be because of channel morphology. However, it is more asymmetrical in SLRs (e.g., SLR2) than in Norm. This difference can be explained from the geometric difference.

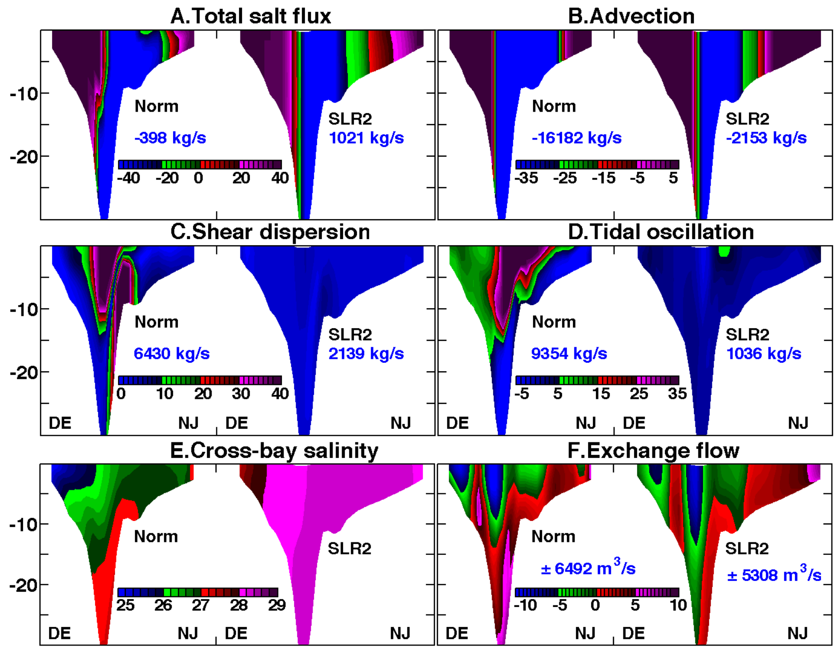

Figure 33. Salt fluxes, cross-Bay salinity and exchange flow, averaged within year 2 at mouth: Norm (left) and SLR2 (right, widened geometry). **A** and **B**. Total and advective salt fluxes (kg/s). **C**. Cross-Bay salinity. **D**. Exchange flow (cm/s) with the blue numbers are the totally integrated inflow/outflow (positive/negative, m^3/s). The blue numbers are the totally integrated salt flux (kg/s, in **A** and **B**) and flux (m^3/s, in **D**) along the whole cross-section. 1000 kg/s salt flux for one year is equivalent to salinity increment of approximate 2.33/2.07 of entire Bay in Norm/SLR2.

For the originally narrow middle and upper Bay, the freshwater from the upper Bay mostly meets directly with the saline oceanic water from the lower Bay to hinder the intrusion of the saline oceanic water, with along-bay salinity gradient and salinity stratification formed However, the freshwater from the upper Bay and the saline oceanic water from the lower Bay tend to slide bay each other in the SLR2-induced wider Bay especially under the Coriolis force. The salt-ridge distance is defined, as the cross-Bay length between the left bank and the highest-salinity location across the Bay, to represent the location of the saltiest inflow from the ocean. In SLR2 the salt-ridge distance can increase up to ~20 kilometers in the middle Bay, as compared to Norm.

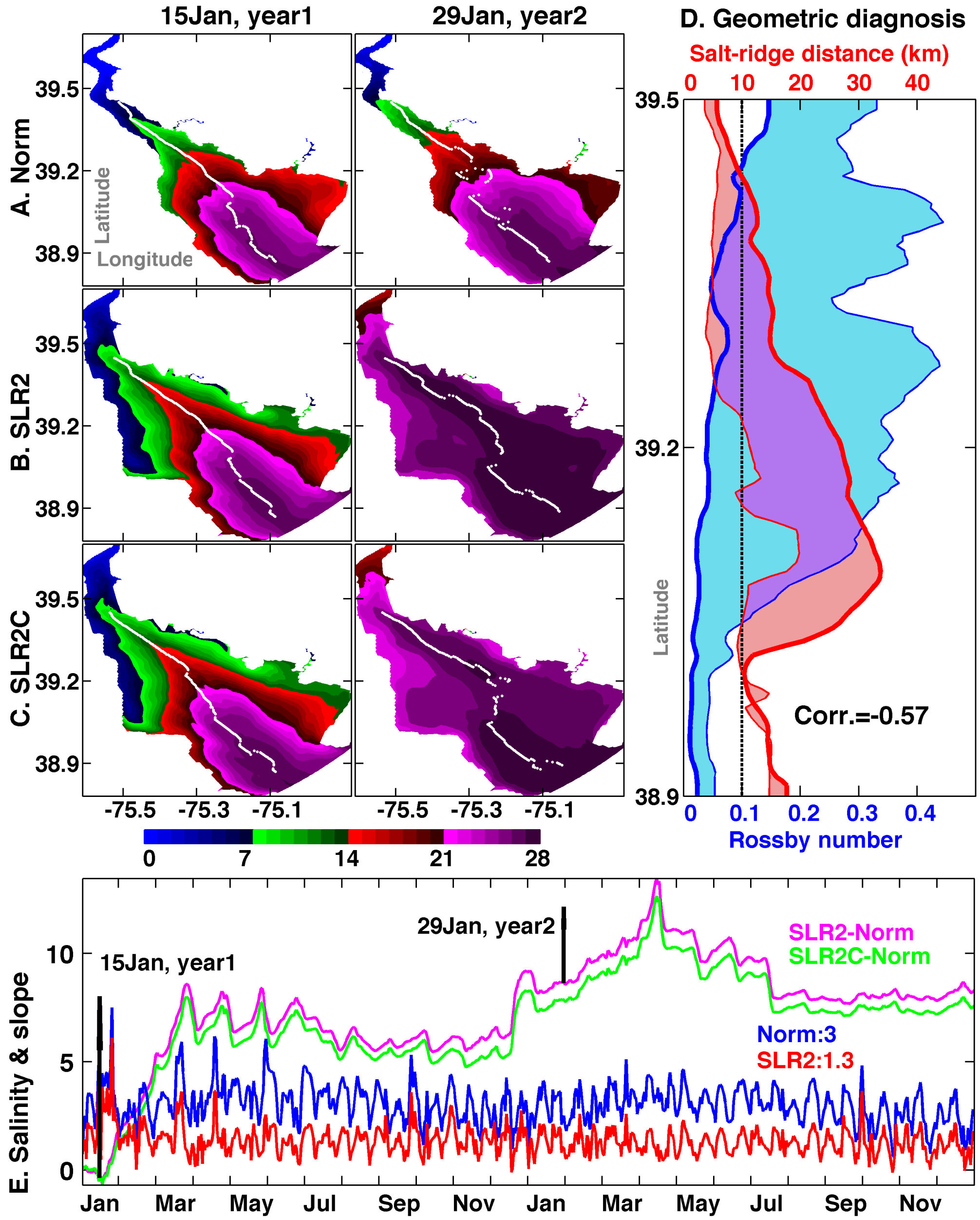

Figure 34. Salinity, sea surface slope and geometric diagnosis. **A**, **B** and **C**: Salinity field vertically averaged on 15 January, year 1 (left) and 29 January, year 2 (right), simulated in cases Norm, SLR2, and SLR2C, respectively. **D**: The along-Bay Rossby number (blue) and salt-ridge distance (km, red) for cases Norm (thin cures) and SLR2 (thick curves). The salt-ridge distance is defined as the cross-Bay length between the left bank and the highest-salinity location indicated by the white dots on column two and representing the location of the saltiest inflow from the ocean. The differences (SLR2 minus Norm) of Rossby number and salt-ridge distance are correlated with correlation coefficient -0.57 (confidence>95%, sample size=148). **E**: Salinity departure of cases SLR2 (magenta) and SLRC (green) relative to Norm as

well as surface slope ($\times 10^{-6}$) from Delaware to New Jersey sides averaged around the mouth (red/blue line for SLR2/Norm).

Speculations on Coriolis force and gradient force: We do not know how important Coriolis force is in the circilation. Rossby number ($R_o = U/f/width$, $f = 2\times 7.292\times 10^{-5}\times sin\varphi$ s^{-1}) is usually used to evaluate the relative importance of Coriolis force (e.g., Knauss, 2005): R_o<0.1, Coriolis force dominates, R_o>1, Coriolis force is omittable. If the width of the bay is used as the horizontal scale, R_o = 0.26 (0.04 ~ 0.50) for case Norm while R_o = 0.05 (0.01 ~ 0.16) for case SLR2, using averaged current in Norm and SLR2, respectively. The differences (SLR2 minus Norm) of Rossby number and salt-ridge distance are correlated with correlation coefficient -0.57 (confidence>95%, however, this correlation may be due to the width difference). If we turn off Coriolis force turned off from case SLR2 (case SLR2C), the salinity averaged in the entire Bay is lower in SLR2C than in SLR2 by only ~1. The widened geometry matters the most importantly as far as the salinity is concerned (Fig. 34 A to D). There is a sea surface slope from Delaware side toward the New Jersey side around the mouth, ~3.0 $\times$ 10^{-6} in Norm and ~1.30 $\times$ 10^{-6} in SLR2 on average. With this slope difference, the along-Bay geostrophic current toward the upper Bay should increase 18 cm/s in SLR2, as compared to that in Norm (Fig. 34E).

§4-7. Summary

Seventeen numerical experiments were carried out to explore the potential impacts on the physical environment of Delaware Bay from the climate changes in sea level, sea surface air temperature, hydrologic conditions, and sea surface winds. Our sensitivity experiments suggest that, as summarized in Figure 35: Delaware Bay should be vulnerable to a 50-100-cm SLR (with 2-m minimum depth required in modeling) that might intensify salt-intrusion and mixing to weaken along-Bay horizontal salinity gradient (with habitable and freshwater area consequently reduced) and that might enlarge the size (width, depth and volume) of the Bay to introduce more salt (~160-190 million tons) into the Bay. With SLR plus the warmer sea surface air, a salty-warm environment would be dominant in the Bay and be unfavorable to oysters because MSX and Dermo diseases might multiply fast under such a salty-warm environment. The SLR-induced salinization might not be offset by the predicted intensified hydrology with river flow. The biggest event in our experiment results is the SLR-induced estuary salinization, with the salinity being much higher and less sensitive to river flow due to much more salt contained in the Bay, compared to the salinity in the Bay without SLR. SLR (e.g., 50 cm, with 2-m minimum depth required in modeling) may deepen the bathymetry and especially widen the geometry in the middle Bay from a narrow "pipe" into a wider "pool", enhace mixing, and changing salinity via the advective salt flux and exchange flow, gaining salt during adjustment and maintaining high salinity state after adjustment via changing the structurte of salinity and circulation.

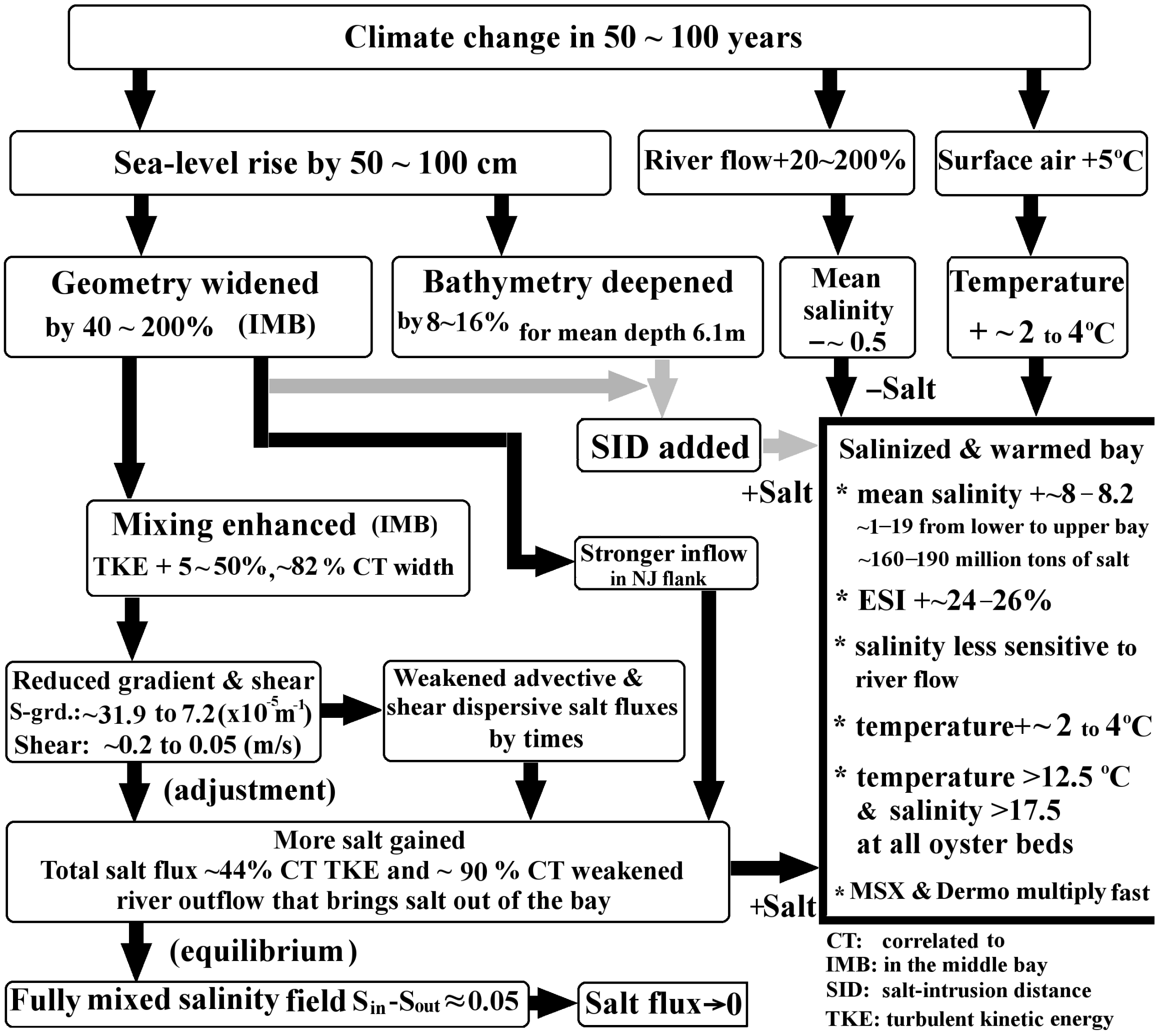

Figure 35. Diagram for climate-change-induced salinized and warmed Delaware Bay. The gray arrows indicate a presumed relationship.

§5. Summary and discussion

Delaware Bay plays important roles in providing biota and fresh-water resource. Its physical environment is highly sensitive and therefore vulnerable to climate changes in SLR, temperature, and hydrology. The largely unknown physical environment (i.e., tracers and circulation) and less numerical modeling in the Bay leave much room for modeling studies. In this study, we develop, validate and apply high-resolution hydro-dynamical model for Delaware Bay using more realistic physics of control equations, dynamical and thermo-dynamical forcing, initial and boundary conditions, and other information missed by theoretical studies, hindcast the largely unknown physical environment of the Bay, study the roles of the physical environment influencing MSX infection prevalence (MSXP), and explore into the future fate of the Bay in response to climate changes.

A series of experiments and data analysis were carried out to determine model parameters (e.g., the resolution, boundary and initial conditions, advection and mixing schemes, bottom friction, the input of heat fluxes, and water type) for the shallow, highly thermally and dynamically sensitive, turbid, and tidal dominated Delaware Bay. The model is driven by tide, hydrologic inputs from six rivers located at middle and upper Bay, and atmospheric forcing of momentum, heat and moisture. The model validation against intensive *in situ* datasets in the years 2000 and 2010-2011 ensures the model to have significant skill in predicting variations in tracers and circulation. The multiple statistical evaluations applied here show the model to have high simulation scores: no drift with time, small systematic biases, proper standard deviations, accurate phases and amplitudes, and correct spatial and temporal structure, as compared between simulations and observations.

The implemented model is applied to inquire into the relationships between water properties and the observed MSXP. To quantify the relationship between observed MSXP and concurrent physical conditions in the Bay, simulations of circulation and tracers in Delaware Bay were performed for five multi-year periods (1974-76, 1979-81, 1984-86, 1990-92, and 2006-09) that displayed different combinations of MSXP and environmental conditions. Subsequent statistical analysis was used to explore the connections between MSXP and (*e.g.*) salinity, temperature and particle transport. Results from the correlation analysis suggest that MSXP may be related to multiple physical factors, depending on location and time of year: An effective upper Bay transport mechanism, river flow, salinity, temperature and salty-warm area (SWA). The negative river flow/salinity and positive river flow/temperature correlations decide a negative temperature/salinity correlation to make the warm and salty condition rarely occur and to help control MSX in the Bay. The reduced MSXP and intensified river flow coincide with the intensified warming during 1993-2009, implying that the intensified warming climate might partially constrain MSX infection by maintaining a Bay with out-of-phase salinity and temperature via providing more river flow into the Bay and reducing the salinity in the Bay.

However, for the Bay to function well to provide proper physical environment, e.g., medium salinity (not too salty) and the negatively correlated temperature and salinity, as the Bay mostly did, needs two important conditions: (1) the precipitation and /or ice-snow melting positively respond to air temperature to decide a positive temperature/river discharge correlation (as was 36~68% positively correlated), and (2) the Bay is sensitive enough to make its salinity negatively respond to freshwater input (as was 59~87% negatively correlated) and its temperature positively respond to air temperature on a short-range climate scale (monthly and seasonally, as was ~98% positively correlated). The persistently drier and warmer Bay in 1984-86 shows an "irregular climate" where MSX was most prevalent, with both temperature and salinity being persistently higher, though not the highest. Will the future climate provide a regular or an irregular climate background for Delaware Bay?

Suggested by our above studies, we inquire into the impacts on physical environment in Delaware Bay from the future climate changes with sensitivity experiments carried out under the climate changes in sea level, sea surface air temperature, hydrologic conditions, and sea surface winds. Our sensitivity experiments suggest that SLR and climate warming may substantially change the original Bay in salinity, temperature and circulation. There are many estuaries similar with Delaware Bay and might be vulnerable to SLR and climate warming.

Our experiments indicated that a fixed coastline, e.g., with a man-made bank in the upper Bay, would substantially mitigate the salinization induced by the SLR but enhance the stratifications of salinity, temperature, and current mainly in the lower Bay (SLR1 and SLR3). Also, to avoid dredging in the lower Bay is also to mitigate the salinization, but in a minor extent (SLR1 and SLR2 and Norm).

The predicted climate may be inaccurate and there are no future data available for us to validate the model according to those future data and the future climate mode. What we can do for reducing the uncertainty is to keep a conservative room for SLR and to use uniform modeling standard in modeling (e.g., with same initial conditions and minimum water depth) and in comparison among cases. Our validated model uses a 2-meter minimum depth that extends to land mask. For all cases, this standard is kept intact for fair. 2-meter minimum depth is required for model to run smoothly and is validated using extensive modern data (I designed a model with even higher resolution and ran with very short time step, which permits a 1-m minimum depth. However, the tidal effect on current and salinity would be weakened with this small minimum depth. Wet-dry scheme is under consideration, but mixing enhancement mainly occurred in spring tide when the water still extends much to minimize the influence from "wet-dry" bathymetry, according to our experiments). If we use a bathymetry that is exactly same as that in Norm, but the coastline is extended to the location same as that in SLR2, the Bay is salinized with the widen geometry, though the shallower depth (0.5 meter less) reduces some salt-intrusion and salinity. If we start from a fresher Bay with zero salinity in the newly formed water, the Bay is still salinized. The larger salinity contrast accelerates the salt exchange and eventually makes the Bay a little bit saltier (Fig. 36). The influences on bathymetry from geological processes (e.g., sediment and sinking) and extreme weather were not included or omitted on a 50-100 year temporal scale. The real gradual SLR would provide much longer adjustment phase than that in the modeling. However, the salinization is caused by widened geometry via enhanced mixing (and probably Coriolis effect). In both adjustment and equilibrium phases, the width of the Bay highly correlates to mixing. The key for salinization is SLR-induced widened geometry, independent the adjustment process.

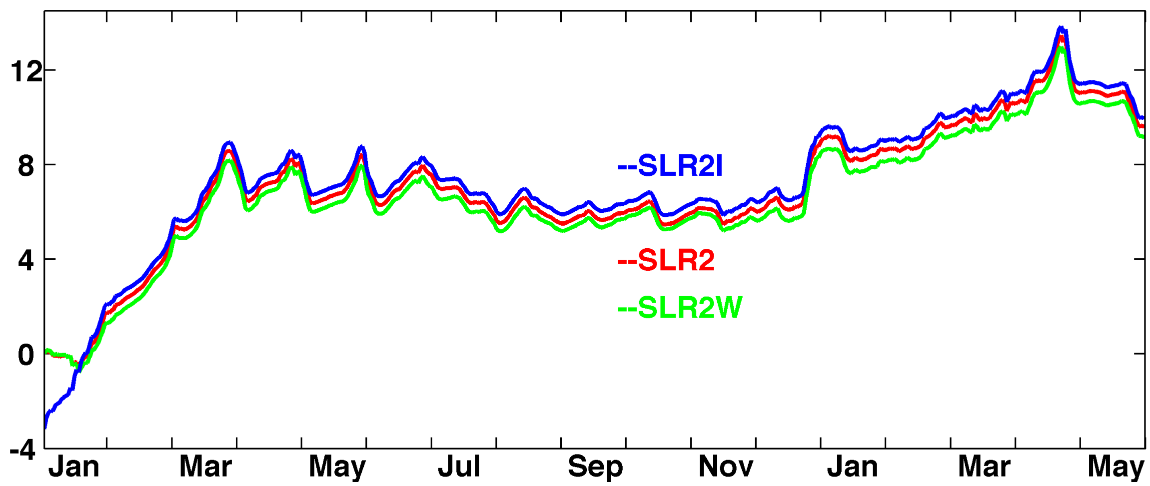

Figure 37. Salinity under further testing circumstances of SLR2, SLR2I and SLR2W (listed in Table 7), with simulated salinity departures averaged within Delaware Bay for the cases SLR2.

Based on the availability of high-resolution topography, seventeen such estuaries including thirty-five Bays were selected along the U.S. coast (Tab. 9). All the Bays have a shallow depth (mean depth<7 meters), small volume (<7.6 km^3 except Chesapeake Bay having a volume of ~67 km^3), and narrow geometry. 50-100 cm SLR will substantially widen their geometry, deepen their depth (>14% their mean depth) and enlarge their volume (19% for Chesapeake Bay, >35% for others). Baffin, Alazan, Copano, Mission, Port, Mud, Winyah, Albemarle, and Chesapeake (Fig. 38) are the representative ones where salinization might occur.

Table 9. SLRs and the sizes of the estuaries picked along the U.S. coast. Seventeen estuaries including thirty-five Bays were selected along the U.S. coast where high-resolution topography are available based on gridded 3-second database provided by the National Geophysical Data Center (NGDC) U.S. Coastal Relief Model. Global gridded 2-minute database from the NGDC U.S. Department of Commerce are also applied here to compute the size of global water and land.

Estuaries along U.S. coast	SLR = 0			SLR = 0.5 m		SLR = 1 m		SLR = 2 m		SLR = 3 m	
	Depth (m) Max/mean	Vol. 10^9 m^3	Area 10^9 m^2	Vol. +%	Area +%	Vol. +%	Area +%	Vol. +%	Area +%	Vol. +%	Area +%
A. North	**12.5/0.7**	**0.16**	**0.218**	**69**	**2**	**141**	**12**	**294**	**15**	**454**	**19**
B. Willapa	**19.0/2.1**	**0.77**	**0.367**	**24**	**2**	**49**	**6**	**100**	**11**	**154**	**17**
C. Tillamook	**0.9/0.2**	**0.01**	**0.037**	**222**	**7**	**459**	**26**	**103**	**46**	**1685**	**61**
D. Coos	**6.3/0.2**	**0.01**	**0.043**	**246**	**12**	**518**	**23**	**113**	**39**	**1819**	**56**
E. Arcata[e+]	**0.1/0.1**	**0.01**	**0.067**	**533**	**10**	**1120**	**60**	**285**	**94**	**4941**	**139**
F. San Pablo[f+]	**87.4/2.4**	**6.05**	**2.533**	**21**	**7**	**44**	**28**	**99**	**50**	**163**	**65**
G. Baffin[g+]	**2.9/1.3**	**0.26**	**0.203**	**39**	**7**	**81**	**32**	**186**	**54**	**309**	**112**
H. Copano[h+]	**5.9/1.3**	**0.90**	**0.716**	**40**	**3**	**82**	**23**	**181**	**49**	**304**	**86**
I. Lavaca[i+]	**12.5/1.1**	**0.33**	**0.293**	**45**	**4**	**92**	**21**	**202**	**45**	**336**	**123**
J. Galveston[j+]	**16.0/1.5**	**1.87**	**1.266**	**34**	**2**	**69**	**18**	**149**	**27**	**235**	**39**
K.Tampa[k+]	**15.7/2.8**	**3.19**	**1.145**	**18**	**3**	**37**	**8**	**76**	**35**	**126**	**59**
L. Mud[l+]	**17.1/1.2**	**0.19**	**0.158**	**41**	**6**	**85**	**22**	**188**	**54**	**319**	**127**
M. Buzzard	**14.2/1.5**	**0.17**	**0.119**	**35**	**12**	**74**	**28**	**166**	**52**	**273**	**74**
N. Stones	**5.3/1.4**	**0.13**	**0.099**	**38**	**8**	**79**	**17**	**170**	**39**	**278**	**57**
O. Albemarle	**13.1/1.6**	**7.56**	**4.879**	**32**	**2**	**65**	**20**	**144**	**39**	**234**	**74**
P.Chesapeake	**112.7/6.3**	**73.61**	**11.67**	**10**	**34**	**21**	**35**	**43**	**40**	**66**	**45**
Q.Delaware	**46.7/6.4**	**13.19**	**2.056**	**12**	**53**	**24**	**55**	**49**	**63**	**75**	**72**
Area change of global water (+) and land (-)	km^2			**140,740**		**232,750**		**2,447,600**		**2,763,300**	
	% (to total area*)			**0.0276**		**0.0456**		**0.4799**		**0.5418**	

e+, Humboldt and South; f+, San Rafeel and San Francisco; g+, Alazan; h+, Mission and Port; i+, Cox, Keller, Chocolate and Carancahua; j+, Trinity and East; k+, Hillsborough, East, McKay and Terra Ceia; l+, Winyah. * **361,320,000 (water area) + 148,740,000 (land area)** km^2.

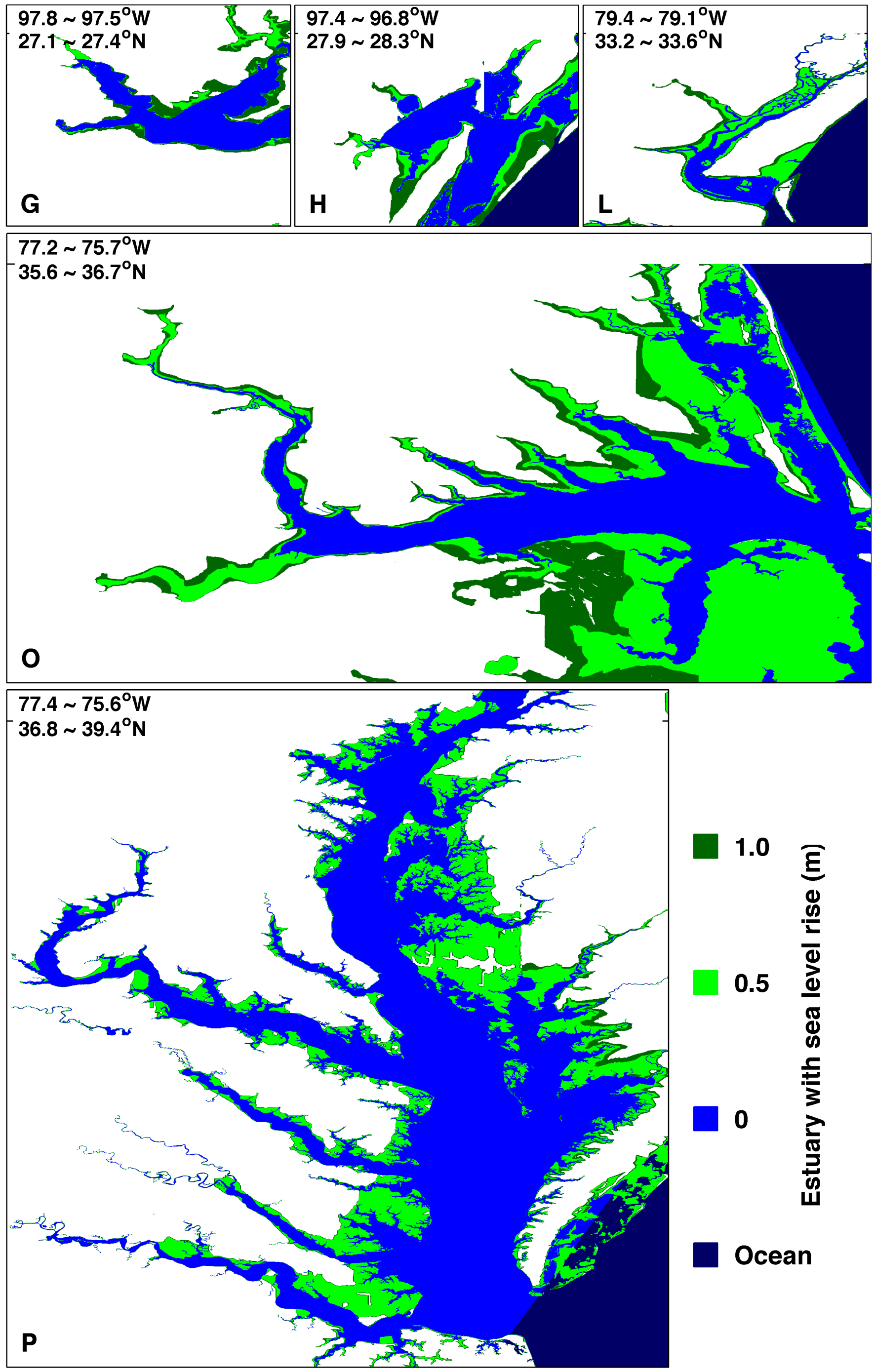

Figure 38. SLRs and the sizes of five estuaries similar to Delaware Bay. The estuaries plotted in **G, H, L, O** and **P** are listed the Table 9 and their longitudes and latitudes are given in the upper corner. Gridded 3-second database used here is from the National Geophysical Data Center U.S. Coastal Relief Model.

References

Adler, R.F., et al., 2003: The version 2 Global Precipitation Climatology Project (GPCP) monthly precipitation analysis (1979-present). *J.Hydrometeorl.,* **4**, 1147-1167.

Andrews, J. D., 1983. *Minchinia nelsoni* (MSX) infections in the James River seed-oyster area and their expulsion in spring. Estuar. Coast. Shelf Sci., *16*, 255-269.

Andrews, J. D., 1966. Oyster mortality studies in Virginia V. Epizootiology of MSX, a protistan pathogen of oysters. Ecology 47:19-31.

Andrews, J. D., 1964. Oyster mortality studies in Virginia. IV. MSX in James River public seed beds. Proc. Nat. Shellfish. Assoc., *53*, 65-84.

Arakawa, A., and V. R. Lamb, 1977. Computational design of the basic dynamical processes of the UCLA general circulation model. *Methods in Computational Physics* , 17 , Academic Press, New York, pp. 173-265.

Aristizabal, M. and R. Chant, 2013. A Numerical Study of Salt Fluxes in Delaware Bay Estuary. *J. Phys. Oceanogr.* **43** (8), p1572DOI: 10.1175/JPO-D-12-0124.1

Austin, H., D.S. Haven and M.S. Moustafa, 1993. The relationship between trends in a condition index of the American oyster, *Crassostrea virginica,* and environmental parameters in three Virginia estuaries. Estuaries 16:362-374.

Bernstein, *et al.* (IPCC Core Writing Team), 2007: Climate Change 2007: Synthesis Report – Summary for Policymakers. Pp.23 in Intergovernmental Panel on Climate Change Fourth Assessment Report.

Burrell, V.G., M.Y. Bobo and J.J. Manzi. 1984. A comparison of seasonal incidence and intensity of *Perkinsus marinus* between subtidal and intertidal oyster populations in South Carolina. J. World Mariculture Soc. *15*, 301-309.

Burreson EM, Stokes NA, Friedman CS, 2000. Increased virulence in an introduced pathogen: Haplosporidium nelson (MSX) in the eastern oyster Crassostrea virginica. *J Aquat An Health,* **12**, 1-8.

Cahill, B., O. Schofield, R. Chant, J. Wilkin, E. Hunter, S. Glenn, and P. Bissett, 2008. Dynamics of turbid buoyant plumes and the feedbacks on near-shore biogeochemistry and physics, *Geophys. Res. Lett., .* **35**, L10605, doi:10.1029/ 2008GL033595.

Chant, R., J. Wilkin, W. Zhang, B. Choi, E. Hunter, R. Castelao, S. Glenn, J. Jurisa, O. Schofield, R.

Houghton and J. Kohut. 2008. Synthesis of observational and numerical studies during LaTTE. *Oceanography,* **21**: 70-89.

Chant, R., W. Geyer, *et al.*, 2007. Estuarine boundary layer mixing processes: insights from dye experiments. *J. Phys. Oceanogr.*, **37**, 1859−1877.

Chapman, D.,1987. Application of wind-forced, long, coastal-trapped wave theory along the California coast. *Journal of Geophysical Research* **92**: 1798-1816.

Chelton, D.B. 1983. Effects of sampling errors in statistical estimation. Deep-Sea Res., *30*, 1083-1101.

Chen, M., P. Xie, and J.E. Janowiak, 2002: Global land precipitation: a 50-yr monthly analysis based on gauge observations. *J. Hydrometeorl.,* **3**, 249-266.

Chen, S. N., and L. P. Sanford, 2009.Axial wind effect on shear and longitudinal salt transport in an idealized, partially mixed estuary. *J.Phys. Oceanogr.,* **39**, 1905-1920.

Church, J.A. and N.J. White, 2006: A 20th century acceleration in global sea-level rise. *Geophys. Res. Lett.,* **33**, L01602, doi: 10.1029/2005GL024826.

Cook, T., M. Folli, J. Klinck, S. Ford, J. Miller, 1998. The Relationship Between Increasing Sea-surface Temperature and the Northward Spread of Perkinsus marinus (Dermo) Disease Epizootics in Oysters.Estuarine, *Coastal and Shelf Science*, **46** (4), 587–597.

Copper, J.A.G., and F. Navas, 2004. Natural bathymetric change as a control on century-scale shoreline behaviour. *Geology*, **32**, 513-561.

Crosby, M.P. and C.F. Roberts. 1990. Seasonal infection intensity cycle of the parasite *Perkinus marinus* (and an absence of *Haplosporidium* spp.) in oysters from a South Carolina salt marsh. *Diseases of Aquatic Organisms*, **9**, 149-155.

Curchitser, Enrique N.,Dale B. Haidvogel, Albert J. Hermann, Elizabeth L. Dobbins, Thomas M. Powell, and Alexey Kaplan, 2005. Multi-scale modeling of the North Pacific Ocean: Assessment and analysis of simulated basin-scale variability (1996-2003). *J. Geophys. Res.,* **110**, C11021, doi:10.1029/2005JC002902.

Davis, G.H., 1987. Land Subsidence and Sea-level Rise on the Atlantic Coastal. *Plain of the United States*.

Davis, R.E., 1976. Predictability of sea surface temperature and sea level pressure anomalies over the North Pacific Ocean. *J. Phys. Oceanogr.*, **6,** 249-266.

Davis, R.E., 1978. Predictability of sea level pressure anomalies over the North Pacific Ocean. *J. Phys. Oceanogr.*, **8,** 233-246.

DiLorenzo J.L., Huang, P-S., Thatcher, M.L.,and Najarian, T.O., 1994. Dredging Impacts on Delaware Estuary Tides, American Society of Civil Engineers, *J. of Waterway, Port, Coastal, and Ocean Engineering,* 86-104.

Divins, D.L. and D. Metzger, 2009. National Geophysical Data Center (NGDC) Coastal Relief Modeldata (http://www.ngdc.noaa.gov/mgg/coastal/coastal.html). Data sources include the US National Ocean Service Hydrographic Database, the US Geological Survey (USGS), Monterey Bay Aquarium Research Institute (MBARI), US Army Corps of Engineers LIDAR (SHOALS), and various other academic institutions.

Durski, S.M., S.M. Glenn, D.B. Haidvogel, 2004. Vertical mixing schemes in the coastal ocean: Comparison of the Level 2.5 Mellor-Yamada scheme with an enhanced version of the K-profile parameterization. *J. Geophys. Res.,* **109**Issue: C1, P C01015.

Emery, W.J. and R. E. Thomson. 1998. Data Analysis Methods in Physical Oceanography, Greg Publishing., first Edition, 634pp.

Ford, S.E., 1985. Effects of salinity on survival of MSX parasite *Haplosporidium nelsoni* (Haskin, Stauber, and Mackin) in oysters. *J. Shellfish Res.*, **5**, 85-90

Ford, S. E. and H. H. Haskin. 1982. History and epizootiology of *Haplosporidium nelsoni* (MSX), an oyster pathogen, in Delaware Bay, 1957-1980. *J. Invertebrate Pathology*, **40**, 118-141.

Ford, S.E. and M.R. Tripp, 1996. Disease and Defense Mechanisms. In: Newell, R.I.E., Kennedy, V.S., and Eble, A.F. (Eds.), The Eastern Oyster: *Crassostrea virginica* . Maryland Sea Grant College, College Park, Maryland, pp. 383-450.

Ford, S.E and D. Bushek, 2012 . Development of resistance to an introduced marine pathogen by a native host. *J. Mar. Res.,* **70**, 205-223.

Ford, S. E., B. Allam and Z. Xu, 2009. Using bivalves as particle collectors and PCR detection to investigate the environmental distribution of *Haplosporidium nelsoni*., *Dis. Aquatic Org*. **83**, 159-168.

Garvine, R.W., 1995. A dynamical system for classifying buoyant coastal discharges. *Continental Shelf Research*, **15**, 1585−1596.

Garvine, R.W., 1991. A dynamical system for classifying buoyant coastal discharges. *Cont. Shelf Res.,* **15**, 1585-1596.

Gornitz, V., 1995: A comparison between recent and late Holocene sea-level trends from eastern North America and other selected regions. *J. Coastal Res.*, **17**, 287–297.

Gornitz, V. and Seeber, 1990, Vertical crustal movements along the East Coast, North America, from historic and late Holocene sea-level data. L. *Tectonophysics* **178**, 127−150.

Haidvogel, D. B. and R. Chant, 2012. Hydrodynamics of Coastal Circulation: Handbook of Environmental Fluid Dynamics (in press).

Haidvogel, D. B., H. Arango, W.P. Budgell, B.D. Cornuelle, E. Curchitser, E.Di Lorenzo, K. Fennel, W.R. Geyer, A.J. Hermann, L. Lanerolle, J. Levin, J.C. McWilliams, A.J. Miller, A.M. Moore, T.M. Powell, A.F. Shchepetkin, C.R. Sherwood, R.P. Signell, J.C. Warner, J. Wilkin, 2008. Ocean forecasting in the terrain-following coordinates: Formulation and skill assessment of the Regional Ocean Modeling System. *J. Computational Physics,* **227**, 3595-3624.

Haidvogel, D.B., H.G. Arango, K. Hedstrom, A. Beckmann, P. Malanotte-Rizzoli, and A.F. Shchepetkin, 2000. Model Evaluation Experiments in the North Atlantic Basin: Simulations in Nonlinear Terrain-Following Coordinates. *Dynamics of Atmospheres and Oceans*, **32**,239-281.

Hansen, D. V. and M. Rattray, 1965. Gravitational circulation in straits and estuaries. *J. Mar. Res.*, **23**, 104-122.

Harleman, D. R. F., and M. L. Thatcher, 1974: Longitudinal dispersion and unsteady salinity intrusion in estuaries. Houille Blanche, 1/2, 25–33.

Haskin, H. H. and J. D. Andrews. 1988. Uncertainties and speculations about the life cycle of the eastern oyster pathogen *Haplosporidium nelsoni* (MSX), *in* Disease Processes in Marine Bivalve Molluscs, Fisher, W. S., ed., American Fisheries Society, 5-22.

Haskin, H. H., and S. E. Ford. 1982. *Haplosporidium nelsoni* (MSX) on Delaware Bay seed oyster beds: a host-parasite relationship along a salinity gradient. *J. Invertebrate Pathology*, **40**, 388-405.

Haskin H.H., Stauber L.A., Mackin J.A., 1966. *Minchinia nelsoni* n. sp. (Haplosporida, Haplosporidiidae): causative agent of the Delaware Bay oyster epizootic. *Science,* **153**, 1414-1416

Hofmann,E., D.Bushek, S.Ford, X.Guo, D.Haidvogel, D.Hedgecock, J.Klinck, C.Milbury, D.Narvaez, E.Powell, Y.Wang, Z.R.Wang, J.Wilkin, L.Zhang, 2009. Understanding How Disease and Environment Combine to Structure Resistance in Estuarine Bivalve Populations. *Oceanography,* **22** (4), 212-231.

Holton, James R. 1992.An Introduction to Dynamic Meteorology (3rd edition). Academic Press.

Kanarska, Y., A. Shchepetkin, J.C. McWilliams, 2007. Algorithm for non-hydrostatic dynamics in the Regional Oceanic Modeling System. *Ocean Modelling,* **18**, 143-174.

Knauss, J.A. (2005), An Introduction to Physical Oceanography, 2nd Ed., *Waveland Press. Inc.*, pp309.

Kasai, A., A.E. Hill, T. Fujiwara, and J.H. Simpson, 2000. Effect of the earth's rotation on the circulation in region of freshwater influence. *J. Geosphys. Res.*, **105**, 16,961-16,969.

Kranenburg, C., 1986: A time scale for long-term salt intrusion in well-mixed estuaries. J. Phys. Oceanogr., 16, 1329–1331.

Lemke, P., J.Pen, R.B.Alley, I.Allison, J.Carrasco, G.Flato, Y.Fujii, G.Kaser, P.Mote, R.H.Thomas and T.Zhang, 2007: Observations: Changes in Snow, Ice and Frozen Ground. In: Climate Change (2007), The Physical Science Basis. Contribution of Working Group I to the Fourth Assessment Report of the Intergovernmental Panel on Climate Change [Solomon, S., D.Qin, M.Manning, Z.Chen, M.Marqis, K.B.Averyt, M.Tignor and H.L.Miller (eds.)]. Cambridge University Press, Cambridge, United Kingdom and New York, NY, USA.

Lerczak, J.A. and W. R. Geyer, 2006. Mechanisms driving the time-dependent salt flux in a partially stratified estuary. *J. Phys. Oceanogr.*, **36**, 2296−2311.

Lerczak, J.A. and W. R. Geyer, 2004. Modeling the lateral circulation in straight, stratified estuaries. *J. Phys. Oceanogr.*, **34**, 1410−1428.

Lerczak, J. A., W. R. Geyer, and R. J. Chant, 2006. Mechanisms driving the time dependent salt flux in a partially stratified estuary. *J. Phys. Oceanogr.*, **36,** 2296-2311.

Littlewood, D.T.J. and S.E. Ford. 1990. Physiological responses to acute temperature elevation in oysters, *Crassostrea virginica* (Gmelin, 1791), parasitized by *Haplosporidium nelsoni* (MSX) (Haskin, Stauber, and Mackin, 1966). *J. Shellfish Res.*, ***9***,159-163.

Lutjeharms, J.R.E., P. Penven, and C. Roy, 2003. Modeling the shear edges of the southern Agulhas Current. *Continental Shelf Res.,* **106**, 7183-7192, 0148-0227/2000JD900719.

MacCready, P., 2007. Estuaries adjustment. *J. Phys. Oceanogr.*, **37**, 2133−2145.

MacCready, P., 2004. Toward a unified theory of tidally-average estuarine salinity structure. *Estuaries,* **27**, 561-570.

MacCready, P. and W.R. Geyer, 2010. Advances in Estuarine Physics. Annu. *Rev. Mar. Sci*., **2**, 35-58.

MacCready, P. and W.R. Geyer, 2001. Estuarine salt flux through an isohaline surface. *J. Geosphys. Res*, **106**, 11629-11637.

Mann, R., M. Southworth, J.M. Harding and J.A. Wessson. 2009. Population studies of the native Eastern oyster, *Crassostrea virginica,* (Gmelin, 1971) in the James River, Virginia, USA. *J. Shellfish Res.*, **28**, 193-220.

Marchesiello, P., J.C. McWilliams, and A. Shehepetkin, 2001. Open boundary conditions for long-term integration of regional ocean models, *Ocean Modell.*, **3**, 1-20.

McCabe, G.J. and M.A. Ayers, 1989. Hydrologic effects of climate change in the Delaware River Basin. *Water Resour Bull*, **25**, 1231-1242.

McLean, R.F., and J.-S. Shen, 2006. From foreshore to fordune: Foredune development over the last 30 years at Moruya Beach, New South Wales, Australia. *J. Coastal Res.*, **22,** 28-36.

Mellor,G.L. and T. Yamada, 1982. Development of a turbulent closure model for geophysical fluid problems. *Reviews of Geophysics and Space Physics,* **20**, 851-875.

Mellor, G. L.   and T. Yamada. A hierarchy of turbulence closure models for planetary boundary layers. J. Atmos. Sci., 31:1791–1806, 1974.

Melsom, A., V.S. Lien, and W.P. Budgell, 2009. Using the Regional Ocean Modeling System (ROMS) to improve the ocean circulation from a GCM 20^{th} century simulation. *Ocean Dynamics*, **59**, Issue 5.

Mesinger, F., G. DiMego, E. Kalnay, K. Mitchell, P. C. Shafran, W. Ebisuzaki, D. Jovi, an, J. Woollen, E. Rogers, E. H. Berbery, M. B. Ek, Y. Fan, R. Grumbine, W. Higgins, H. Li, Y. Lin, G. Manikin, D. Parrish, and W. Shi, 2006. North American Regional Reanalysis, *Bulletin of the American Meteorological Society*, **87**(3), 343-360.

Mitchell, T.D., and P.D.Jones, 2005. An improved method of constructing a database of monthly climate observations and associated high-resolution grids. *Int. J.Climatol.,* **25**, 693-712.

Monismith, S. G., W. Kimmerer, J. R. Burau, and M. T. Stecey, 2002. Structure and flow-induced variability of subtidal salinity field in northern san francisco bay. *J. Phys. Oceanogr.*, **32**, 3003.

Najjar, R.G., L.Patterson, and S.Graham, 2009. Climate simulations of major estuarine watersheds in the Mid-Atlantic region of the US. *Climate Change*, **95**, 139-168.

Najjar, R.G., C.P. Pyke, M.B. Adams, D. Breitburg, C. Hershner, M. Kemp, R. Howarth, M.R. Mulholland, M.Paolisso, D.Secor, K.Sellner, D.Wardrop, and R.Wood, 2010. Potential climate-change impacts on the Chesapeake Bay. *Estuarine, Coastal and Ahelf Science,* **86**, 1-20.

Narváez, D. A., J. M. Klinck, E. N. Powell, E. E. Hofmann, J. Wilkin and D. B. Haidvogel, 2012. Modeling the dispersal of eastern oyster (*Crassostrea virginica*) larvae at Delaware Estuary. *J. Mar. Res.,* **70**, 381-409.

NASA-JPL: The National Aeronautics and Space Administration (NASA) Physical Oceanography Distributed Active Archive Center at the Jet Propulsion Laboratory, California Institute of Technology.

Nguyen, A. D., 2008. Salt Intrusion, Tides and Mixing in Multi-channel Estuaries, Taylor & Francis/Balkema (PO Box 447, 2300 AK Leiden, The Netherlands), 174pp.

Nikitina, D.L., J.E. Pizzuto, R.A. Schwimmer, and K.W. Ramsey, 2000. An updated Holocene sea-level curve for the Delaware coast. *Marine Geology,* **171**, 7-20.

NWLP and NWLON: The National Water Level Program (NWLP) and the National Water Level Observation Network (NWLON), http://tidesandcurrents.noaa.gov/nwlon.html.

Paulson, C.A. and J.J. Simpson, 1977. Irradiance measurements in the upper ocean, *J.Phys. Oceanogr.,* **7**, 952-956.

Peltier, W. R., 1996: Global sea-level rise and glacial isostatic adjustment: An analysis of data from the east coast of North America. Geophys. *Res. Lett.*, **23**, 717–720.

Penven, P., V. Echevin, J. Pasapera, F. Colas, and J. Tam, 2005. Average circulation, seasonal cycle, and mesoscale dynamics of the Peru Current System: A modeling approach, *J.Geophys. Res.,* **110**, doi:10.1029/2005JC002945.

Penven, P., Laurent Debreu, Patrick Marchesiello, and James C. McWilliams, 2006. Evaluation and application of the ROMS 1-way embedding procedure to the central California upwelling system. *Ocean Modelling* **12**, 157-187.

Perlin, Natalie, Eric D. Skyllingstad, Roger M. Samelson, Philip L. Barbour, 2007. Numerical Simulation of Air–Sea Coupling during Coastal Upwelling. *J. Phys. Oceanogr*., **37**, 2081-2093.

Peterson, T.C. and R.S. Vose, 1997. An overview of the Global Historical Climatology Network temperature database. *Bull. Amer. Meteor. Soc.,* **78**, 2837-2849.

Pollard, David: pollard@essc.psu.edu Pennsylvania State University EMS Earth and Environmental Systems Institute 2217 Earth-Engineering Sciences Building tel: (814) 865-2022 University Park, PA 16802-6813 fax: (814) 865-3191

Powell, E. N., A. A. Kathryn, J.N. Kraeuter, S.E. Ford, D. Bushek, 2008. Long-term trends in oyster population dynamics in Delaware Bay: regime shifts and response to disease. *J. of Shellfish Research,* **27**, 729-755.

Powell, E.N., D.A. Kreeger, J.M. Morson, D. B. Haidvogel, Z.Wang, R. Thomas, J. E. Gius, 2012. Oyster food supply in Delaware Bay: Estimation from a hydrodynamic model and interaction with the oyster population. J. Marine Res., 70, 469-503 (DOI: http://dx.doi.org/10.1357/002224012802851904).

Ralston, D. K., W. R. Geyer, and J. A. Lerczak, 2008. Subtidal salinity and velocity in the hudson river estuary: observations and modeling. *J. Phys. Oceanogr.*, **38**, 753-770.

Rudolf, B., H. Hauschild, W. Rueth, and U.Schneider, 1994. Terrestrial precipitation analysis: Operational method and required density of point measurements. In: Global Precipitations and Climate Change [M. Bubois, and F. Désalmand (eds.)]. NATO ASI Series I, **26**, Springer Verlag, Berlin, 173-186.

Scully, M.E., W. R. Geyer, and J. A. Lerczak, 2009. The influence of lateral advection on the residual estuarine circulation: A numerical modeling study of the Hudson River Estuary. *J. Phys. Oceanogr.,* **39**, 107-124.

Sharp, J.H., K.Yoshiyama, A.E. Parker, M.C. Schwartz, S.E. Curless, A.Y. Beauregard, J.E. Ossolinski, and A.R. Davis, 2009. A biogeochemical view of estuarine eutrophication: Seasonal and spatial treands and correlations in the Delaware Estuary. *Estuaries and Coast,* **32**, 1023-1043.

Shchepetkin, A.F., McWilliams, J.C., 2006. Computational kernel algorithms for fine-scale, multi-process, long-time oceanic simulations. In: Ternam, R., Tribbia, J.(Eds), Handbook of Numerical Analysis: Special Volume: Computational Methods for the Atmosphere and the Oceans. Elsevier.

Shchepetkin, A.F., McWilliams, J.C., 2005. The Regional Ocean Modeling System: A split-explicit, free-surface, topography-following coordinate oceanic model. *Ocean Modelling*, **9**, 347-404.

Shchepetkin, A.F., McWilliams, J.C., 2003. A method for computing horizontal pressure-gradient force in an oceanic model with a non-aligned vertical coordinate. *J. Geophys. Res.* **108**, 3090-3124.

Shchepetkin, A.F., McWilliams, J.C., 1998. Quasi-monotone advection schemes based on explicit locally adaptive dissipation. *Mon. Weather Rev.* **126**, 1541-1580.

Simpson, J. H., A. CM and M. NGC. 1978. Fronts on the continental shelf. *J.Geophys. Res.,* **83**: 4609-4614.

Smolarkiewicz, P.K., and J. Szmelter, 2005. MPDATA: An edge-based unstructured-grid formulation, *J. Computational Physics,* **206**, 624-649.

Song, Y.T., 1998. A general pressure gradient formulation for ocean models. Part I: Scheme design and diagnostic analysis. *MWR*, **126**, 3213-3230.

Song, Y.T. and D.G. Wright, 1998.A general pressure gradient formulation for ocean models. Part II: Energy, momentum and bottom torque consistency. *WMR*, **126**, 3231-3247.

Song, Y., Haidvogel, D.B., 1994. A semi-implicit ocean circulation model using a generalized topography-following coordinate. *J. Comput. Phys.* **115**, 228-244.

Sprague V., 1979. Classification of the Haplosporidia. *Mar Fish Rev*, **41**, 40-44.

Stommel, H., 1961. Thermohaline Convection with Two Stable Regimes of Flow, *Tellus,* **2**, 224-230.

Taylor, K. E., 2001. Summarizing multiple aspects of model performance in a single diagram. *J. Geophys. Res.,* **110**, C11021, doi:10.1029/2005JC002902.

The Delaware Department of Natural Resources and Environmental Control: http://www.dnrec.delaware.gov.

Tilburg, C. E., J. T. Reager, and M. M. Whitney, 2005. The physics of blue crab larval recruitment in Delaware Bay: A model study. *J. Marine Research,* **63**, 471-475.

Trenberth, K.E., P.D.Jones, P.Ambenje, R.Bojariu, D.Easterling, A.Klein Tank, D.Parker, F.Rahimzadeh, J.A.Renwick, M.Rusticucci, B.Soden and P.Zhai, 2007. Observations: Surface and Atmospheric Climate Change. In: Climate Change 2007: The Physical Science Basis. Contribution of Working Group I to the Fourth Assessment Report of the Intergovernmental Panel on Climate Change [Solomon, S., D.Qin, M.Manning, Z.Chen, M.Marqis, K.B.Averyt, M.Tignor and H.L.Miller (eds.)]. Cambridge University Press, Cambridge, United Kingdom and New York, NY, USA.

Tsimplis, M.N., A.G.P. Shaw, R.A. Flather and D.K. Woolf, 2006. The influence of the North Atlantic Oscillation on the sea level around the northern European coasts reconsidered: the thermosteric effects.

Phlios. T. Roy. Soc. A, **364**, 845-856.

Umlauf, L., and H. Burchard, 2003. A generic length-scale equation for geophysical turbulence models, *J.Mar.Res.,* **61**,235-265.

UCS: Union of Scientists (www.ucsusa.org), 2006. The Changing Northeast Climate summarized from *Climate Change in the U.S. Northeast*, a report of the Northeast Climate Impacts Assessment (NECIA, 2006) and two studies by K.Hayhoe, C.Wake, and collaborators on the NECIA Climate Team.

Wang, Z., D. Haidvogel, D.Bushek, S.Ford, E. Hofmann, E.Powell, and J. Wilkin, 2012. Circulation and Water properties and Their Relationship to the Oyster Disease MSX in Delaware Bay, *J. Marine Res.,* **70**, 279-308 (DOI: http://dx.doi.org/10.1357/002224012802851931).

Warner, J.C., N. Perlin and E.D. Skyllingstad, 2008A. Using the Model Coupling Toolkit to couple earth system models. *Environmental Modelling & Software*. **23**, 10-11, 1240-1249.

Warner, John C., Christopher R. Sherwood, Richard P. Signell, Courtney K. Harris, Hernan G. Arango, 2008B. Development of a three-dimensional, regional, coupled wave, current, and sediment-transport model. *Computers & Geoscience*, **34**, 1284-1306.

Warner, J. C., C. R. Sherwood, H. G. Arango, and R. P. Signell, 2005a: Performance of four turbulence closure methods implemented using a generic length scale method, *Ocean Modelling*, **8**, 81-113.

Warner, J. C., W. R. Geyer, and J. A. Lerczak, 2005b. Numerical modeling of an estuary: A comprehensive skill assessment. *J Geophys. Res.,* **110**, 1-13. C05001, doi:10.1029/2004JC002691.

Whitney, M.M, and R.W. Garvine, 2006. Simulating the Delaware Bay Buoyant Outflow: Comparison with Observations. *J. Phys. Oceanogr.,* **36**, 3-21.

Wong, K.C., 1994A. On the nature of transverse variability in a coastal plain estuary. *J Geophys. Res.,* **99**, 14,209-14,222.

Wong, K.C., 1994B. On the relationship between long-term salinity variations and river discharge in the middle reach of the Delaware Estuary.*J Geophys. Res.,***100**, 20,705-20,713.

Zhang, W. F., Wilkin, J. L., Levin, J. C., Arango, H. G., 2009. An adjoint sensitivity study of buoyancy- and wind-driven circulation on the new jersey inner shelf. *J. Phys. Oceanogr*. **39** (7), 1652-1668.